SWECLIM
SWEDISH REGIONAL CLIMATE MODELLING PROGRAMME

SMHI

No 101, Jan 2003

Reports Meteorology and Climatology

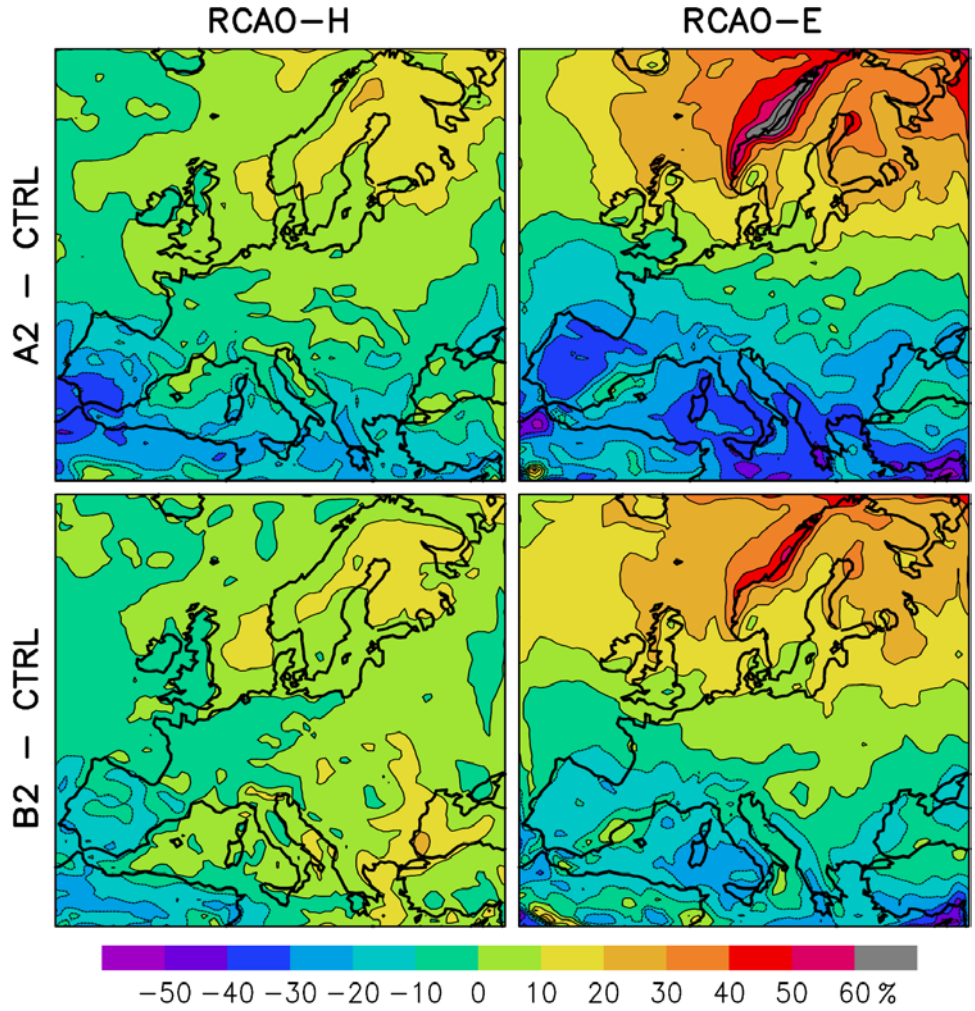

GCM driven simulations of recent and future climate with the Rossby Centre coupled atmosphere – Baltic Sea regional climate model RCAO

Jouni Räisänen, Ulf Hansson, Anders Ullerstig, Ralf Döscher, L. Phil Graham, Colin Jones, Markus Meier, Patrick Samuelsson and Ulrika Willén

Rossby Centre

Cover illustration: Changes in mean annual precipitation (in per cent of the control run mean) in the HadAM3H-driven (left) and the ECHAM4/OPYC3-driven (right) regional climate change simulations.

RMK No. 101, January 2003

GCM driven simulations of recent and future climate with the Rossby Centre coupled atmosphere – Baltic Sea regional climate model RCAO

Jouni Räisänen, Ulf Hansson, Anders Ullerstig, Ralf Döscher, L. Phil Graham, Colin Jones, Markus Meier, Patrick Samuelsson and Ulrika Willén

Rossby Centre, SMHI

Report Summary / Rapportsammanfattning

Issuing Agency/Utgivare	Report number/Publikation
Swedish Meteorological and Hydrological Institute S-601 76 NORRKÖPING Sweden	RMK No. 101
	Report date/Utgivningsdatum January 2003

Author (s)/Författare

Jouni Räisänen, Ulf Hansson, Anders Ullerstig, Ralf Döscher, L. Phil Graham, Colin Jones, Markus Meier, Patrick Samuelsson and Ulrika Willén

Title (and Subtitle/Titel

GCM driven simulations of recent and future climate with the Rossby Centre coupled atmosphere – Baltic Sea regional climate model RCAO

Abstract/Sammandrag

A series of six general circulation model (GCM) driven regional climate simulations made at the Rossby Centre, SMHI, during the year 2002 are documented. For both the two driving GCMs HadAM3H and ECHAM4/OPYC3, a 30-year (1961-1990) control run and two 30-year (2071-2100) scenario runs have been made. The scenario runs are based on the IPCC SRES A2 and B2 forcing scenarios. These simulations were made at 49 km atmospheric resolution and they are part of the European PRUDENCE project.

Many aspects of the simulated control climates compare favourably with observations, but some problems are also evident. For example, the simulated cloudiness and precipitation appear generally too abundant in northern Europe (although biases in precipitation measurements complicate the interpretation), whereas too clear and dry conditions prevail in southern Europe. There is a lot of similarity between the HadAM3H-driven (RCAO-H) and ECHAM4/OPYC3-driven (RCAO-E) control simulations, although the problems associated with the hydrological cycle and cloudiness are somewhat larger in the latter.

The simulated climate changes (2071-2100 minus 1961-1990) depend on both the forcing scenario (the changes are generally larger for A2 than B2) and the driving global model (the largest changes tend to occur in RCAO-E). In all the scenario simulations, the warming in northern Europe is largest in winter or autumn. In central and southern Europe, the warming peaks in summer and reaches in the RCAO-E A2 simulation locally 10°C. The four simulations agree on a general increase in precipitation in northern Europe especially in winter and on a general decrease in precipitation in southern and central Europe in summer, but the magnitude and the geographical patterns of the change differ a lot between RCAO-H and RCAO-E. This reflects very different changes in the atmospheric circulation during the winter half-year, which also have a large impact on the simulated changes in windiness. A very large increase in the lowest minimum temperatures occurs in a large part of Europe, most probably due to reduced snow cover. Extreme daily precipitation increases even in most of those areas where the mean annual precipitation decreases.

Key words/sök-, nyckelord

Climate change, climate scenario, regional climate modelling, Europe, PRUDENCE

Supplementary notes/Tillägg	Number of pages/Antal sidor	Language/Språk
This work is a part of the SWECLIM programme and of the EU PRUDENCE project.	61	English

ISSN and title/ISSN och title

0347-2116 SMHI Reports Meteorology Climatology

Report available from/Rapporten kan köpas från:

SMHI
S-601 76 NORRKÖPING
Sweden

Contents

1 Introduction

The Rossby Centre, part of SMHI and the Swedish Regional Climate Modelling Programme SWECLIM, has recently conducted a set of new regional climate change simulations. Six 30-year regional model runs have been made, using boundary data from the two global general circulation models (GCMs) HadAM3H and ECHAM4/OPYC3. Two of these runs represent the recent (1961-1990) climate and the remaining four the climate in the late 21st century (2071-2100) under two different assumptions of future atmospheric composition. These simulations contribute to the European PRUDENCE project.

This report gives an overview of the results of the mentioned simulations. Both the quality of the simulated recent climate (1961-1990) and the climate changes projected for 2071-2100 are discussed, with some more emphasis on the latter. The focus is largely on the atmospheric near-surface climate, including both the time mean state and some measures of variability and extremes. However, it is impossible to cover all relevant topics in one report. For example, user-oriented parameters like growing season length, wind energy potential, heating or cooling degree days etc. are excluded here. Another important question that we do not address explicitly is comparison between the regional climate model and the driving GCM simulations. However, the differences between our HadAM3H- and ECHAM4-driven experiments underline the point that many aspects of regional climate simulations are strongly governed by the driving GCM. This conclusion is well in line with earlier research (e.g., Noguer et al. 1998; Rummukainen et al. 2001; Räisänen et al. 2001).

The outline of this report is as follows. We first describe the regional climate model, the GCMs that provided boundary data for it, the emission scenarios used in the climate change simulations, and other issues related to the design of the experiments (Section 2). In Section 3, the control simulations (1961-1990) are discussed and compared with observational estimates of climate in the same period. After this, the projected climate changes for the period 2071-2100 are studied. First, in Section 4, a descriptive overview of the simulated changes is given. Then, in Section 5, some statistical aspects are addressed, including the significance of the changes with respect to unforced climate variability and the relative similarity, or lack thereof, between the results of the HadAM3H- and ECHAM4-driven simulations. Finally, the conclusions are given in Section 6.

2 The experimental design

2.1 The coupled regional climate model RCAO

The coupled regional climate model RCAO consists of the atmospheric model RCA2 (Jones 2001; Bringfelt et al. 2001), the three-dimensional Baltic Sea ocean model RCO (Meier et al. 1999; Meier 2001; Meier et al. 2002) and the lake model PROBE (Ljungemyr et al. 1996) applied in an area approximately covering the Baltic Sea drainage basin. In the experiments described here the atmospheric model was run in a

rotated latitude-longitude grid with a resolution of 0.44° (approximately 49 km) in both horizontal directions and with 24 levels in the vertical. The integration domain covered an area of 106 ×102 grid boxes, of which the outermost eight at each side were used as boundary relaxation zones. The ocean model RCO was run with 6 nm (approximately 11 km) horizontal resolution and with 41 levels in the vertical, in an area covering the Baltic Sea and the Kattegat.

The atmospheric model domain is shown in Fig. 1, which also indicates four subregions used for portraying the results. The ones that are most frequently used are Sweden (which is of special interest from a local Swedish perspective but also often gives a good idea of the results in northern Europe in general) and land south of 49°N (which provides a general impression of the model behaviour in the southern half of the domain). Only grid boxes with at least 50% of land are included in these two areas. Where space admits and this gives significant additional information, some area means are also shown for the whole Baltic Sea runoff area (including Sweden but excluding the Baltic Sea) and the Baltic Sea itself. As also indicated in Fig. 1, most figures in this report exclude the boundary relaxation zones and the two outermost rows and columns in the ordinary model area, which are still very markedly affected by boundary problems such as sharp gradients in cloudiness and precipitation.

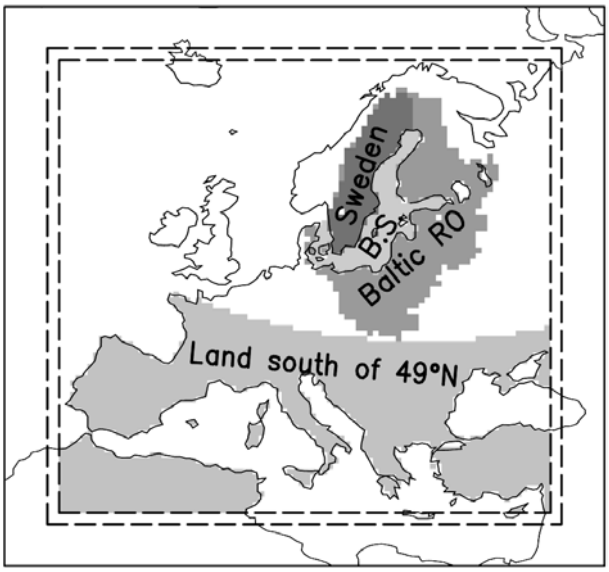

Figure 1. *The RCAO model domain. The outer dashed lines indicate the boundary relaxation zones and the inner dashed lines the area shown in most figures of this report and used for the statistics in Section 5. Also shown are four subareas for which some of the results are shown separately: Sweden, the Baltic Sea runoff area (which includes Sweden), the Baltic Sea and land south of 49˚N.*

Since the focus in this report is on atmospheric and land surface results, the main features of RCA2 are discussed in some more detail below. The model is structured within the HIRLAM reference system and uses the HIRLAM model semi-Lagrangian dynamical core described in McDonald and Haugen (1992, 1993) with 6th order implicit horizontal diffusion (McDonald 1994). However, most of the original HIRLAM physical parameterisations have been exchanged for newer schemes. The fast but highly simplified radiation scheme described in Savijärvi (1990) and Sass et al. (1994) is still

used, but with some modifications added by Räisänen et al. (2000b) to allow, in particular, changes in the CO_2 concentration between different model runs. Subgrid scale vertical mixing is treated with the scheme of Cuxart et al. (2000), which includes turbulent kinetic energy as a prognostic variable. The Kain-Fritsch convection scheme (Fritsch and Chappell 1980; Kain and Fritsch 1990) parameterises both deep and shallow convective mixing. The parameterisation of resolved condensation processes follows that described in Rasch and Kristjánsson (1998). Cloud water is a prognostic variable, whereas resolved cloud fraction is diagnosed from relative humidity following Slingo (1987). There is a tight coupling between convection and resolved condensation with detrained convective cloud water and moisture acting as a source term for resolved condensation within the same time step. Finally, the land surface-soil scheme has two prognostic layers for temperature and soil moisture, plus an additional bottom temperature layer whose temperature is derived from the driving GCM simulation. A weighted vegetation fraction is used to parameterise the effect of vegetation on the prognostic variables. A full description of the surface-soil scheme can be found in Bringfelt et al. (2001).

2.2 The driving GCM simulations

Data from two global climate models, HadAM3H and ECHAM4/OPYC3, were used to drive RCAO. ECHAM4/OPYC3 (Roeckner et al. 1999) is a coupled atmosphere-ocean GCM, whose atmospheric component ECHAM4 was run at T42 spectral resolution (formally equivalent to a grid spacing of 2.8° lon × 2.8° lat). HadAM3H is a high-resolution (1.875° lon × 1.25° lat) version of the atmospheric component of the Hadley Centre coupled atmosphere ocean GCM HadCM3 (Gordon et al. 2000). Because HadAM3H excludes the ocean, the simulations with this model used sea surface temperature (SST) and sea ice distributions derived from observations and earlier, lower resolution HadCM3 climate change experiments (see below).

The two coupled atmosphere-ocean models HadCM3 and ECHAM4/OPYC3 were first run from 1860 to 1990, using observed or estimated changes in atmospheric composition. From 1990 on, the simulations were divided to two using two different scenarios of future anthropogenic greenhouse gas and aerosol emissions: IPCC SRES A2 and B2 (Nakićenović et al. 2000). The A2 scenario assumes relatively large (in comparison with the other SRES scenarios) and continuously increasing emissions of the major anthropogenic greenhouse gases, CO_2, CH_4 and N_2O. The B2 scenario also features an increase in the CO_2 and CH_4 emissions, but this is slower, in the lower midrange of the SRES scenarios. However, sulphur emissions are also larger in A2 than in B2, which partly compensates the climatic effects of the larger greenhouse gas emissions.

For driving RCAO, two 30-year time slices (1960/1961-1990 and 2070-2100) of the HadAM3H and ECHAM4/OPYC3 simulations were used. HadAM3H itself was run for these periods only, using presecribed SST and sea ice distributions. For the control run (1960-1990), observed sea surface conditions were used. For the period 2070-2100, the SST and ice distributions were modified using the HadCM3-simulated changes in SST and ice. For SST the modification was relatively simple. The HadCM3-simulated change in SST was represented by its 30-year seasonally varying mean value (2071-2100 minus 1961-1990) plus the best-fit linear trend within the 30-year period (to account for the increase in greenhouse gases from 2070 to 2100). This change was then

added to the observed SST time series for 1960-1990. For sea ice, the principle was the same but a slightly more complicated adjustment procedure was needed to account for the differences in ice edge between HadCM3 in 1961-1990 and the observations (http://dmiweb.dmi.dk/pub/prudence/hadam3h_ hadrm3h_ info.html).

The motivation to not employ HadCM3 data directly to drive regional climate models derives from the relatively poor control climate in HadCM3, which does not use flux adjustments. There are substantial biases in SST in some ocean areas including the northern North Atlantic (Gordon et al. 2000), as well as in aspects of the simulated atmospheric climate. For example, the annual mean surface air temperatures in Sweden are about 3°C too low. The use of observed SSTs and the higher resolution in HadAM3H allowed a more realistic control climate, even though it is not possible to verify that the simulation of climate changes was also improved.

2.3 Representation of forcing in RCAO

The IPCC SRES scenarios include changes in the concentrations of several atmospheric greenhouse gases and aerosol types. Because of the simplicity of the RCA2 radiation code, the net effect of these changes was approximated by an "equivalent" increase in the CO_2 concentration. The control run value of 353 ppmv was raised in the B2 simulations to 822 ppmv and in the A2 simulations to 1143 ppmv, which values were held constant over the whole 30-year period. These values were selected so that the resulting increase in global mean radiative forcing, approximated following Ramaswamy et al. (2001, p. 358) as

$$\Delta F = 5.35\ \mathrm{Wm}^{-2}\Delta(\ln[\mathrm{CO}_2]) \quad (1)$$

would equal the projected 2071-2100 minus 1961-1990 changes in total anthropogenic radiative forcing for the B2 and the A2 scenarios, respectively. The estimates for the latter (4.5 W m^{-2} for B2 and 6.2 W m^{-2} for A2) were obtained from Houghton et al. (2001, pp. 66 and 823). This method of treating the forcing is crude, but it is justified by the fact that the sensitivity of regional climate models to the local radiative forcing is small (Räisänen et al. 2000, 2001). The model feels the "global warming" mainly through the change in boundary conditions, that is, through the inflow of warmer and moister air from the driving global model and through the higher prescribed SSTs and (in the case of RCA2) deep soil temperatures. Note that the actual projected increases in the CO_2 concentration are smaller, with values reaching slightly over 600 and nearly 850 ppmv by 2100 in the B2 and A2 scenarios, respectively (Houghton et al. 2001, p. 65).

2.4 Spin-up

The atmospheric results shown in this report were calculated using the full simulated 30-year periods 1961-1990 and 2071-2100. These 30-year periods were preceded by a 4-month spin-up period, which in all three HadAM3H-based runs (hereafter RCAO-H) and the ECHAM4/OPYC3-based (hereafter RCAO-E) A2 and B2 scenario runs used boundary data for the autumn 1960 or 2070. However, because ECHAM4/OPYC3 boundary data were not available at a sufficient time resolution in 1960, the RCAO-E control run spin-up was made using boundary data for September-December 1961. This procedure creates an abrupt change in boundary conditions between the end and the rebeginning of the year 1961, but at least in the atmosphere, the resulting shock was found to die out within the first two simulated days of the new year.

The Baltic Sea model RCO was initialised using observational data for September 1960, both for the control and the scenario runs. The use of observations to initialise the scenario runs is problematic, since the observed water temperatures in 1960 are not representative of the simulated warmer climate in the 2070's. We therefore exclude the first winter (2070-2071) when discussing the simulated changes in Baltic Sea ice conditions. Although this problem may also have an effect on the atmospheric conditions around the Baltic Sea in the year 2071, this effect appears to be small in comparison with the interannual variability.

2.5 The ice thickness problem

In the RCAO-H simulations, an instability in the PROBE lake model occasionally generated abrupt, unphysically large increases in ice thickness. As a result, the ice thickness in some lakes exceeded 10 meters in some winters, and the thick ice cover occasionally survived over the following summer (see Fig. 2a for an example). The problem only occurred in deep lakes that include, in the RCAO implementation of PROBE, Lake Ladoga, Lake Onega and a number of Swedish lakes.

An excessively thick ice cover affects the overlaying atmosphere, particularly the surface air temperature in summer. To approximately correct for this problem, the monthly mean files were rewritten applying a simple adjustment scheme to those grid boxes where the ice thickness had exceeded 1.5 m during the previous nine months (Appendix). Comparison between the original and adjusted files indicates that the problem had a serious impact only over large lakes (such as Lake Ladoga) that cover a substantial fraction of an atmospheric grid box (see Fig. 2b). In most of those about 60 grid boxes (less than 1% of the model area) where adjustments were made, the two sets of files are almost identical. No such adjustments have been made to the daily and the six-hourly files, however.

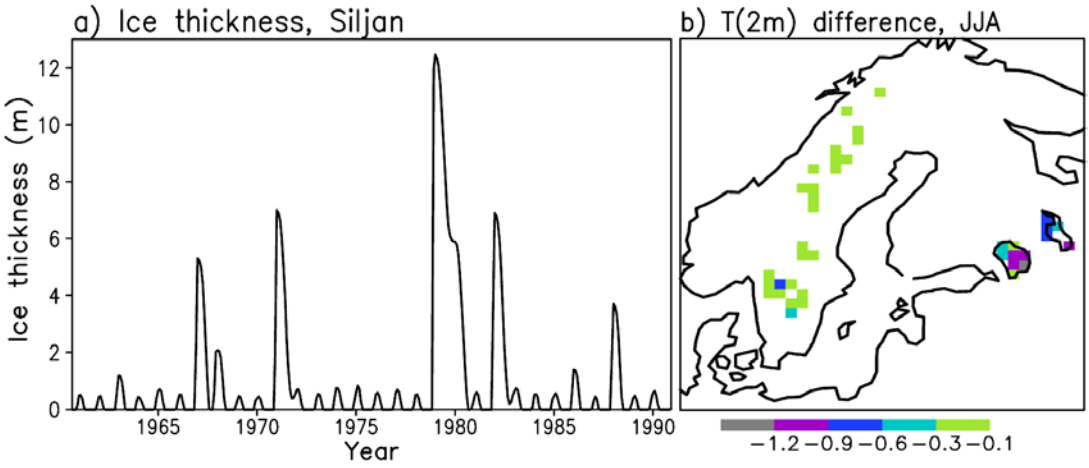

Figure 2. *(a) Ice thickness in Lake Siljan (60.9°N, 14.8°E) in the RCAO-H control run. (b) Difference (°C) in June-July-August mean 2 m temperature between the original and adjusted files (original minus adjusted) in the RCAO-H control run. The differences in the other seasons are smaller.*

This problem was detected when analysing the RCAO-H control run, but for consistency the same version of PROBE was used even in the two RCAO-H scenario

runs. For all the RCAO-E simulations, the problem was eliminated by a simple fix to the PROBE model code.

2.6 Output parameters of the atmospheric model

A list of the saved RCA2 output parameters and their time resolution is given Table 1.

Table 1. *The RCA2 output and its time resolution. 6H indicates instantaneous six-hourly values, and 24H and M daily and monthly means estimated from these. The values marked as 6H* are means or extremes over the previous six hours, and 24H* and M* daily and monthly means or extremes calculated from these. M** is the monthly mean of daily extremes. MC indicates monthly means stored separately for different times of the day (00, 06, 12 and 18 UTC). Surf = surface; LW = long-wave; SW = short-wave.*

Pressure level data (300, 500, 700, 850 and 925 hPa)		Fluxes of water (continued)	
Temperature	M + 500 and 850 hPa 6H	Evaporation	M*, 24H*
Wind components	M + 500 and 850 hPa 6H	Interception evaporation	M*, 24H*
Relative humidity	M + 500 and 850 hPa 6H	Runoff	M*, 24H*
Vertical velocity (ω)	M + 500 and 850 hPa 6H		
Geopotential height	M + 500 and 850 hPa 6H	Other surface data	
		Temperature, 2 m	M, MC, 24H, 6H
Other free atmospheric data		Max temperature, 2 m	M**, 24H*
Integrated water vapor	M, 6H	Min temperature, 2 m	M**, 24H*
Integrated cloud water	M, MC	Soil temperature (top)	M, 6H
Low cloud cover	M, MC	Max soil temperature (top)	M**, 24H*
Mid-level cloud cover	M, MC	Min soil temperature (top)	M**, 24H*
High cloud cover	M, MC	Soil temperature (deep)	M, 24H
		Soil temperature (bottom)	M
Fluxes of energy, water and momentum		Soil moisture (top)	M, 24H
Latent heat flux (surf)	M*, 6H*	Soil moisture (deep)	M, 24H
Potential latent heat flux	M*, 6H*	Wind components, 10 m	M, 6H
Sensible heat flux (surf)	M*, 6H*	Max wind speed, 10 m	6H*
Momentum flux (surf)	M*, 6H*	Mean wind peed, 10 m	M
Net SW radiation (surf)	M*, 6H*	Relative humidity, 2 m	M, 6H
Net LW radiation (surf)	M*, 6H*	Sea level pressure	M, 6H
Downward SW rad. (surf)	M*, 6H*	Surface pressure	M, 6H
Downward LW rad. (surf)	M*, 6H*	Total cloud cover	M, 6H
Net SW radiation (top)	M*, MC*	Sunshine hours	M*, 24H*
Net LW radiation (top)	M*, MC*	Snow water equivalent	M, 24H
Downward SW rad. (top)	M*	Snow fraction	M, 24H
Precipitation	M*, 24H*	Ice cover	M, 24H
Large-scale precipitation	M*, 6H*	Ice thickness	M, 24H
Convective precipitation	M*, 6H*	Water temperature	M, 24H
Snowfall	M*, 6H*		

3 The control simulations

In this section, the control period (1961-1990) climates in the HadAM3H-driven (RCAO-H) and ECHAM4/OPYC3-driven (RCAO-E) regional experiments are discussed and compared with observational estimates of the climate in this period. The focus is on surface and near-surface climate and mainly on time-mean conditions. For a few variables (surface air temperature, precipitation and wind speed), aspects of

variability and extremes are also discussed. For an overview of the order of discussion, the reader is referred to the table of contents. Because of the importance of these variables for interpreting some of the temperature- and precipitation-related results, the discussion begins from sea level pressure (Section 3.1) and total cloudiness (Section 3.2).

3.1 Sea level pressure

The gross features of the observed time mean sea level pressure are well reproduced in the RCAO control simulations, that is, the biases are generally small compared with the overall geographical variation (Fig. 3). The biases that do exist tend to be of somewhat larger magnitude in RCAO-E than in RCAO-H. The pressure in the RCAO-E simulation is, in most of the year, too high in the southwestern and northeastern parts of the domain, with a smaller (positive or negative) bias in-between. This indicates too cyclonic time-mean conditions (and possibly too frequent cyclone activity) in the middle of the domain. The biases in RCAO-H are more seasonally variable. For example, the pattern in winter indicates too strong westerly flow from the Atlantic Ocean to southern Scandinavia and the western parts of central Europe, whereas the reverse is true in spring and autumn.

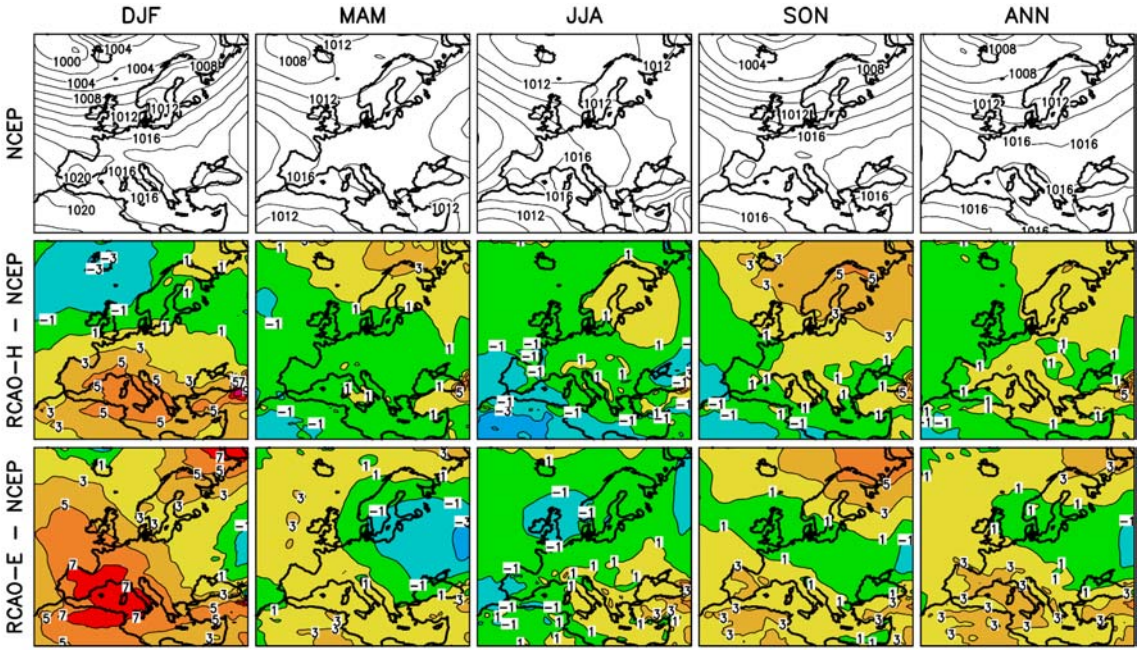

Figure 3. *Top: seasonal (DJF = December–February, MAM = March–May, JJA = June–August, SON = September–November) and annual (ANN) means of sea level pressure in 1961-1990 (contours every 2 hPa) according to the NCEP reanalysis (Kalnay et al. 1996; Kistler et al. 2001). Middle and bottom: the differences RCAO-H – NCEP and RCAO-E – NCEP (contours and shading at ±1, ±3, ±5 and ±7 hPa). The maps show the whole RCAO domain, including the boundary relaxation zones.*

3.2 Total cloudiness

The analysis of surface observations by CRU, the University of East Anglia Climate Research Unit (New et al. 1999, 2000) reveals a contrast in annual mean cloudiness between northern and southern Europe, with more clouds in the north than in the south (Fig. 4). The north-south contrast in the RCAO simulations is qualitatively similar but

stronger. The northern half of the model domain is, on the average, too cloudy in comparison with the CRU climatology, and the southern half too clear. Qualitatively the same pattern of biases was found in the reanalysis-driven RCA2 simulations analysed by Bringfelt et al. (2001) although, in these, the positive bias in northern Europe was smaller.

The bottom two panels of Fig. 4 show the 30-year mean seasonal cycles of cloudiness averaged over Sweden and the land area south of 49ºN. The positive bias in cloudiness in Sweden and elsewhere in northern Europe persists througout the year, being in the summer half-year larger in RCAO-E (in which the pressure pattern indicates more cyclonic flow conditions) than in RCAO-H. The annual mean cloudiness in Sweden is 66% in the CRU data set, 77% in RCAO-H and 80% in RCAO-E. In the land area south of 49ºN, both simulations appear to underestimate the average cloudiness in almost all months (although there are large variations within this area), with a larger underestimate in RCAO-E than in RCAO-H

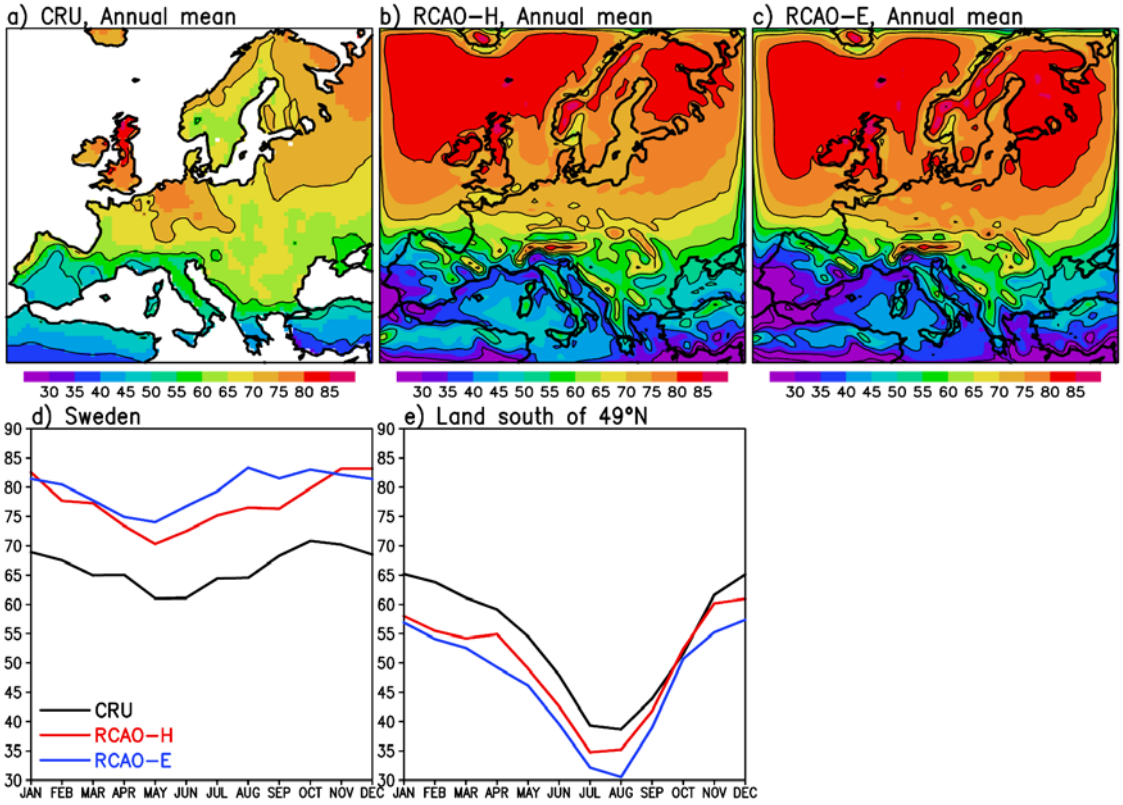

Figure 4. *Top: annual mean total cloudiness (%) from the CRU climatology (land only) and in the RCAO-H and RCAO-E control simulations. Bottom: the seasonal cycles of cloudiness from CRU (black), RCAO-H (red) and RCAO-E (blue) in Sweden and in the land area south of 49°N. The boundary relaxation zones and the two outermost rows and columns in the ordinary model area are excluded from the figure. In (a)-(c), the shading interval is 5%, but contours are drawn at every 10% only and the labels are excluded for legibility.*

The CRU cloud climatology itself is not an exact truth. When the sun is under the horizon, surface observations tend to underestimate the true cloud cover, because thin clouds remain easily unnoticed (e.g., Hahn et al. 1995). Conversely, high cumulus- or cumulonimbus clouds (which are most common in summer, and more common in the

southern than the northern parts of the RCAO domain) generally seem to cover a larger part of the sky than is their actual projection against the Earth surface (the quantity simulated by models). In Scandinavia, satellite observations indicate about 5% larger (smaller) winter (summer) cloudiness than surface observations (Karlsson 2001). However, satellite observations also have their own sources of uncertainty, especially in winter.

3.3 Surface air temperature

3.3.1 Time mean temperature

Figure 5 shows the seasonal and annual biases in the simulated mean surface air (2 m) temperature with respect to the CRU temperature climatology. A simple adjustment is applied for differences in surface height between the CRU data base and the model, assuming a constant lapse rate of 5.5°C km^{-1} (in most areas the impact of this adjustment is small).

The simulated temperatures are generally close but mostly slightly above those analysed, with an average annual mean bias of about 1°C. The largest warm biases occur, in both RCAO-H and RCAO-E, in the southeastern part of the domain in summer (which is apparently associated with too dry conditions there, Section 3.4.1) and in northern Scandinavia in winter. The latter bias may be partly an artefact, because there are suggestions that the CRU climatology is too cold in this area (see the discussion in Bringfelt et al. 2001). Overall, the biases in the two experiments are quite similar, even though a closer inspection also reveals some differences in the seasonal and geographical details.

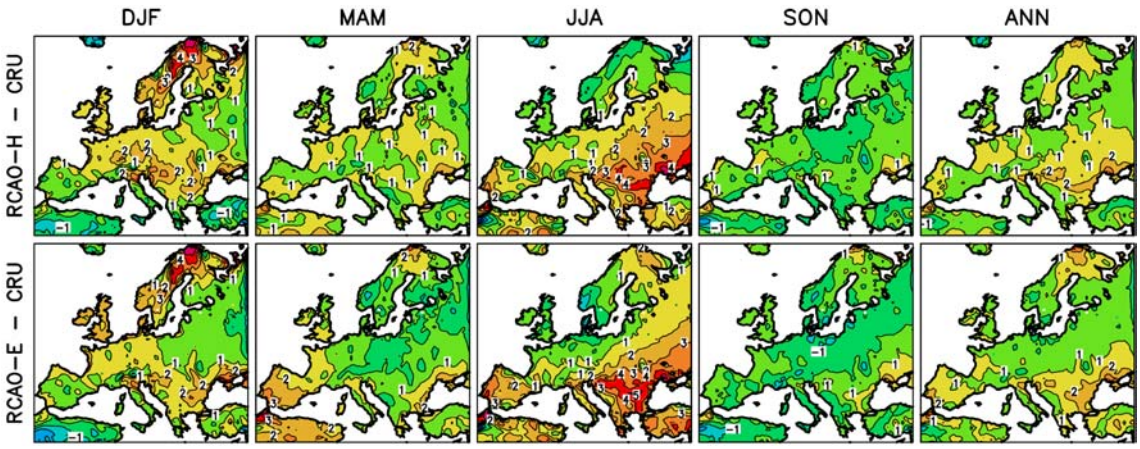

Figure 5. *Seasonal and annual mean biases in surface air (2 m) temperature (°C) relative to the CRU climatology in the RCAO-H (top) and RCAO-E (bottom) control runs.*

3.3.2 Interannual variability of monthly mean temperatures

Both in the real world and in model simulations, temperature varies irregularly from year to year. This variation is characterised in Fig. 6 by the interannual standard deviation of monthly mean temperatures. The top three panels, which show the mean of the standard deviations for the 12 individual calendar months, reveal a generally good agreement between the CRU analysis and the two RCAO control simulations. In all cases, the largerst variability occurs in the northeastern part of the domain and the

smallest in south and west. However, the simulated variability in the southern half of the model domain tends to be somewhat larger than that observed.

The lower part of Fig. 6 shows the seasonal cycles of the standard deviation in Sweden and the land area south of 49°N. In Sweden and in northern Europe in general, the observed seasonal cycle of variability is well reproduced in the model, except for undersimulated variability in the first two or three months of the year. The overestimate in variability in the land area south of 49°N is in relatively terms largest (about 40%) in summer. The differences between RCAO-H and RCAO-E are relatively modest. It should be noted that the magnitude of variability in a limited sample of data may vary a lot by chance. There is no simple way to quantify this sampling uncertainty for standard deviations averaged over several grid boxes, but the consistency of the RCAO – CRU differences from month to month indicates that these differences are not entirely due to chance.

It is important to note that the simulated interannual variations of temperature (and other climate elements) are generally not in phase with the observed variations in 1961-1990. Thus, years that were warm in the real world may be either warm or cold in the model. Because of the use of the observed SSTs over the Atlantic Ocean, this might appear surprising for RCAO-H. In practice, however, the impact of SST variations on the European climate is relatively small compared with the effects of chaotic atmospheric variability (see also Räisänen et al. 2002).

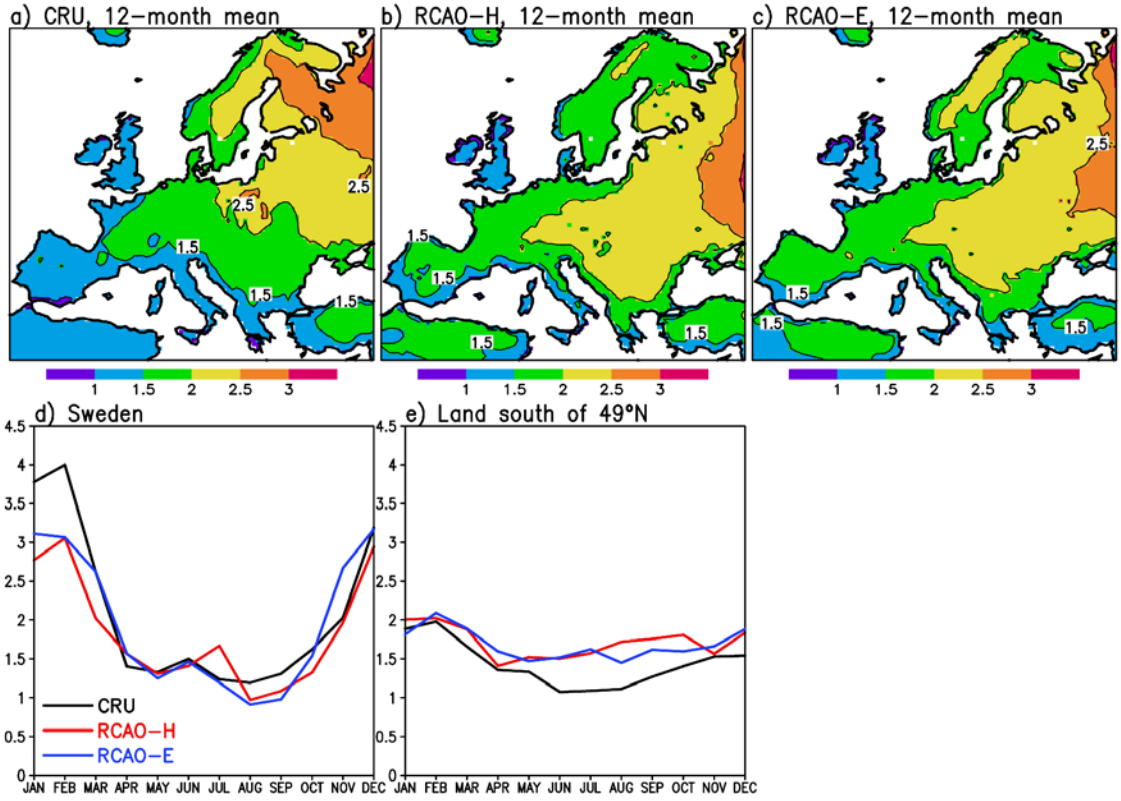

Figure 6. *Top: the interannual standard deviation of monthly mean temperature (°C) in 1961-1990 averaged over the 12 calendar months, as derived from the CRU analysis and from the RCAO-H and RCAO-E control simulations. Bottom: the seasonal cycles of the area mean of the standard deviation from CRU (black), RCAO-H (red) and RCAO-E (blue) in Sweden and in the land area south of 49°N.*

3.3.3 Diurnal temperature range

The simulated diurnal temperature range, defined as the average difference between the daily maximum and minimum temperature, is compared with the CRU analysis in Fig. 7. Again, RCAO-H and RCAO-E are more similar with each other than with the observations. In both two simulations, the diurnal range is reasonable in the southern part of the model domain but too small further north. For example, the annual area mean for Sweden is 8.5°C in CRU, but only 5.2°C in RCAO-H and 5.1°C in RCAO-E.

Several factors likely contribute to these differences. One is the fact that the surface temperature in the model represents the top 7 cm soil layer, rather than the actual skin temperature. In addition, the model includes subgrid scale lakes, which also slightly reduce the grid box mean temperature range compared with land area observations especially in northern Europe. Furthermore, the biases in the simulated cloudiness, with too cloudy conditions in the northern parts of the domain and too clear skies in the south, act to reduce the diurnal variability in the north and amplify it in the south. Finally, the distribution of precipitation biases (Section 3.4.1) has a similar effect via its impact on soil moisture. All these factors are expected to reduce the diurnal temperature range in northern Europe, whereas the latter two are expected to increase it in the south.

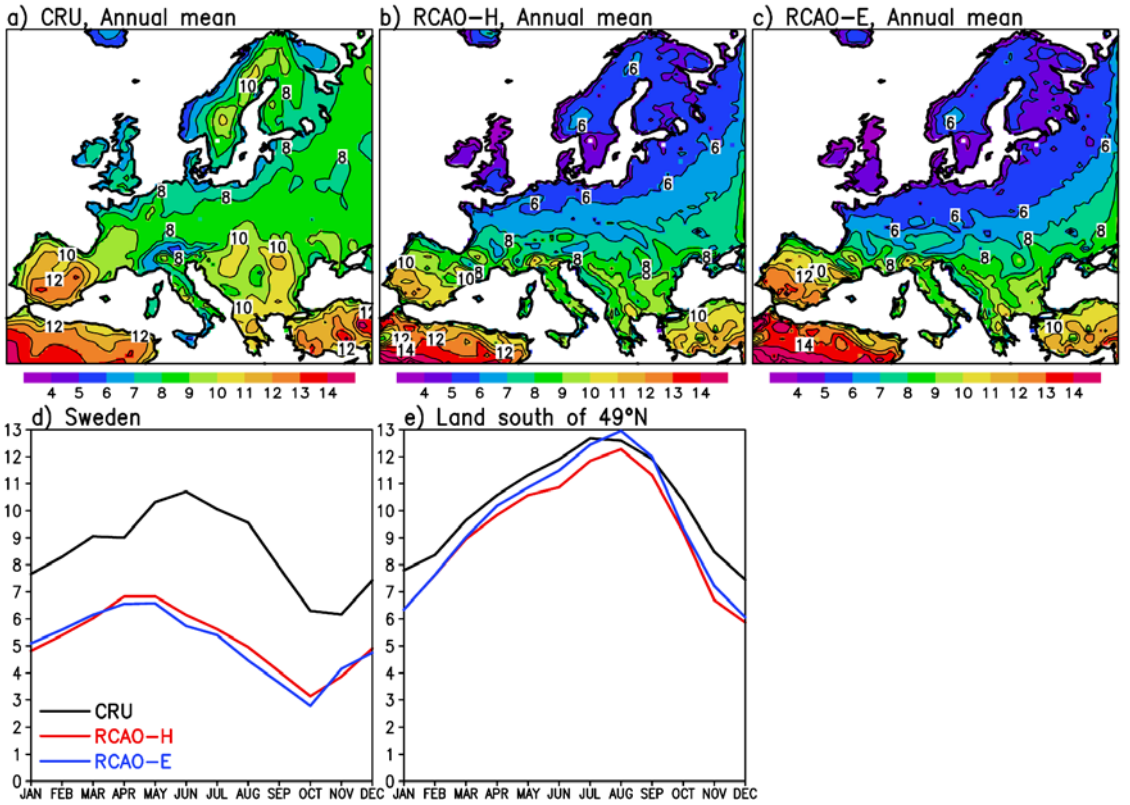

Figure 7. *Top: the 30-year annual mean diurnal temperature range (°C) in CRU, RCAO-H and RCAO-E. Bottom: the average seasonal cycles of the diurnal range in Sweden and in the land area south of 49°N.*

3.3.4 Temperature extremes

The extremes of the simulated temperatures are characterised in Fig. 8 by the 30-year means of the year's highest maximum and lowest minimum temperature. No gridded observations are available for these statistics, but as expected from the small diurnal temperature range and abundant cloud cover, the highest temperatures in northern Europe are relatively modest. For example, in an average summer, the highest temperature occurring in any grid box Sweden is 28.9°C in RCAO-H and only 26.4°C in RCAO-E. In reality, 30°C is exceeded in almost all summers. The lower value in RCAO-E is consistent with the more abundant cloud cover and precipitation (Section 3.4.1) in this simulation. The absolute 30-year maximum temperature in Sweden is 33.8°C in RCAO-H and 30.7°C in RCAO-E, whereas 36.4°C was measured in Lessebo in southeastern Sweden in August 1975.

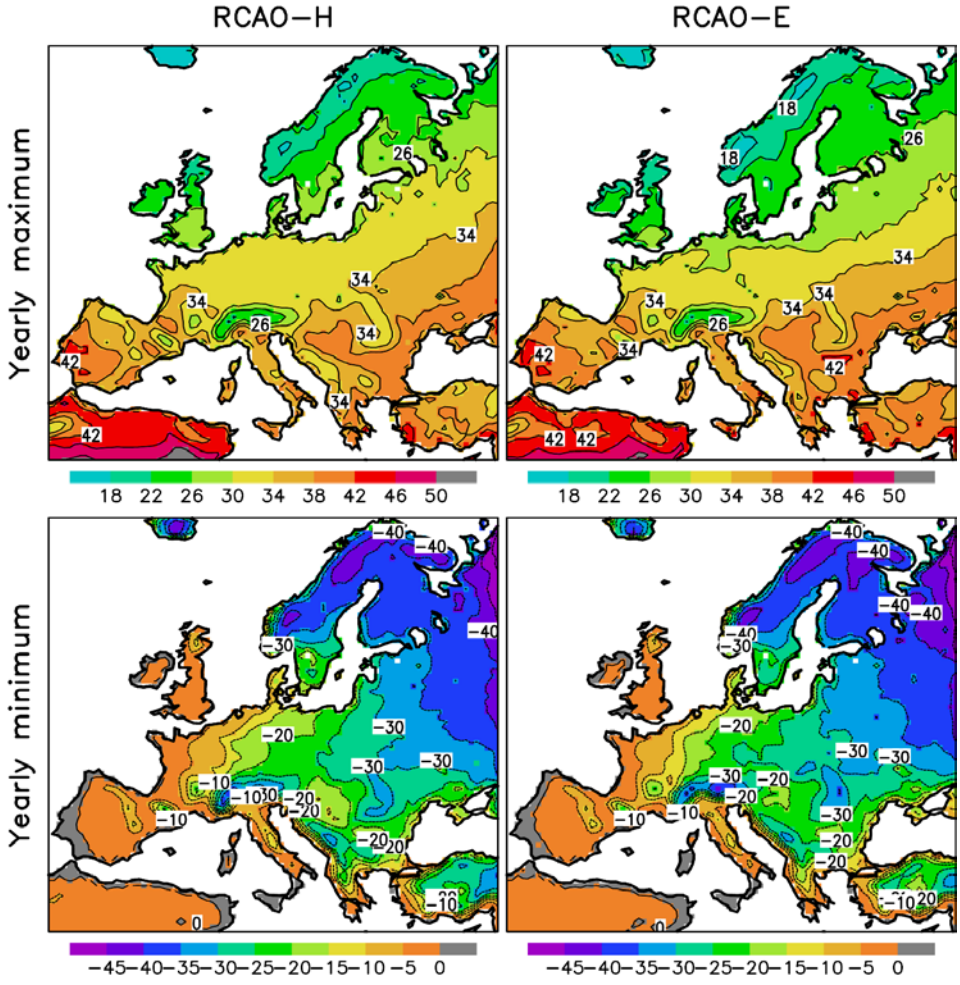

Figure 8. *Average annual temperature extremes in RCAO-H (left) and RCAO-E (right). The maps of yearly maxima are contoured and shaded at every 4°C and those of yearly minima at every 5°C.*

Despite the average warm bias and the average underestimate in diurnal variability, the coldest winter temperatures in RCAO are low. The absolute 30-year minima in Sweden are –56.0°C in RCAO-H and –55.6°C in RCAO-E, whereas the lowest officially recorded value in 1961-1990 (in Vuoggatjålme in February 1966) was –52.6°C. In an average winter, the lowest temperature occurring somewhere in Sweden is –47.4°C in

RCAO-H and –47.2°C in RCAO-E, and very low temperatures occasionally occur even in southern Sweden. For example in Norrköping 150 km southwest of Stockholm, the temperature falls below –30°C in five winters in RCAO-H (with an absolute minimum of -39.6°C) and in three winters in RCAO-E (with an absolute minimum of -34.4°C). In reality this only happened once, in February 1966, with a minimum of –33.5°C. The model apparently creates excessively sharp surface inversions in some rare weather situations, possibly because cooling by long-wave radiation is too efficient.

3.4 Precipitation

3.4.1 Time mean precipitation

The average annual precipitation from the CRU climatology is shown in Fig. 9a. The precipitation in the two RCAO control runs has largely similar geographical patterns as the CRU precipitation, but there are marked quantitative differences (Fig. 9b-c). The simulated precipitation is generally above the CRU estimate in northern Europe, especially in RCAO-E, but mostly below the CRU estimate in the southern parts of the domain. As shown in the lower part of the figure, the seasonal cycles of precipitation in Sweden are in good agreement between the model and CRU, disregarding the annual difference which amounts to 36% (48%) of the CRU value in RCAO-H (RCAO-E). The RCAO-E simulation is wetter than RCAO-H especially in the summer half-year. Similar conclusions hold for the Baltic Sea drainage basin as a whole, where the annual bias relative to CRU is 24% in RCAO-H and 42% in RCAO-E. In the southern parts of the model domain, however, both two simulations are too dry in summer, with a larger negative bias in RCAO-E than in RCAO-H.

The interpretation of these findings is complicated by the well-known negative bias in precipitation measurements, especially where the simulated precipitation exceeds the CRU estimate. Following Jones and Ullerstig (2002), Fig. 9e also shows an alternative, most likely more realistic estimate of actual precipitation for the Baltic Sea drainage basin (GPCP2/Rubel). This estimate is based on the second version of the Global Precipitation Climatology Project dataset (Huffman et al. 1997), which has been adjusted for the undercatch problem and was further tuned for the Baltic Sea drainage basin using the monthly correction coefficients of Rubel and Hantel (2001). As the GPCP2 data only exist from 1979, the ratio between the GPCP2/Rubel precipitation and CRU precipitation was calculated for the common period of these data sets and was then used to multiply the CRU means for 1961-1990. This estimate gives 19% larger annual mean precipitation and 40% larger winter precipitation than CRU. The RCAO-H simulation is in good agreement with it, whereas the precipitation in RCAO-E still appears somewhat high. Corrections of similar magnitude would probably be needed for the CRU precipitation in Sweden alone. Further south in the domain, where the fraction of solid precipitation is lower, the appropriate correction would probably be smaller.

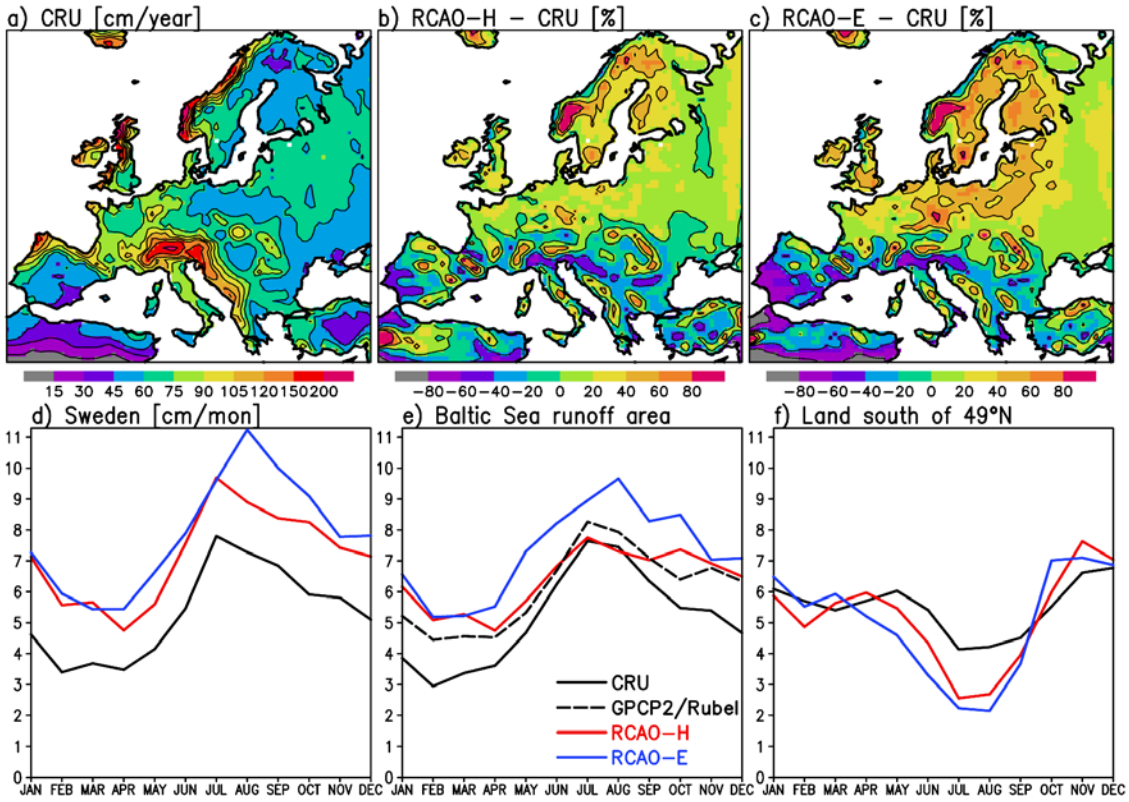

Figure 9. *Top left: average annual precipitation in 1961-1990 according to the CRU analysis. Top middle and right: the difference in precipitation between the RCAO control simulations and CRU, in per cent of the CRU precipitation. Bottom: the average seasonal cycles of precipitation in the three land areas shown in Fig 1. For the Baltic Sea runoff area, an alternative observational estimate of precipitation is also given (GPCP2/Rubel; see the text for details).*

3.4.1 Interannual variability of monthly precipitation

The relative (standard deviation divided by mean precipitation) interannual variability of monthly precipitation is studied in Fig. 10. The two model simulations agree with the CRU data in indicating larger relative variability in the southern than in the northern part of the model domain, but the contrast is too large in the model. In northern Europe, the relative variability is smaller than observed, especially in RCAO-E. This is consistent with the large number of simulated precipitation days in this area, which is discussed in the next subsection (as noted by Räisänen (2002), the relative variability tends to increase with decreasing number of precipitation days). In the Mediterranean area, by contrast, the simulated relative variability is larger than observed, with a generally larger bias in RCAO-E. The underestimate in the north is most pronounced in winter and the overestimate in the south in summer.

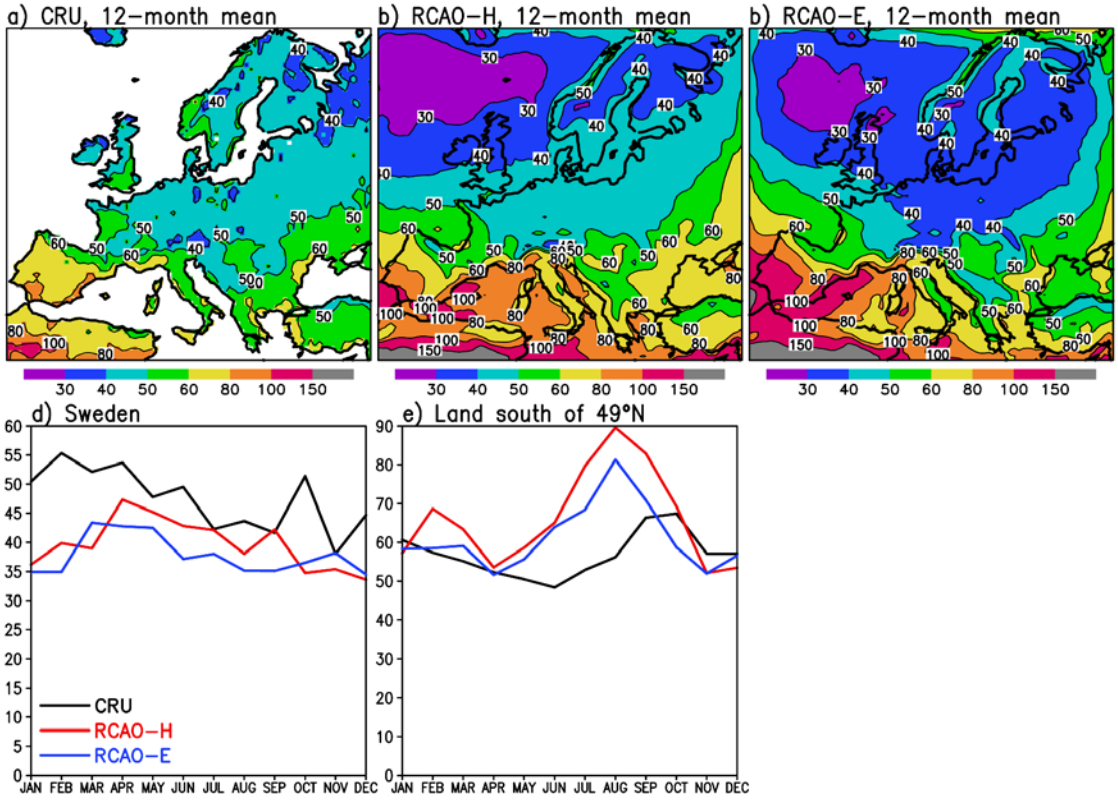

Figure 10. *Top: the ratio between the 12-month means of the interannual standard deviation of precipitation and the mean precipitation, as calculated from the CRU data for 1961-1990 and the two RCAO control simulations. Bottom: the ratio between the area means of the standard deviation and the time mean precipitation in Sweden and in the land area south of 49°N. All values have been multiplied by 100.*

3.4.2 Number of precipitation days

The annual number of wet days (often defined as days with precipitation exceeding some nonzero threshold) is a commonly used indicator of daily precipitation variability. Figure 11 shows this statistics for the RCAO control simulations, using the three thresholds 0.1, 1 and 10 mm day^{-1}. For Sweden, these maps can be compared with Raab and Vedin (1995, p. 84).

In northern Europe and even more strikingly over the northern North Atlantic, completely dry days (with less than 0.1 mm of precipitation) are infrequent in the model. In Sweden on the average, over three days out of four have simulated precipitation, whereas the observed fraction is about one of two (however, the geographical gradients are similar in the two cases). Part of this difference may be explained by the fact that the model grid boxes represent a much larger area (2400 km^2) than station measurements and are not affected by the undercatch in measurements. These complications also need to be recalled when considering the results for larger thresholds. However, the number of days with at least 1 mm of precipitation also appears excessive in Sweden (on the average 175 in RCAO-H and 181 in RCAO-E, in contrast with observed values varying on both sides of 120), whereas the 10 mm threshold is exceeded approximately as frequently as observed (17 days in RCAO-H and 20 days in RCAO-E). From this comparison with point measurements, the excess in mean precipitation mostly appears to result from too many days with light or moderate precipitation.

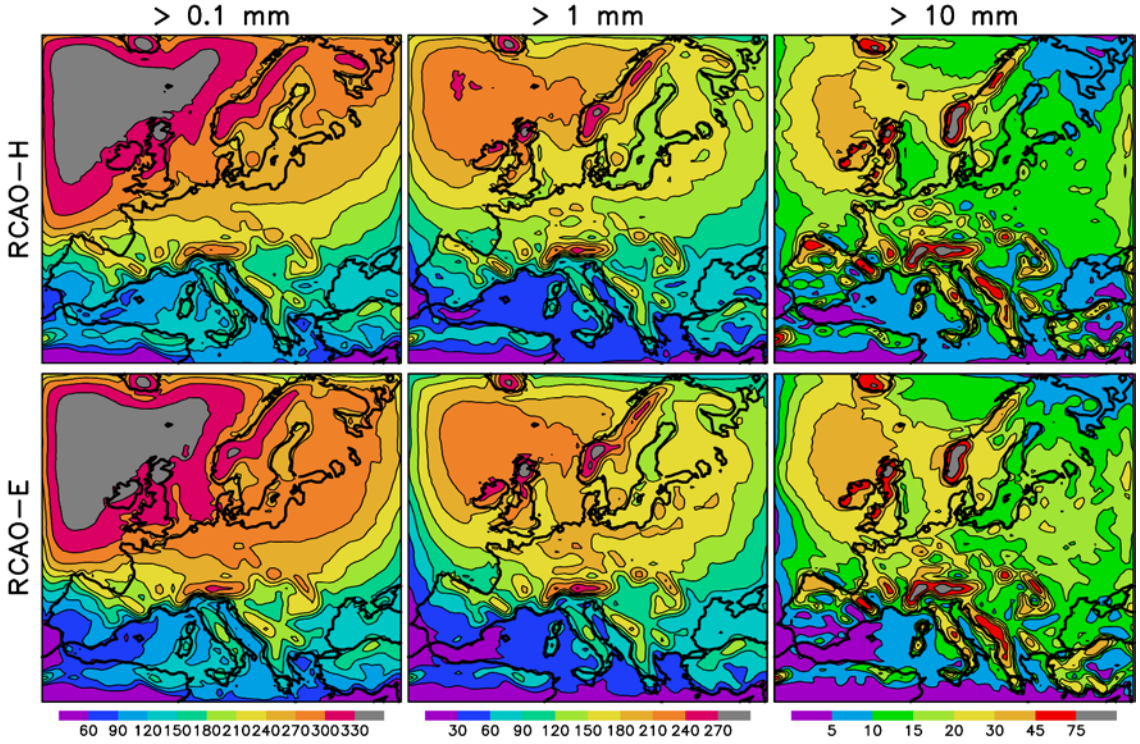

Figure 11. *The mean annual number of days with precipitation above 0.1 mm (left), 1 mm (middle) and 10 mm (right) in RCAO-H (top) and RCAO-E (bottom). The colour scale varies with the precipitation threshold.*

3.4.3 Extreme daily precipitation

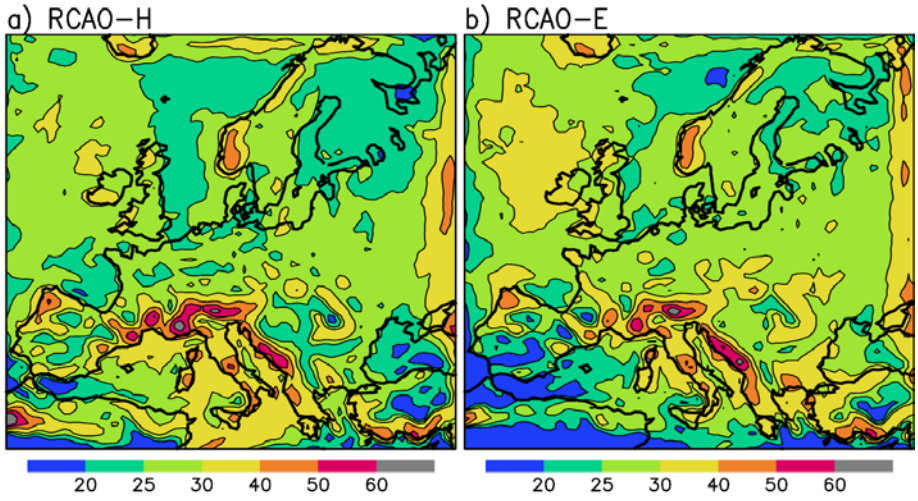

Figure 12. *The average yearly maximum one-day precipitation (mm) in RCAO-H and RCAO-E.*

Figure 12 shows the 30-year means of the annual maximum one-day precipitation in the two control simulations. These fields exhibit less geographical variation than the time mean precipitation. The average for Sweden is 27 mm in both RCAO-H and RCAO-E, or somewhat below the observed values in 1961-1990 that varied mostly from 30 to 35 mm with slightly larger values near the coasts and in the mountains (Raab and Vedin 1995, p. 84). Toward even more extreme events, the gap between the model results and the station observations increases. The single largest one-day precipitation anywhere in Sweden in the whole 30-year period is 69 mm in RCAO-H and 97 mm in RCAO-E,

whereas 179 mm was measured in Söderköping in southeastern Sweden in July 1973. The absolutely largest simulated amounts in the whole model domain are of the order of 130 mm per day. Again, however, comparison between the 2400 km^2 grid box values and the local station observations is not completely fair.

3.5 Wind speed

3.5.1 Time mean wind speed

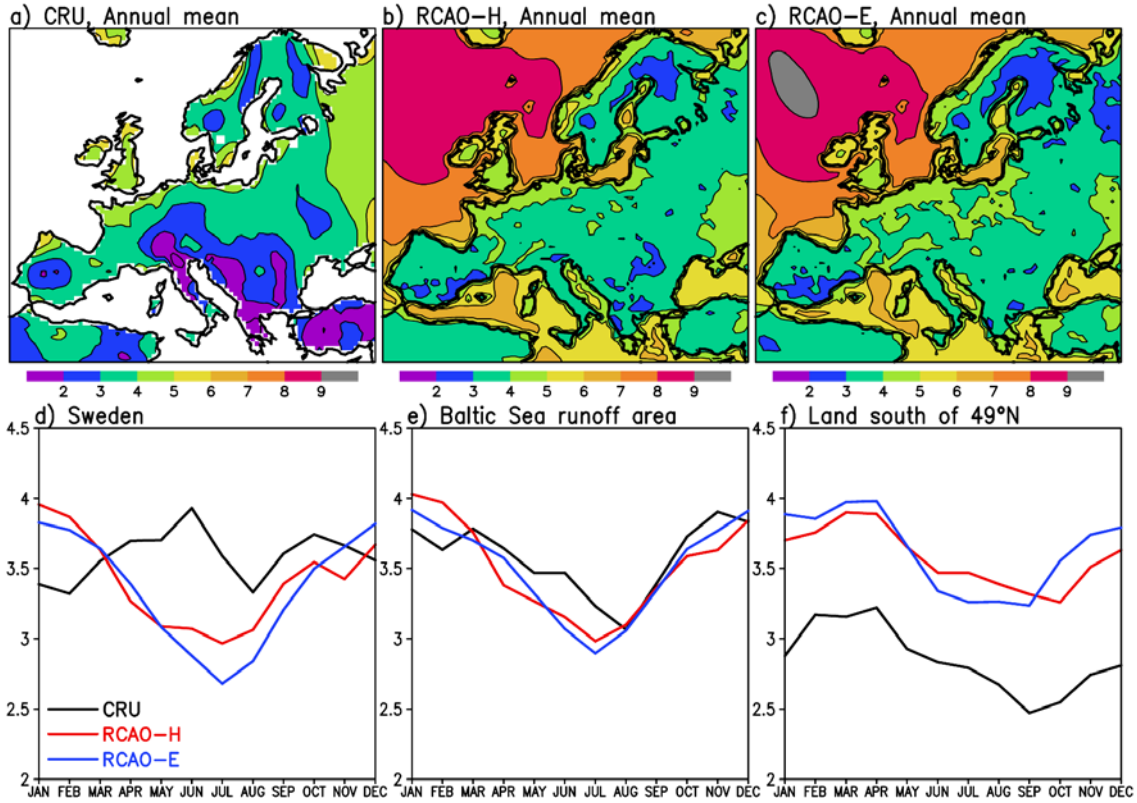

Figure 13. *Top: annual mean 10 m level wind speed (m s^{-1}) in 1961-1990 according to the CRU analysis and in the RCAO-H and RCAO-E control simulations. Bottom: the average seasonal cycles of wind speed in Sweden, the Baltic Sea runoff area and the land area south of 49°N.*

The near-surface wind speed is an important meteorological variable for practical applications, but it is both difficult to simulate (because it is strongly dependent on the boundary layer structure and local geography) and to verify (because measurement practices vary). Figure 13 compares the time mean 10 m level wind speed in RCAO with the CRU analysis. The annual means in northern Europe are in reasonable agreement, although there are many differences in the geographical patterns. Both model weaknesses and biases in observations may contribute to these. In southern Europe, the wind speeds in RCAO exceed the CRU values, which appear in this area surprisingly low. The seasonal cycles of the simulated and the analysed wind speed are in good agreement for the Baltic Sea runoff area as a whole and for land south of 49°N. In Sweden, however, both two simulations overestimate the average observed wind speeds in winter and underestimate them in summer. This suggests a problem in the simulation of boundary layer stability conditions or in the stability dependence of the near-surface wind speed. However, this comparison might also be to some extent affected by the

unveven distribution of the observation stations on which the CRU climatology is based. An uproportionally large fraction of the stations especially in northern Sweden are located in valleys, which are particularly in winter less windy than higher terrain.

3.5.2 Extremes of wind speed

As already noted by Rummukainen et al. (1998) for the first version of the RCA model, the highest wind speeds in RCAO are relatively modest (Fig. 14). The average annual maximum values over land are typically 9-12 m s^{-1}, and even over the Baltic Sea wind speeds exceeding 20 m s^{-1} are very rare. The absolutely highest wind speed occurring over the Baltic Sea during the 30-year period is 23.5 m s^{-1} in RCAO-H and 25 m s^{-1} in RCAO-E. However, the fact the model in principle simulates mean winds for the 2400 km^2 grid boxes may act to smooth out the local extremes.

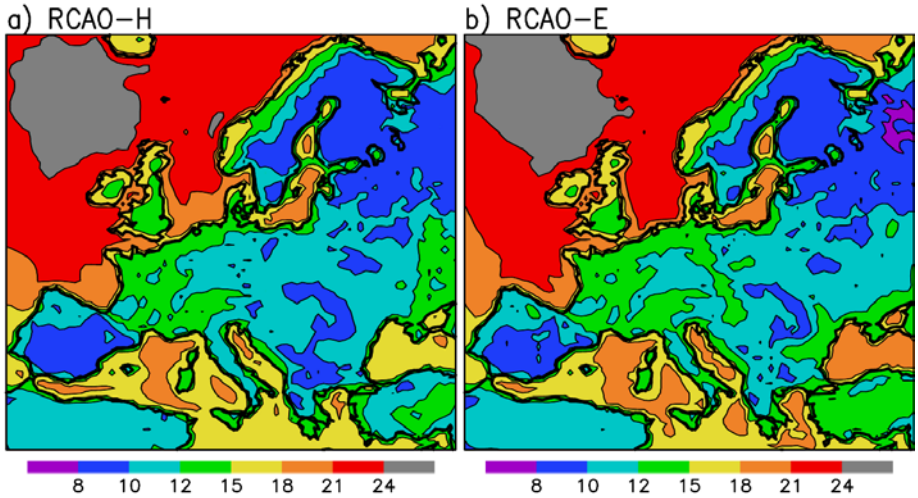

Figure 14. *The average annual maximum 10 m wind speed (m s^{-1}) in the RCAO-H and RCAO-E control simulations.*

3.6 Snow conditions

The simulated snow conditions are illustrated in Fig. 15 with two statistics: the average annual duration of the snow season and the average annual maximum water content of the snow pack. The former quantity is somewhat sensitive to the exact definition; here the areal snow fraction predicted by RCAO2 is used (for example; a monthly mean snow fraction of 0.5 is intepreted as 15 days with snow cover). Nevertheless, the agreement with observations in Sweden (Raab and Vedin 1995, p. 94) appears good. For the maximum water content of the snow pack, quantitative comparison with station observations is done in Table 2. For most locations, the model is in good agreement with the observations. However, the simulated values tend to be slightly too low in southern and too high in northern Sweden. The former bias likely results from the somewhat too warm simulated temperatures and the latter from too abundant precipitation. The positive bias in the simulated snow maxima is particularly large at two stations in the inland of northern Sweden (Jokkmokk and Hemavan). This is related to the fact that the abundant orographic precipitation, which in reality mainly falls over the western side of the Scandinavian mountains, partly spills over to the eastern side in the model. For improvement, higher model resolution would be needed. The differences between RCAO-H and RCAO-E are relatively modest, although in southern Sweden RCAO-E tends to have somewhat more snow and a longer snow season than RCAO-H.

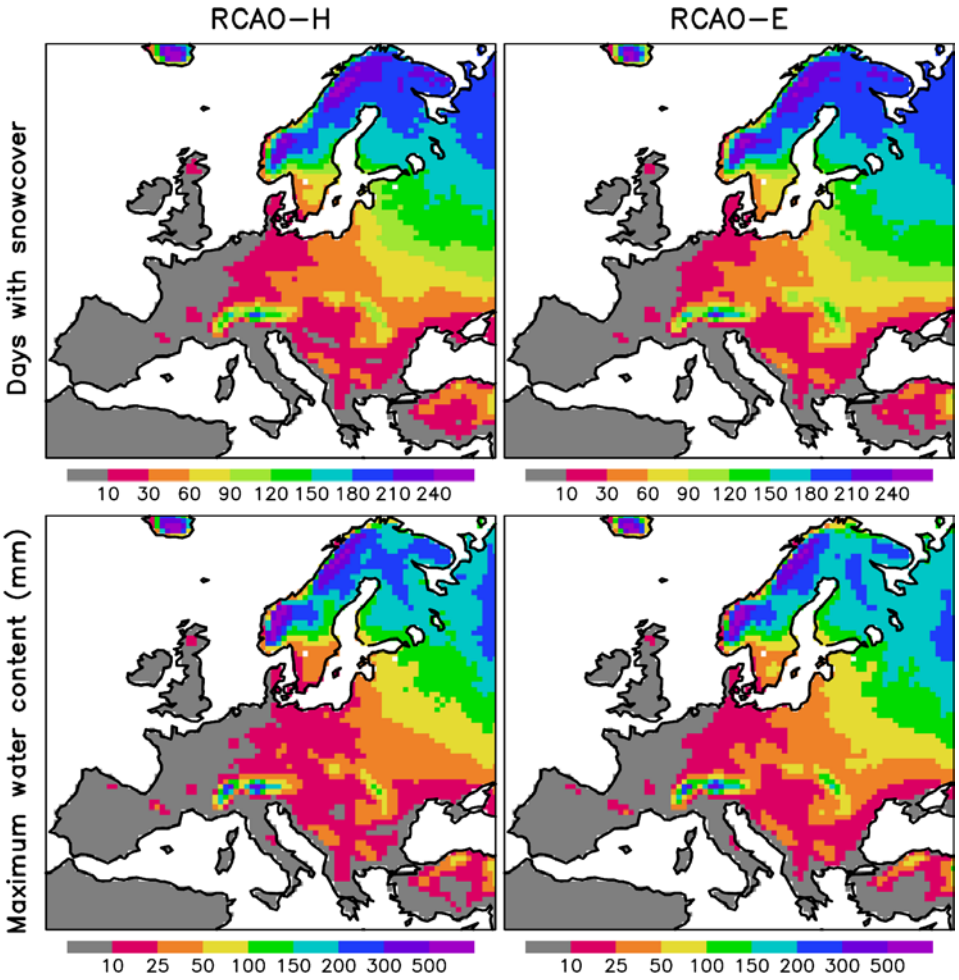

Figure 15. *The average annual duration of the snow season (top) and the average yearly maximum water content of the snow pack (bottom) in the RCAO control runs.*

Table 2. *Average annual maximum water content of the snow pack (mm) at selected Swedish locations. The observations (Raab and Vedin 1995, p. 96) represent the period 1968-1993, the model results the simulated years 1961-1990.*

Location	Latitude	Longitude	Observed	RCAO-H	RCAO-E
Katterjåkk	68.7°N	18.2°E	386	419	382
Jokkmokk	66.5°N	20.2°E	116	203	210
Hemavan	65.8°N	15.1°E	252	472	460
Haparanda	65.5°N	24.2°E	135	175	161
Umeå	63.8°N	20.3°E	130	164	163
Söderhamn	61.3°N	17.1°E	95	86	106
Malung	60.7°N	13.7°E	107	147	156
Karlstad	59.4°N	13.3°E	47	37	47
Stockholm	59.4°N	18.0°E	37	29	42
Göteborg	57.8°N	11.9°E	34	18	19
Nässjö	57.6°N	14.7°E	72	43	54
Kalmar	56.7°N	16.3°E	36	24	36
Falsterbo	55.4°N	12.8°E	17	13	18

3.7 Other aspects of the surface hydrology

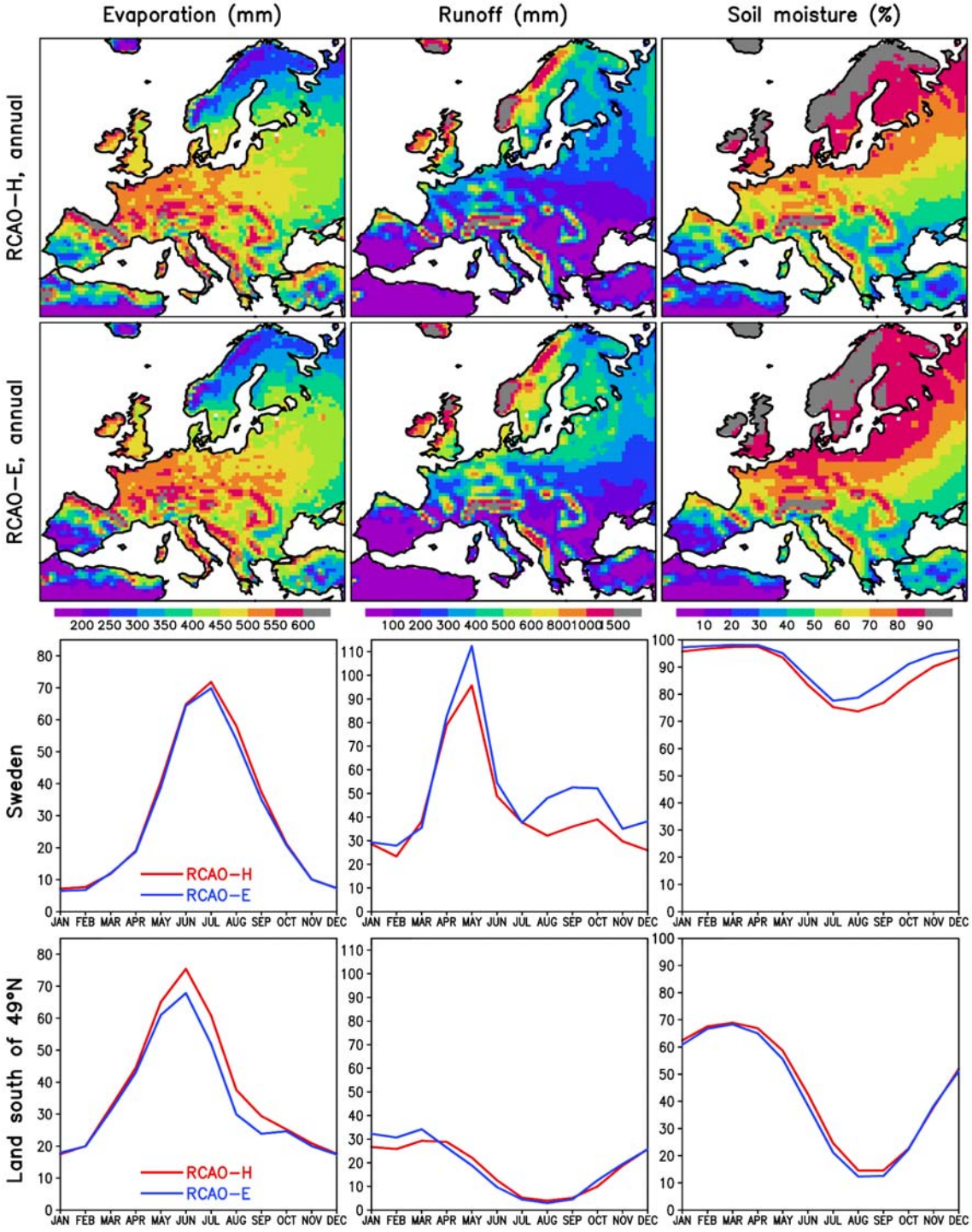

Figure 16. *Evaporation (left), point runoff (middle) and fractional soil moisture (per cent of a maximum of 242 mm) in the RCAO control simulations. The first two rows show the 30-year annual means in RCAO-H and RCAO-E, and the last two rows the average seasonal cycles in Sweden and the land area south of 49°N.*

The simulated precipitation (Section 3.4) and snow conditions (Section 3.6) have already been discussed. Results related to some other aspects of the surface hydrology are shown in Fig. 16. The first two columns display the simulated evaporation and

runoff generation, both scaled from the 360-day model year to a 365-day year, and the third the total soil moisture, summed over the surface and deep soil layers and expressed in per cent of the maximum capacity of 242 mm.

In the northern parts of the model domain, evaporation is slightly larger in RCAO-H than in RCAO-E, despite the more abundant precipitation in the latter. The annual area mean in Sweden is 357 mm in RCAO-H and 344 mm in RCAO-E, both close to the estimate 370 mm given by Raab and Vedin (1995, p. 111). The simulated soil moisture content in Sweden and other parts of northern Europe is close to saturation in most of the year, especially in RCAO-E, and evaporation is governed more by the availability of energy than water. The slightly lower summer evaporation in RCAO-E in Sweden reflects larger cloudiness, which reduces the solar radiation reaching the surface.

The larger precipitation together with the slightly smaller evaporation makes runoff in Sweden substantially larger in RCAO-E (606 mm per year) than in RCAO-H (514 mm per year). Both values exceed the observational estimate of Raab and Vedin (1995, p. 111), 380 mm per year. For the whole Baltic Sea runoff area as well, runoff is much larger in RCAO-E than in RCAO-H (468 vs. 362 mm per year).

The simulated hydrological regime in the southern part of the model domain is very different from that in the north. The soil is dry, especially in late summer and autumn, and evaporation is severely restricted by the lack of moisture. Most of the modest runoff occurs in winter. Because of the negative bias in precipitation, the model most likely underestimates runoff generation in this area.

3.8 Ice conditions

3.8.1 Lake ice

Figure 17 provides a comparison between the long-term mean observed (Eklund 1998, 1999) and simulated ice conditions in a number of Swedish lakes. The observational data cover lakes of widely varying size but are mostly for relatively large lakes (medium area about 30 km^2). For both the two parameters, the average ice season length and the annual maximum ice thickness, the first-order observed geographical variation is captured in the simulations. Lakes in southern (northern) Sweden have mild (severe) ice conditions in both the model and in nature. However, the simulated ice season is in most lakes somewhat too short, with the ice forming too late and melting too early. The observed mean over the 37 lakes with data available is 170 days, and the simulated values are 147 days in RCAO-H and 154 days in RCAO-E. This is qualitatively consistent with the relatively mild winter climate in the simulations. However, there is no systematic underestimate of the average annual maximum ice thickness. The observed value, averaged over 26 lakes, is 40 cm, whereas those for RCAO-H and RCAO-E are 40 and 44 cm. A similar apparent discrepancy between the simulated ice season length and maximum ice thickness already occurred in the earlier RCA1 simulations (Rummukainen et al. 2001).

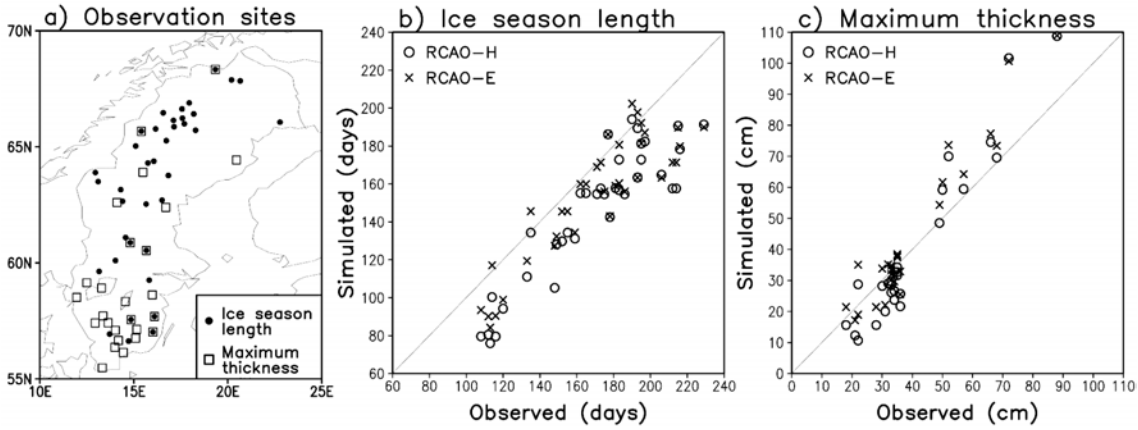

Figure 17. *Comparison between simulated and observed ice conditions in Swedish lakes. (a) The locations of the 37 lakes with observations of average ice season length (closed circles) and 26 lakes with observations of mean annual maximum ice thickness (boxes). (b) Scatter diagram between the average observed and average simulated ice season length (open circles for RCAO-H and crosses for RCAO-E). (c) As (b) but for the mean annual maximum ice thickness.*

Ice season length and especially the maximum ice thickness in RCAO-H are strongly affected by the problem described in Section 2.5. The results for RCAO-H in Fig. 17 therefore exclude all winters when the ice thickness exceeded 1.5 m.

3.8.2 Baltic Sea ice cover

Figure 18 shows the simulated 30-year time series of annual maximum ice area in the Baltic Sea including the Kattegat. As expected from the colder winters in this simulation, there is on the average slightly more ice in RCAO-E (mean 231 × 10^3 km^2, range from 113 × 10^3 km^2 to 398 × 10^3 km^2) than in RCAO-H (mean 196 × 10^3 km^2, range from 100 × 10^3 km^2 to 376 × 10^3 km^2). These values are in reasonable agreement with observations for 1961-1990 by the Finnish Marine Research Institute (mean 204 × 10^3 km^2, range from 52 × 10^3 km^2 to 405 × 10^3 km^2). The simulated Baltic Sea climate will be reported in more detail elsewhere.

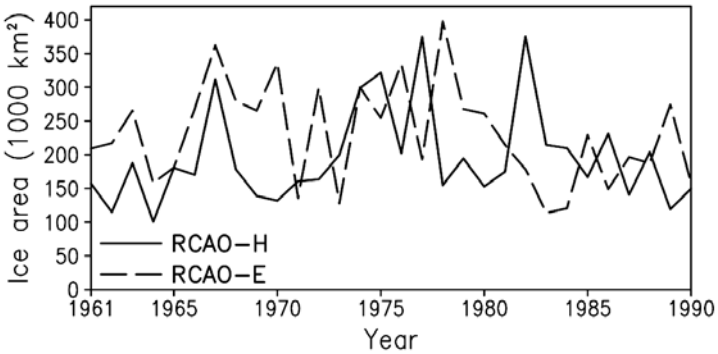

Figure 18. *Yearly maximum Baltic Sea ice area in the RCAO-H (solid) and RCAO-E (dashed) control runs.*

4 Simulated climate changes for the period 2071-2100

In this and the following section, the simulated climate changes, defined as differences in climate between the scenario (2071-2100) and the control period (1961-1990) are described. Altogether, the two driving global models and the two forcing scenarios give four scenarios of regional climate change. A gallery of figures and some tables are provided in this section to illustrate the similarities and the differences between these scenarios. The largely descriptive approach in this section will be complemented in Section 5 by a more quantitative statistical approach.

The order of discussion in this section follows that in the previous one. The changes in sea level pressure and cloudiness are discussed in the first two subsections, since they are useful for understanding some of the other changes. It should be emphasised right from the outset, however, that the largest (in comparison with natural variability) simulated change in surface climate is the general increase in temperature (Section 4.3).

4.1 Sea level pressure

4.1.1 Time mean sea level pressure

Most of the interannual variability of temperature, precipitation and other aspects of surface climate in Europe results from variations in the atmospheric circulation. Likewise, systematic changes in the circulation with changing atmospheric composition might modify the changes in surface climate in an important manner, over the more direct thermodynamic aspects of global warming. It is, however, not clear how the circulation will respond to changes in radiative forcing. As illustrated for the time mean sea level pressure in Fig. 19, the RCAO-H and RCAO-E scenario simulations give in some seasons quite different answers to this. These differences are essentially inhereted as such from the driving GCM simulations (not shown).

Beginning from the A2 minus control run climate changes, the RCAO-H experiment indicates very little annual mean pressure change, even though this results partly for opposing changes in different seasons. For example, a wintertime pressure decrease centred over the southern Norvegian Sea is to a large extent balanced by a pressure increase in the same area in summer and autumn. Except for summer, the pressure changes in RCAO-H are relatively weak compared with the simulated natural variability (Section 5.1). In RCAO-E, the changes are larger and more consistent between different seasons. In the annual mean there is a slight increase in pressure over central Europe and a strong decrease over northern Scandinavia and the Arctic Ocean. Some variant of this pattern is seen in all four seasons, although it migrates somewhat to the south in winter and to the north in summer. The pressure decrease near the northern boundary of the model domain is largest (over 10 hPa) in winter and spring. This pattern indicates an increase in the time-mean westerly geostrophic winds over northern Europe and the northern North Atlantic, and it also suggests a northward shift in cyclone activity.

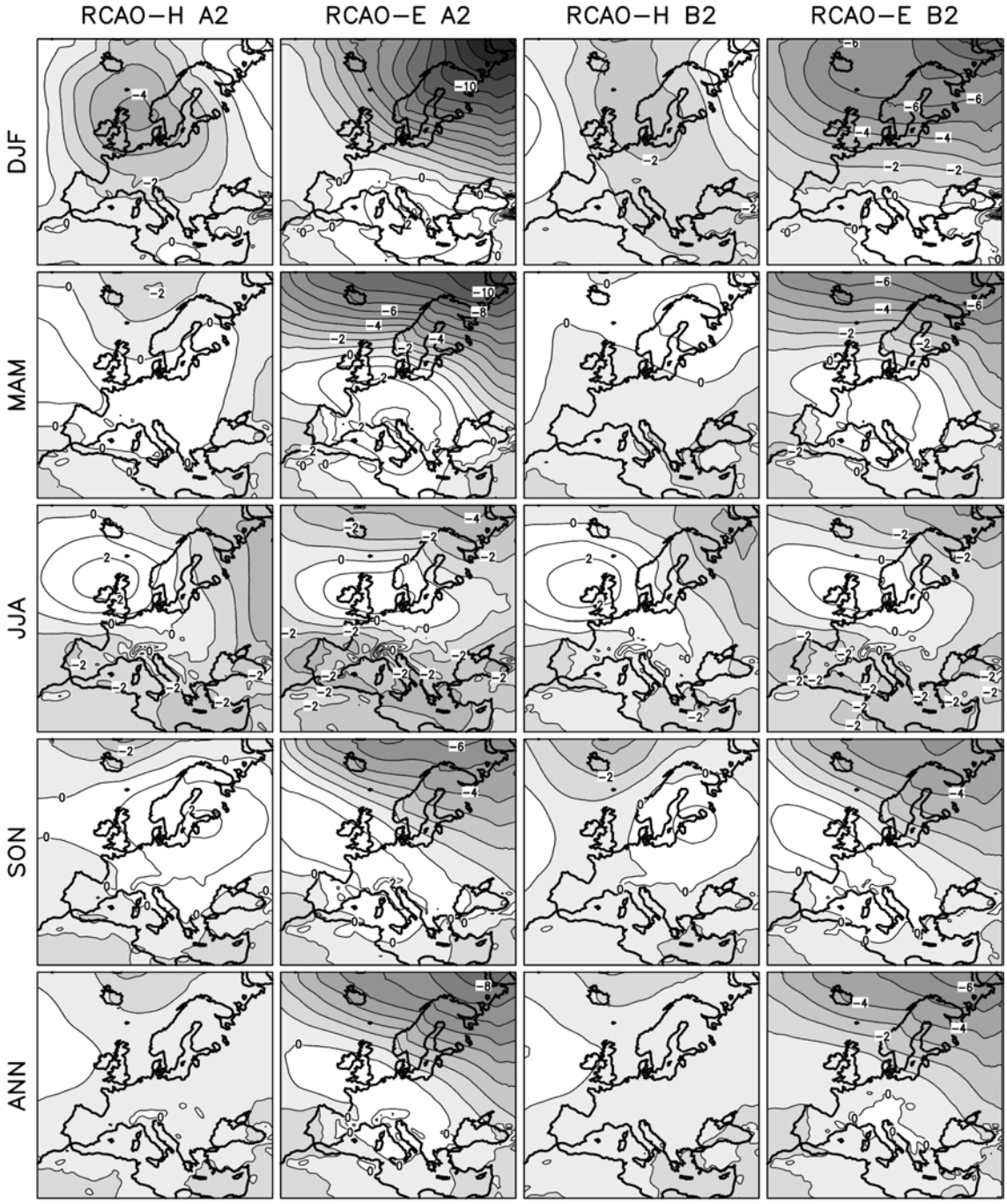

Figure 19. *Changes in seasonal and annual mean sea level pressure (differences from the corresponding control run 30-year means) in the RCAO climate change simulations. Contours at every 1 hPa; negative values are shaded.*

The B2 simulations redproduce most of the changes in A2, although with smaller amplitude[1]. Some qualitative differences do occur. For example, in RCAO-H in spring, the B2 simulation indicates a slight increase in pressure over northern Scandinavia, in contrast to the slight decrease in A2. Similarly, the strong pressure decrease in RCAO-E

[1] The A2 minus control and B2 minus control climate changes are not independent from each other, because the same control run has been used in defining both of them. This tends to produce some apparent similarity between the changes in A2 and B2 even when the statistical significance of the changes is weak.

in winter extends further southwest to the northern North Atlantic in the B2 than in the A2 simulation. However, some differences of this type would be expected simply from the substantial natural variability of the atmospheric circulation. As will be discussed in Section 5.1, any signs of real (statistically significant) nonlinearity between the climate changes in the A2 and B2 simulations are relatively weak.

4.1.2 Band-pass filtered variability

The changes in synoptic time scale pressure variability are illustrated in Fig. 20 using the band-pass filtered standard deviation of sea level pressure. The traditional band-pass filter of Blackmon (1976) is used, which passes variations in approximately the 2.5 to 6-day period range. Results are shown only for the winter when the differences in time mean pressure change between RCAO-H and RCAO-E are greatest, and only for the A2 scenario in which the changes are largest. More frequently, the 500 hPa geopotential height variability is analysed in this context but the choice of the level does not affect the basic conclusions.

The strongest variability in the control runs occurs over the northwestern Atlantic Ocean, from where a reasonably well-defined "storm track" extends towards northern Europe and the Arctic Ocean. In the A2 scenario run, the area of large variability extends further eastward in both RCAO-H and RCAO-E, but the change is larger in RCAO-E. In addition, the increase in variability in RCAO-H occurs mainly on the southern side of the control run storm track, whereas the pattern in RCAO-E represents a more direct eastward or northeastward extension of variability. These differences between the two experiments are largely as expected from the differences in the winter time mean pressure change in Fig. 19.

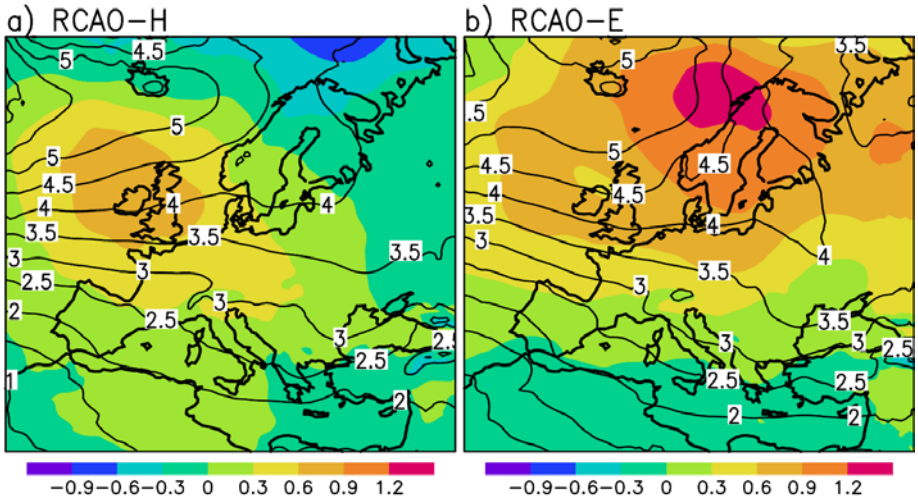

Figure 20. *The band-pass filtered standard deviation of sea level pressure in December-February in the RCAO-H and RCAO-E control runs (contours at every 0.5 hPa) and the change in this from the control run to the A2 scenario run (shading).*

The band-pass filtered variability measures the combined effect of transient cyclones and anticyclones but is unable to separate between these. The time mean pressure changes in Fig. 19 suggest that the cyclones in RCAO-E become more frequent or intense especially over the northern flank of the area where the variability increases, whereas anticyclonic activity primarily increases over the southern flank of this area.

4.2 Total cloudiness

Clouds and their interaction with radiation are probably the single most important source of uncertainty in the magnitude of greenhouse-gas-induced global mean warming (Stocker et al. 2001). Changes in cloudiness might also have important effects on regional climates, but it is important to remember that the impact of clouds on temperature is twofold. By reflecting sunlight clouds act to cool the surface especially in summer and during the daylight hours, but by absorbing terrestrial long-wave radiation they also act to warm the surface. The net cloud feedback on temperature changes therefore depends, in addition to the change in the total cloud cover, on the diurnal cycle of the change and the time of the year, on the height in the atmosphere where cloudiness increases or decreases, and on other possible changes in cloud properties.

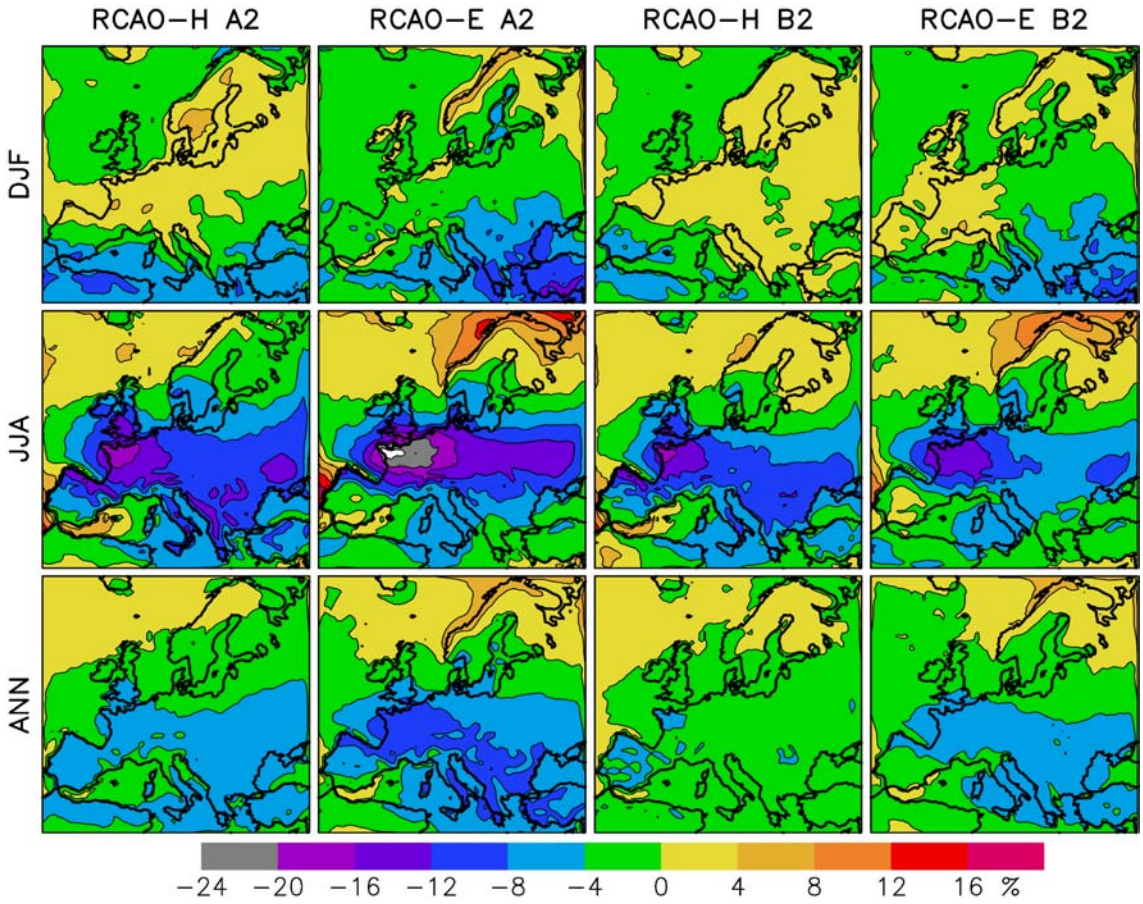

Figure 21. *Changes in December-Febaruary, June-August and annual mean cloud cover (in per cent of full sky) in the RCAO climate change simulations. The colour scale is given below the figure.*

Figure 21 shows the RCAO-simulated changes in average cloud cover in winter, summer and the annual mean (the changes in spring and autumn are generally between those in winter and summer). The changes in the A2 and B2 scenario runs tend to be of the same sign, but the magnitude of the changes is larger in A2 than in B2. In winter, cloudiness increases slightly in most of northern Europe in both RCAO-H A2 and B2. In RCAO-E, the increase is less widespread, being largest at the west coast of Norway, where the increased westerly flow indicated by the change in the time mean sea level pressure (Fig. 19) leads to increased orographic uplift of air. The decrease in cloudiness

on the eastern side of the Scandinavian mountains especially in RCAO-E A2 also most likely results from the stronger westerly flow. Further south, in the Mediterranean area, the RCAO-H and RCAO-E experiments both indicate a general decrease in cloudiness, although with substantial differences in the patterns of change.

The changes in summer are dominated by a large reduction in cloud cover over central Europe, especially its western parts. The largest changes occur in RCAO-E A2, in which summer mean cloud cover locally decreases by 24% (of full sky) in France. Part of this decrease may be explained by changes in atmospheric circulation: the increase in time mean easterly flow indicated by the pattern of pressure change in all four scenario runs suggests suppressed moisture supply from the Atlantic Ocean to western and central Europe. However, local thermodynamic feedbacks between reduced precipitation, soil moisture and evaporation (Sections 4.4 and 4.7) might play an even more important role. Smaller reductions in cloudiness extend southward to the Mediterranean area and northward to southern Scandinavia. Even further north and at the west coast of Norway summer cloudiness increases, especially in the two RCAO-E simulations. The smaller decrease in cloudiness in the Mediterranean area than in central Europe may result at least partly from the fact that the summer mean cloudiness in the Mediterranean region is very low even in the control simulations.

The annual mean total cloudiness decreases in most of the model domain in all four scenario simulations, excluding some parts of northern Europe.

4.3 Surface air temperature

4.3.1 Time mean temperature

Maps of seasonal and annual mean surface air temperature change in the RCAO experiments are shown in Fig. 22. These reveal several features of interest:

- For both the A2 and the B2 scenarios, the warming is in most areas and seasons larger in RCAO-E than in RCAO-H.
- The maximum annual mean warming occurs in central and southern rather than northern Europe, at least excluding RCAO-H B2.
- In northern Europe, the warming is largest in autumn and winter, as is commonly the case even in global climate models (Räisänen 2000). However, the warming in winter is distinctly larger in RCAO-E than in RCAO-H. This results, at least in part, from the increase in westerly winds in RCAO-E and the absence of such an increase in RCAO-H.
- The warming over the Atlantic Ocean, which is dictated by the SST change in the driving global model, is much larger in RCAO-E than in RCAO-H. This may be related to different changes in the Atlantic thermohaline circulation. In ECHAM4/OPYC3, there is no change in the strength of this circulation with increasing greenhouse gas forcing (Latif et. al 2000), whereas HadCM3 simulates a roughly 20% decrease in circulation strength in both the A2 and B2 scenario runs by 2100 (http://www.meteoffice.gov.uk/research/hadleycentre/pubs/brochures/B2000/predictions.html). These differences in the SST change probably also explain some part of the difference in warming over Europe.

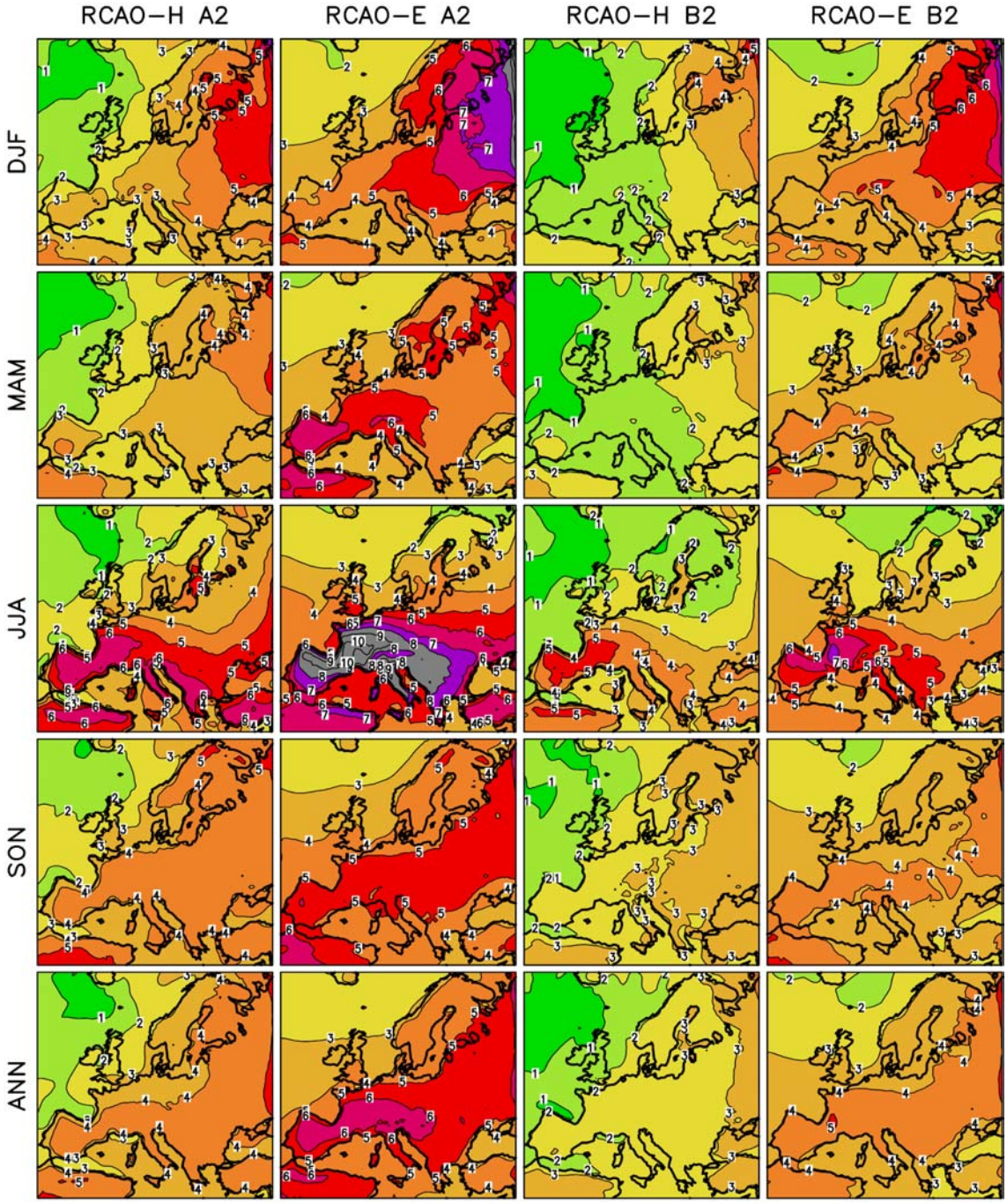

Figure 22. *Changes in seasonal and annual mean surface air temperature (differences from the corresponding control run 30-year means) in the RCAO climate change simulations. Contours and shading at every 1°C.*

- In southern and central Europe, the warming peaks in summer. In RCAO-E, in particular, the warming in southwestern Europe is extremely large, with a maximum of over 10°C in France in the A2 scenario and 7°C even in the B2 scenario. This very large warming is accompanied by substantially reduced cloudiness (Section 4.2), precipitation (Section 4.4), and soil moisture (Section 4.7). These changes most probably reinforce each other via the feedback loop described by Wetherald and Manabe (1995). However, as noted for cloudiness in Section 4.2, changes in atmospheric circulation may also play a role.

- It is not quite clear why the summertime warming in central and southwestern Europe is so much larger in RCAO-E than in RCAO-H, especially as the changes in the pressure pattern (Fig. 19) in this season are similar. One factor that likely plays a role are different changes in the atmospheric circulation in spring. The RCAO-E simulations show a centre of increasing MAM mean sea level pressure over central Europe, whereas the pattern in the RCAO-H simulations is relatively diffuse. This leads to a substantial decrease in spring cloudiness (not shown) and precipitation (Section 4.4.1) over central and southwestern Europe in RCAO-E, in contrast with relatively small changes in RCAO-H. Consequently, the soil dries out earlier and more severely in RCAO-E than in RCAO-H (Section 4.7).
- The temperature changes over the Baltic Sea are largely determined by the SST and sea ice changes simulated by the RCO model, and they occasionally differ from the temperature changes in the surrounding land areas. In particular, the air (and surface water) over the southern and central parts of the Baltic Sea warms more in summer than the air over nearby land areas, especially in the RCAO-H simulations. On the other hand, a local minimum of warming occurs over the northern Bothnian Bay in RCAO-E. The dynamics of these sea-land differences still need to be investigated. Possible causes might include changes in the Baltic Sea ocean circulation and temperature stratification.
- The A2 and B2 scenario simulations give qualitatively very similar results, although the magnitude of the warming is smaller in B2 than in A2. It is also of interest to note that the annual mean warming is in most of the domain very similar between RCAO-H A2 and RCAO-E B2.

4.3.2 Interannual variability of monthly mean temperatures

The time-averaged warming is accompanied in the RCAO simulations by a decrease in interannual temperature variability in northern Europe in winter (see Figs. 23e-f for results for Sweden), with a larger change in RCAO-E than in RCAO-H. In summer, variability changes little in northern Europe but tends to increase further south (Figs. 23g-h). The seasonal and geographical details of the change vary a lot between the A2 and B2 scenarios, probably because these changes have a relatively low signal-to-noise ratio. For example, the RCAO-H B2 simulation shows an area of increased annually averaged variability in eastern Europe that is absent in RCAO-H A2 (Figs. 23a,c).

A tendency towards reduced mid- and high-latitude temperature variability in winter in a warmer climate also occurs in global climate models, most likely due to a reduction of snow and ice (Räisänen 2002). A slight increase in midlatitude temperature variability in summer is likewise a common model result, which probably reflects reduced soil moisture. When the soil becomes sufficiently dry, the capability of evaporation to cool the surface decreases. This acts to increase both the average summer temperatures and their interannual variability, because the lack of evaporative cooling has its largest effect in those summers when the atmospheric circulation favours warm conditions and, with sufficient soil moisture, large evaporation (Delworth and Manabe 1988, 1989; Tett et al. 1997).

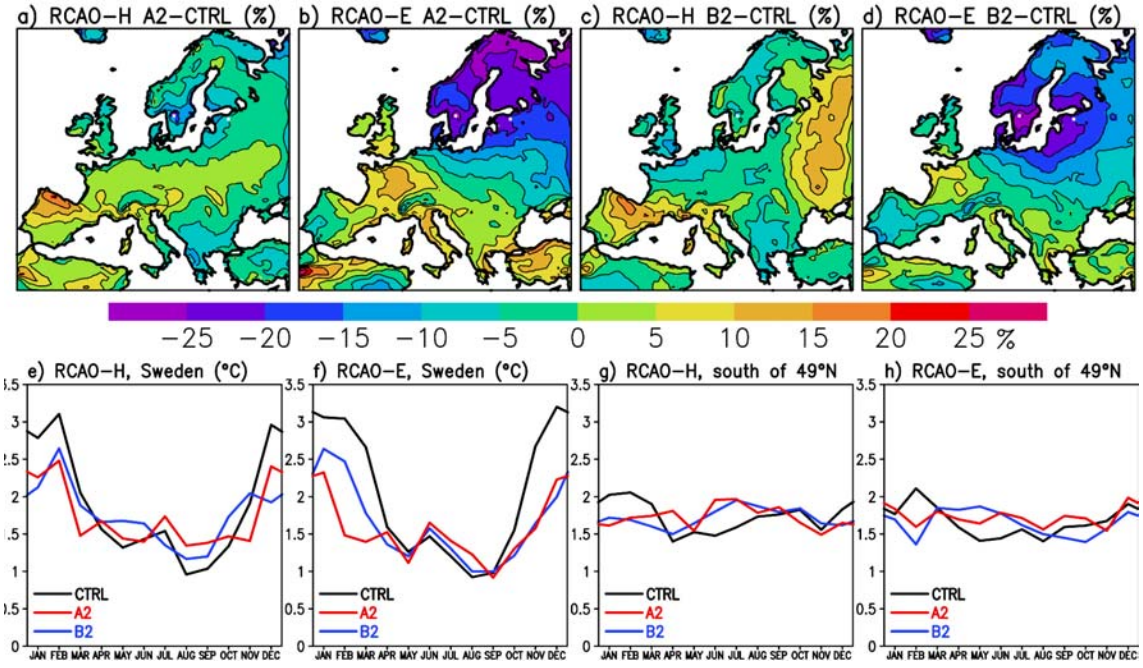

Figure 23. *Top: Changes in the 12-month mean interannual standard deviation of monthly mean temperature (per cent differences from the corresponding control run 12-month means). Bottom: the seasonal cycles of the area mean of the standard deviation (in °C) in Sweden and in the land area south of 49°N. Both the control run and the scenario run temperature series were detrended before the calculation of the standard deviations to remove any biases associated with the gradual change in forcing. In this and the following figure only land areas are shown, because temperature varies much less over sea than over land.*

4.3.3 Diurnal temperature range

The changes in the average diurnal temperature range (Fig. 24) show some resemblance with the changes in interannual variability. The annual mean diurnal range decreases in northern Europe, locally by over 25% in the RCAO-E A2 simulation. Further south the variability increases, with the largest relative increase in those parts of southwestern Europe (in particular France) where the decrease in cloudiness is largest. However, the magnitude of the change varies substantially between the four scenario simulations.

In the southern half of the model area as a whole (Fig. 24g-h), the diurnal temperature range increases slightly in most of the year. In Sweden (Fig. 24e-f) and in northern Europe in general, the decrease in variability is largest from late autumn to spring. The decrease in snow cover (Section 4.6), which prevents temperature from falling to very low levels in clear nights, is a main suspect for this. It should be noted, though, that regular night-to-day temperature variability in northern Europe in midwinter is weak. The diurnal temperature range and changes in this between different model runs are therefore also affected by irregular day-to-day temperature variations (see Räisänen et al. 1999).

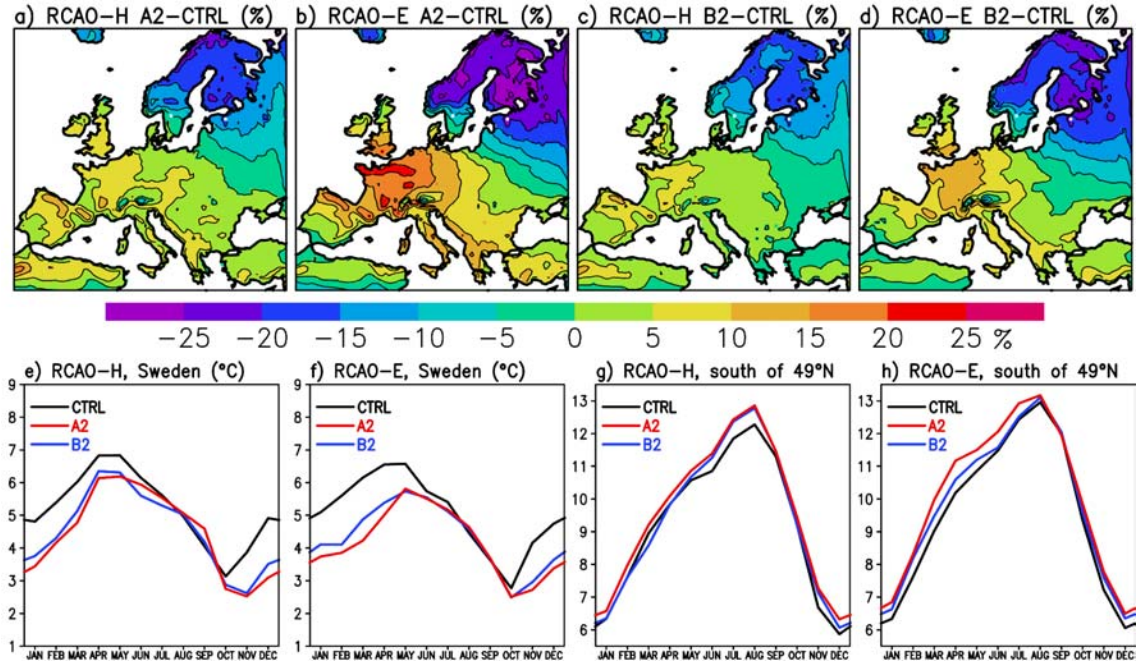

Figure 24. *Top: changes in the 30-year annual mean diurnal temperature range (in per cent of the corresponding control run 30-year means). Bottom: the seasonal cycles of the average diurnal temperature range (in °C) in Sweden and in the land area south of 49°N.*

4.3.4 Temperature extremes

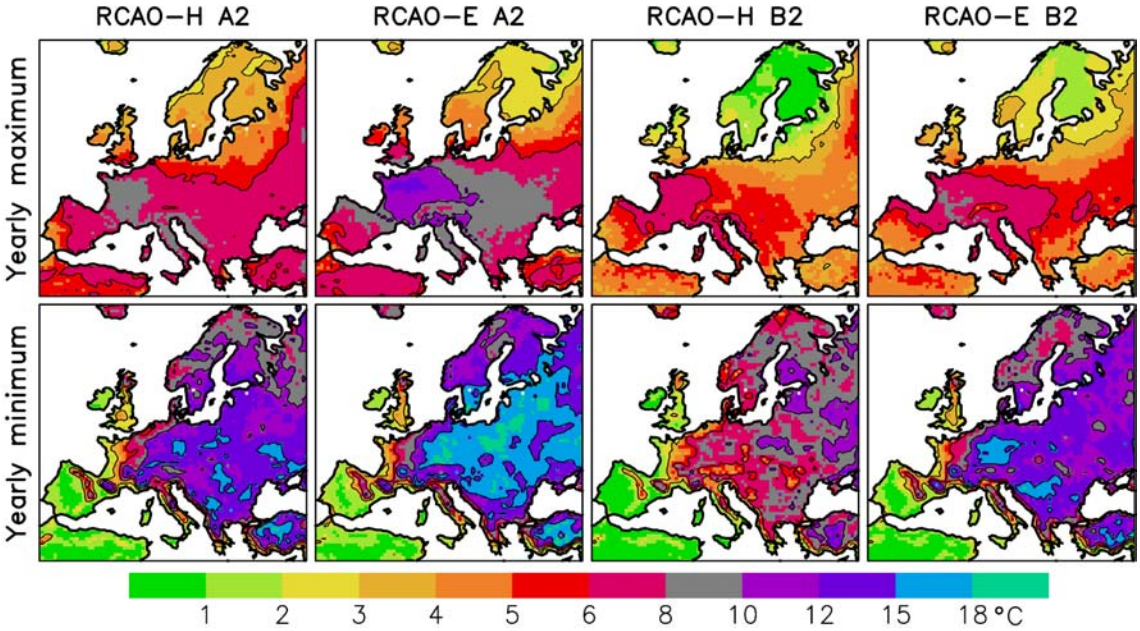

Figure 25. *Changes in average yearly temperature extremes from the control runs to the A2 and B2 scenario runs. The colour scale is given below the figure. Contours are drawn at 3, 6, 10 and 15°C only*

The control run average yearly temperature extremes were shown in Fig. 8. Figure 25 shows the changes in these in the A2 and B2 scenario runs. In northern Europe, the increase in yearly maximum temperatures is broadly the same as that in the June-July-August mean temperature (Fig. 22). Further south, the warm extremes generally increase

more than the mean temperature, even though the summer time mean warming is also very large. In France in RCAO-E A2, the highest yearly maximum temperatures increase by up to 12°C. This is consitent with the increased interannual and diurnal temperature variability discussed in the previous subsections.

The lowest winter minimum temperatures increase in most of Europe much more than the December-February mean temperature (the lower half of Fig. 25 and the first row of Fig. 22). The largest changes occur in southern Scandinavia and central-eastern Europe, where the increase exceeds 15°C in RCAO-E A2. This corresponds to the areas where a more or less significant snow cover occurs in the control runs but which become almost snow-free in the scenario runs (Section 4.6). In southwestern Europe, which is snow-free even in the control runs, the change in the lowest winter temperatures is more modest. Even in northern Scandinavia, where a good deal of snow remains even in the scenario runs, the changes in the lowest minimum temperatures tend to be somewhat smaller than those in eastern and central Europe.

For the sake of curiosity, Table 3 lists some statistics of absolute geographical temperature extremes (i.e., highest and lowest temperatures occurring somewhere within a given geographical area). Although the temperature never reaches 40°C in Sweden in any of the scenario runs, the absolutely highest temperatures near the southern edge of the map domain (in northern Africa) are well above the current world record of 56.7°C. As far north as in the southern Netherlands, temperature once exceeds 50°C in RCAO-E A2. Looking at the other end of the distribution, severe cold occasionally occurs in the northernmost parts of the model domain even in the scenario runs, but the difference from the control run values is nevertheless quite large.

Table 3. *Absolute temperature extremes (°C) in the RCAO simulations. The values for Sweden give the absolutely highest or lowest temperatures occurring in any grid box in Sweden in an average year (rows 1 and 4) or once in the 30-year simulations (rows 2 and 5). Rows 3 and 6 show the absolute 30-year extremes for the whole map domain.*

	RCAO-H			RCAO-E		
	CTRL	A2	B2	CTRL	A2	B2
yearly maximum, Sweden	28.9	33.1	30.9	26.4	32.1	29.5
30-year maximum, Sweden	33.8	38.9	35.0	30.7	38.4	35.9
30-year maximum, all points	57.0	61.5	59.0	54.5	61.4	60.8
yearly minimum, Sweden	-47.4	-37.9	-39.5	-47.2	-37.9	-39.6
30-year minimum, Sweden	-56.0	-45.9	-49.4	-55.6	-44.2	-49.6
30-year minimum, all points	-65.0	-49.5	-56.7	-60.8	-46.7	-50.7

4.4 Precipitation

4.4.1 Time mean precipitation

The changes in the 30-year seasonal and annual mean precipitation, expressed in per cent of the control run values, are shown in Fig. 26. There are large geographical and

seasonal variations in the change, and also some substantial differences between the HadAM3H- and ECHAM4-driven simulations. The main features include the following:

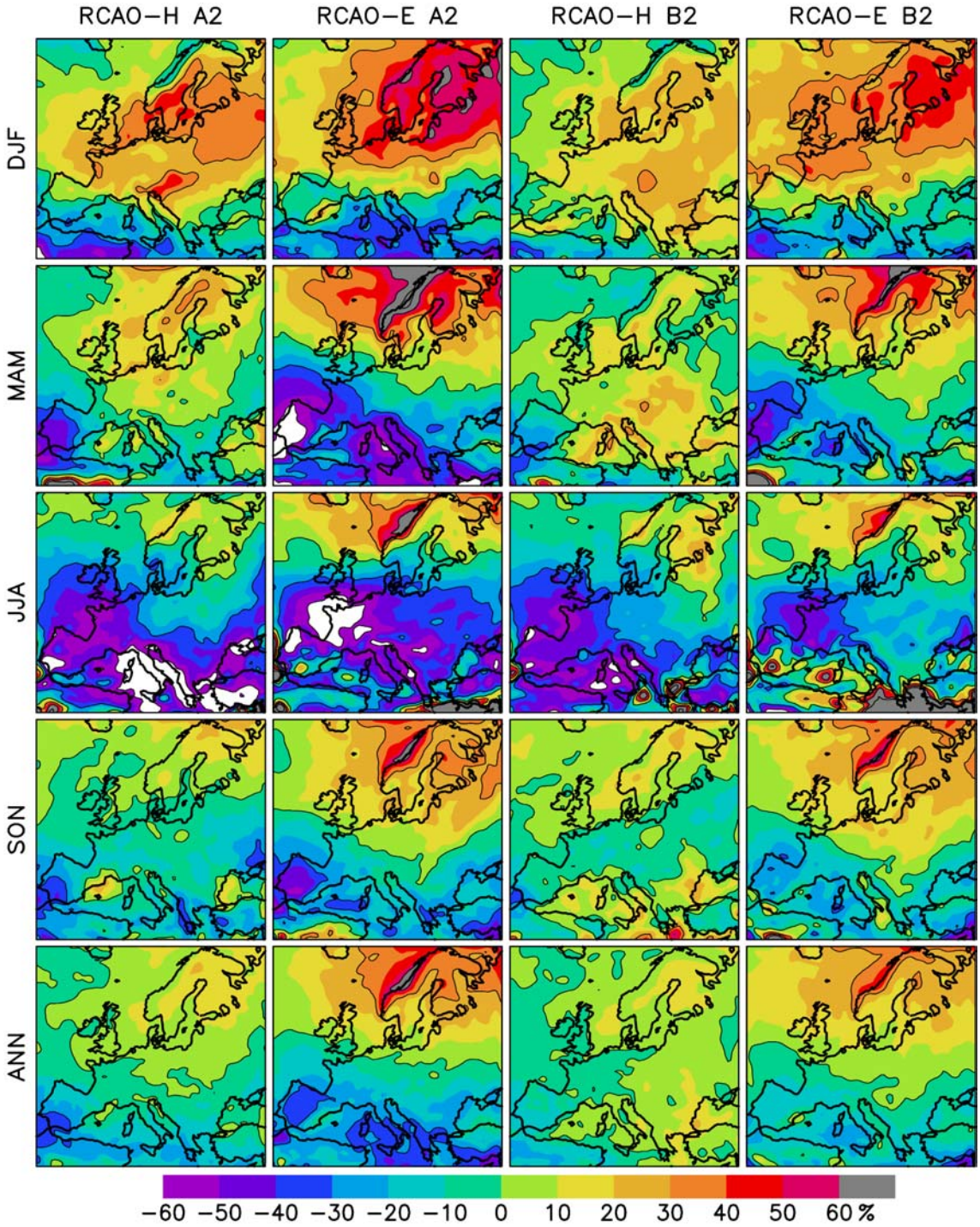

Figure 26. *Changes in seasonal and annual mean precipitation (per cent differences from the corresponding control run 30-year means) in the RCAO climate change simulations. The colour scale is given below the figure. Contours are drawn at every 30% only. A slight smoothing is applied for legibility.*

- All four scenario simulations agree on a general increase in precipitation in northern and central Europe in winter. They also agree on a general and in some areas very large (up to 70% in the A2 scenario runs) decrease in summer

precipitation in southern and central Europe. A smaller decrease in summer precipitation extends up to central Scandinavia in the north. Thus, the changes in northern and central Europe have a very pronounced seasonal cycle.

- The mean annual precipitation increases in northern Europe and decreases further south, except for RCAO-H B2 in which an increase occurs even in much of southeastern Europe. However, this north-south contrast is stronger in the RCAO-E than in the RCAO-H simulations. This reflects most probably the northward shift in cyclone activity in RCAO-E that is absent in RCAO-H (Section 4.1).
- At the west coast of Norway, where precipitation is strongly governed by wind direction, the differences between RCAO-H and RCAO-E are huge. The increase in westerly winds leads to a large increase in annual precipitation in RCAO-E (up to 70% in the A2 and over 40% even in the B2 scenario run), whereas the increase in RCAO-H A2 and B2 is only 0-10%. In winter, when the time mean westerly wind decreases in the RCAO-H scenario simulations, precipitation in northwestern Norway decreases in them. As the control run (and observed) precipitation in western Norway is very large, these differences are even more dramatic in absolute terms.
- The changes in the B2 simulations are in most cases qualitatively similar to but smaller than those in the A2 simulations. However, some exceptions occur. One of the most notable is the contrast between decreasing annual precipitation in southeastern Europe in RCAO-H A2 and increasing precipitation in B2. Similarly, the increase in annual precipitation extends slightly further south in RCAO-E B2 than RCAO-E A2. However, the unforced variability of precipitation is large and is likely to explain a substantial part of these apparent discrepancies (Section 5.1)

4.4.2 Interannual variability of monthly precipitation

The top row of Fig. 27 shows the per cent changes in the 12-month mean of the interannual standard deviation of monthly precipitation. The patterns are noisy and highly variable between the different scenario runs, but the general picture is one of increasing standard deviation in northern Europe and decreasing standard deviation in southern Europe. Thus, as the first approximation, the changes in the absolute amplitude of interannual precipitation variability tend to follow those in the mean precipitation (cf. Fig. 26). This behaviour has been documented well in earlier studies (e.g., Räisänen 2002) and is qualitatively expected since precipitation is bounded from below by zero.

A more interesting question is if there is any systematic difference between the per cent changes in the standard deviation and the mean (i.e., does the coefficient of variation of precipitation change). This is addressed in the lower half of Fig. 27 by comparing the seasonal cycles of the changes in the mean and the standard deviation in Sweden and in the land area south of 49°N. In Sweden, the two changes tend to follow each other, but in winter all four scenario runs show a smaller increase in the standard deviation than in the mean (excluding RCAO-E B2 in February). This difference is particularly pronounced in RCAO-E A2. South of 49°N, the situation is reversed, with the mean precipitation decreasing in most months more than the standard deviation (most regularly so in RCAO-E A2). This implies that, in the southern parts of the model area, the low extremes of monthly precipitation decrease by an even larger per cent fraction than the mean precipitation, while the high extremes decrease less.

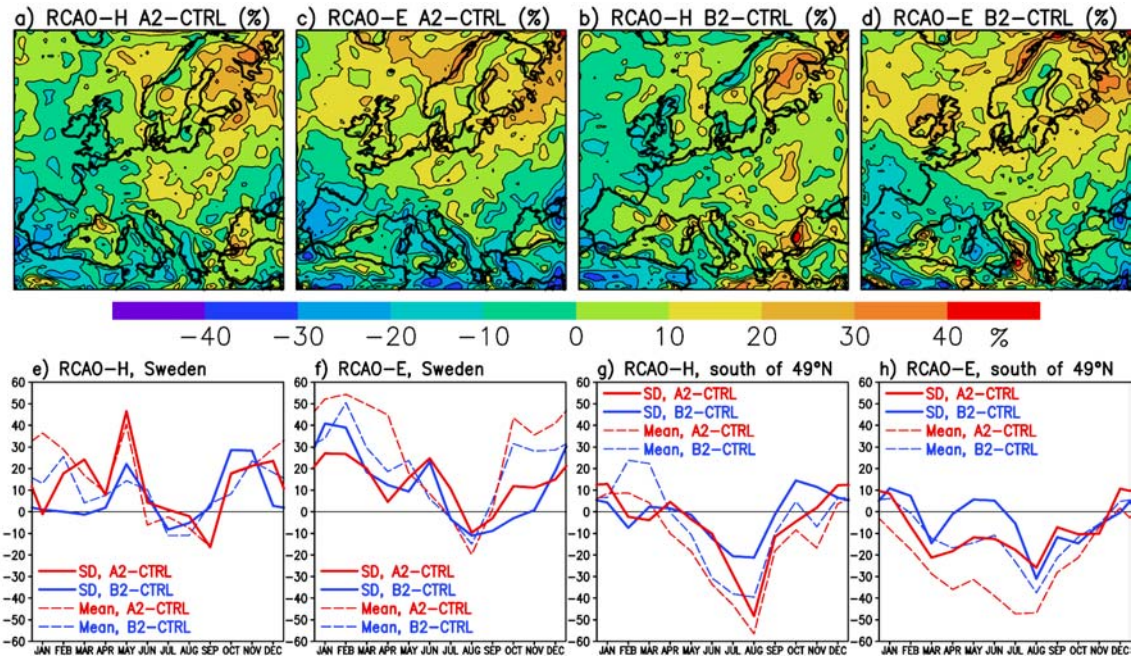

Figure 27. *Top: Changes (per cent differences from the control run values) in the 12-month mean interannual standard deviation of monthly precipitation. Bottom: per cent changes in the area means of the standard deviation (solid lines) and the time mean precipitation (dashed lines) in Sweden and the land area south of 49ºN.*

All other factors being the same, the coefficient of variation of monthly precipitation increases with decreasing number of precipitation days (Räisänen 2002). Thus, one would expect from these results a decrease in the number of precipitation days in the sourthern part of the model area and an increase in the north, with the largest changes in RCAO-E A2. This is actually the case.

4.4.3 Number of precipitation days

The simulated changes in the annual number of days with at least light (≥ 0.1 mm), at least moderate (≥ 1.0 mm) and heavy precipitation (≥ 10 mm) are shown in Fig. 28. Using the lowest threshold, the number of precipitation days increases in northern Europe excluding southern Scandinavia, and decreases in southern and central Europe. These changes are larger for the A2 than the B2 scenario, and in RCAO-E than RCAO-H. Thus, in northern Europe, completely dry days that are infrequent even in the control runs become on an annual basis even less common in the scenario runs. Further south, the number of dry days increases. The results for the 1.0 mm threshold are similar. Using either of these two thresholds, the decrease in the number of precipitation days extends further north than the decrease in annual precipitation (Fig. 26).

The number of days with heavy (≥ 10 mm) precipitation also increases in northern Europe and decreases in most of southern Europe excluding RCAO-H B2, but the area of increase extends further south than in the case of the first two thresholds. The largest absolute increases and decreases occur, as expected, in those mountain areas where heavy precipitation is most frequent in the control simulations.

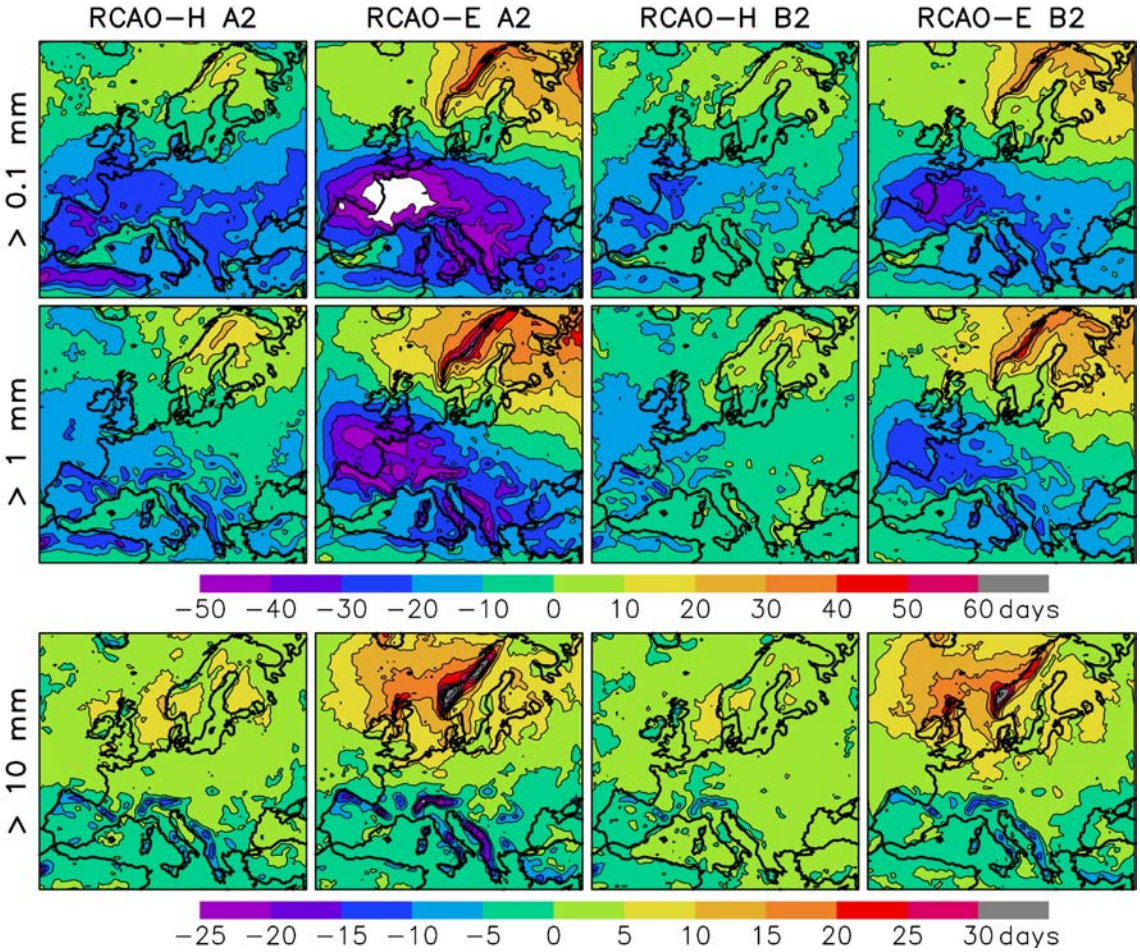

Figure 28. *Changes (A2 or B2 scenario run minus control run) in the average annual number of days with at least 0.1 mm (top), 1 mm (middle) and 10 mm (bottom) of precipitation. The colour scale differs between the first two rows and the last row.*

Table 4. *Area mean changes in the number of days with precipitation exceeding varying thresholds (from 0.1 to 20 mm). Values are given in absolute units (days per year) and in per cent (in parentheses). Results are shown for Sweden and for the land area south of 49ºN.*

	P (mm)	RCA-H, A2	RCA-E, A2	RCA-H, B2	RCA-E, B2
Sweden	≥ 0.1	2.1 (1%)	10.8 (4%)	2.4 (1%)	8.6 (3%)
	≥ 1.0	7.6 (4%)	19.0 (11%)	3.9 (2%)	14.5 (8%)
	≥ 5.0	8.2 (15%)	16.6 (27%)	5.5 (10%)	12.0 (19%)
	≥ 10	4.5 (28%)	9.6 (49%)	3.3 (20%)	7.0 (36%)
	≥ 20	0.8 (42%)	1.9 (79%)	0.6 (29%)	1.3 (57%)
< 49°N	≥ 0.1	-21.7 (-14%)	-30.1 (-20%)	-11.6 (-14%)	-16.5 (-11%)
	≥ 1.0	-13.7 (-15%)	-22.0 (-24%)	-6.4 (-15%)	-11.8 (-13%)
	≥ 5.0	-5.2 (-13%)	-9.5 (-26%)	-1.6 (-13%)	-4.4 (-12%)
	≥ 10	-1.7 (-10%)	-3.6 (-21%)	0.1 (-10%)	-1.2 (-7%)
	≥ 20	0.1 (2%)	-0.3 (-6%)	0.5 (12%)	0.3 (7%)

Table 4 gives the area mean changes in the number of precipitation days for various lower thresholds for Sweden and the land area south of 49°N. Here, both absolute (days per year) and relative (per cent of the control run mean) changes are given. The higher

the threshold used, the larger is the relative increase in the number of days with precipitation above that threshold in Sweden and elsewhere in northern Europe. In this sense there is an "unproportional" increase in the *number* of very wet days in northern Europe, even though this does not imply that the *magnitude* of the extremes would increase more than the mean precipitation (Section 4.4.4). In the land area south of 49°N the total number of precipitation days decreases substantially, but the decrease is much smaller or reversed to an increase for the highest threshold (20 mm) used.

4.4.4 Extreme daily precipitation

Figure 29 shows the simulated changes in the 30-year mean yearly maximum one-day precipitation. The patterns of change are very noisy, but all four scenario runs indicate an overall increase in the yearly extremes even in those parts of southern and central Europe where the mean annual precipitation decreases. Very similar results were reported by Räisänen and Joelsson (2001) for the previous Rossby Centre regional climate change simulations made with the RCA1 model. In that paper it was also shown that, although the changes in individual grid boxes were very heavily affected by internal variability, the statistical significance of the changes increased dramatically when they were averaged over a sufficiently large area. Table 5 compares the changes in the area means of mean annual precipitation and the yearly maximum one-day precipitation in two areas, Sweden and all land south of 49°N. Also included in this comparison are the area means of the absolutely largest one-day precipitation occurring within the whole 30-year simulations.

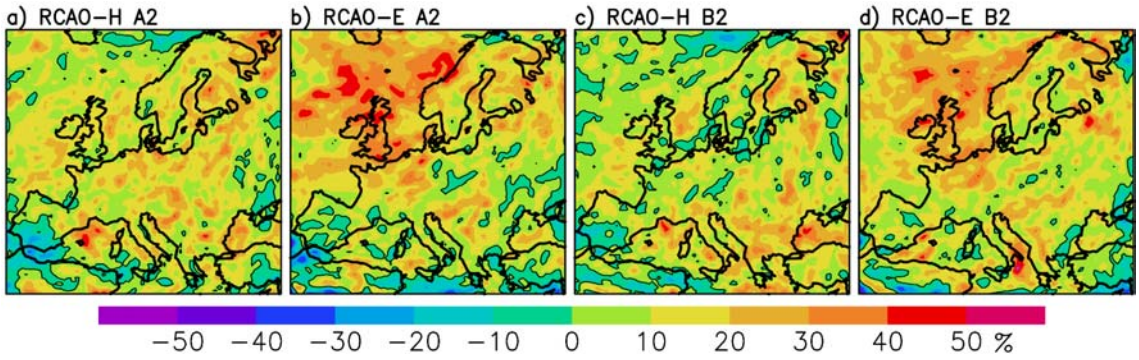

Figure 29. *Per cent changes in the 30-year means of yearly maximum one-day precipitation from the control runs to the A2 and B2 scenario runs. The colour scale is given below the figure. Contours are omitted except for 0%.*

In an area mean sense, the average yearly and 30-year precipitation extremes increase in both two areas and all four scenario runs. There is a tendency for the 30-year extremes to increase more (even in per cent terms) than the yearly extremes, but this is not the case for the two B2 simulations in Sweden. The increases in the extremes are by and large similar between the two areas, although the changes in the mean precipitation are not. All four scenario runs show a decrease of time and area mean precipitation in the area south of 49°N but an increase in Sweden (which is in RCAO-E A2 and B2 larger than the increase in extremes). These apparently contradictory results are consistent with the different changes in the number of precipitation days in these areas. In Sweden, both the intensity and (especially in RCAO-E) annual number of precipitation events increase, which leads to a relatively large increase in the time mean precipitation. In the

southern parts of the model domain, any increases in precipitation intensity are more than compensated by a decrease in the number of precipitation days.

Table 5. *Per cent changes in the area means of mean annual precipitation (rows 1 and 4), the average yearly maximum one-day precipitation (rows 2 and 5) and the absolute (30-year) maximum daily precipitation (rows 3 and 6). Results are shown for Sweden and for the land area south of 49°N.*

		RCA-H, A2	RCA-E, A2	RCA-H, B2	RCA-E, B2
Sweden	Mean	12	23	8	17
	Max (1 yr)	13	14	7	11
	Max (30 yr)	23	15	6	9
< 49°N	Mean	-11	-21	-2	-9
	Max (1 yr)	8	7	9	9
	Max (30 yr)	16	19	12	14

4.5 Wind speed

4.5.1 Time mean wind speed

As expected from the different changes in mean sea level pressure and transient activity (Section 4.1), the changes in the average 10 m wind speed differ substantially between the RCAO-H and RCAO-E experiments. In the annual mean (upper row of Fig. 30), the changes in the two RCAO-H scenario runs are very modest (within ±4% in virtually the whole of Europe). In RCAO-E, larger changes occur. Wind speeds increase in northern Europe, in the Nordic area typically by about 8% in RCAO-E A2, and decrease in the Mediterranean region. As shown in the lower half of Fig. 30, the increase in Sweden (and in northern Europe in general) is largest in winter and early spring, when the increase in the north-south pressure gradient in RCAO-E is largest (Fig. 19). The decrease in the southern half of the model domain is more seasonally uniform but occurs mainly in the summer half-year.

Figure 30g shows the seasonal cycles of the change over the Baltic Sea, where the simulated wind changes are substantially modified by stability effects associated with changes in SST and ice cover. In winter, the mean wind speed in RCAO-E increases even more over the Baltic Sea than over the surrounding land areas, with the largest increase over the central and northern parts that have a decent ice cover in the control runs but lose most of it in the scenario runs (Section 4.8). Most probably for the same reason a small increase occurs in winter even in RCAO-H, although there is no systematic change in the surrounding land areas. In summer the difference between RCAO-H and RCAO-E is reversed, with more positive changes in RCAO-H than in RCAO-E. The increase in summer windiness over the Baltic Sea in RCAO-H apparently reflects the large increase in Baltic Sea SSTs in this experiment, which is revealed by the pronounced land-sea contrast in warming in Fig. 22 and leads to reduced surface layer stability.

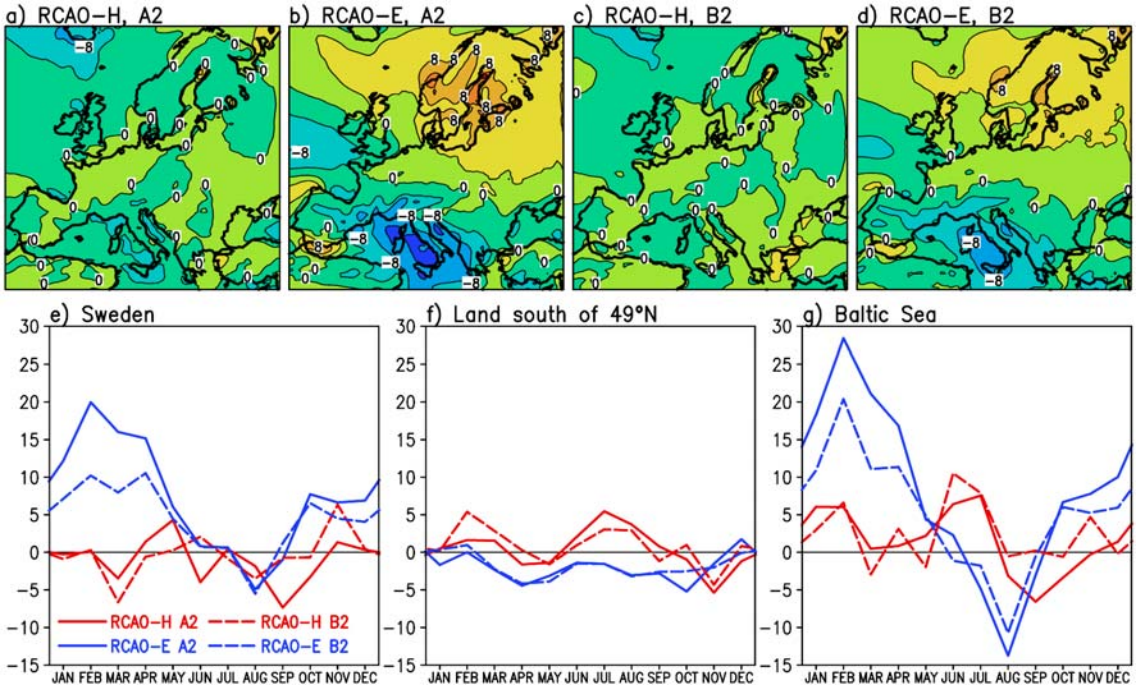

Figure 30. *Top: changes in the 30-year annual mean wind speed (per cent differences from the corresponding control run 30-year means). Bottom: the seasonal cycles of the change in Sweden, the land area south of 49°, and the Baltic Sea (see the panel for Sweden for the identification of the different simulations).*

4.5.2 Extremes of wind speed

The changes in the average yearly maximum wind speed (Fig. 31) tend to follow the changes in the time mean wind speed. The changes in the two RCAO-H scenario runs are generally small, whereas the RCAO-E simulations indicate a general increase in wind extremes in northern Europe. Similar conclusions hold for the absolute 30-year extremes of wind speed (not shown).

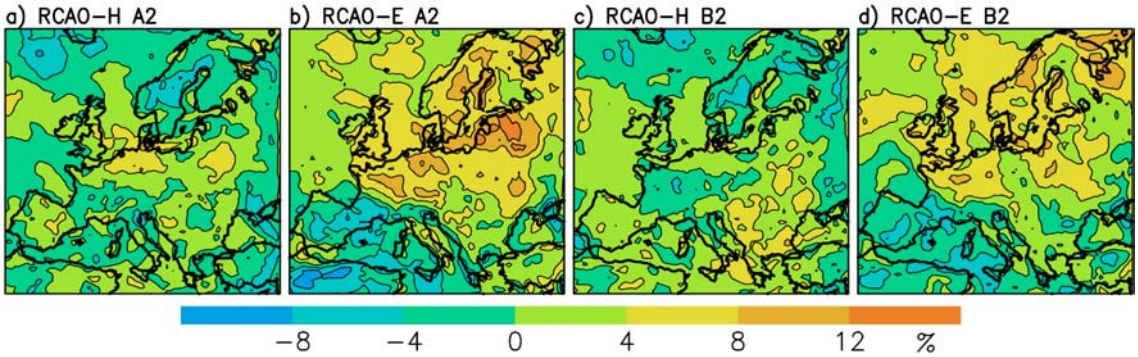

Figure 31. *Per cent changes in the average yearly maximum wind speed from the RCAO control runs to the A2 and B2 scenario runs. Contours and shading at every 4%.*

4.6 Snow conditions

The warming in the RCAO scenario runs leads to a substantial shortening of the snow season (upper row of Fig. 32). Following the magnitude of the warming, the decrease in the snow season length is larger in the A2 than in the B2 simulations, and larger in RCAO-E than in RCAO-H. However, the largest changes (from 45 to over 90 days

depending of the simulation) occur in all cases in the same areas: in a belt extending from central Scandinavia to the Baltic states, at the west coast of Norway and over the Alps. These areas have a comparably decent snow season in the control runs but are milder and therefore more sensitive to temperature increase than northern Scandinavia, where the decrease in snow season length is smaller. In areas like southernmost Scandinavia and central Europe where the snow season is short even in the control runs, the decrease in the snow season length is also smaller in absolute terms but large in relative terms. For example, those parts of southwestern Sweden that have 30-60 snow days in the control runs become almost snow-free (less than 10 snow-covered days) in both the two A2 scenario runs (not shown).

The lower row of Fig. 32 shows the changes in the average yearly maximum snow water equivalent. The magnitude of the changes depends on the simulation but the largest per cent decreases from the control run values occur in those areas that had relatively little snow even in the control simulations. In northern Finland and over the Scandinavian mountains, the change is relatively small but still negative. This might appear surprising: given the large simulated increases in winter precipitation and the fact that the winter mean temperature remains in these areas well below zero even in the scenario runs, one would expect the amount of snowfall to increase. This is actually the case in the midwinter (December-February) in most of these areas, excluding the southern parts of the Scandinavian mountains in RCAO-E A2 (not shown). However, the increase in midwinter snowfall is more than compensated by less snowfall in early and late winter, and by more frequent melting episodes.

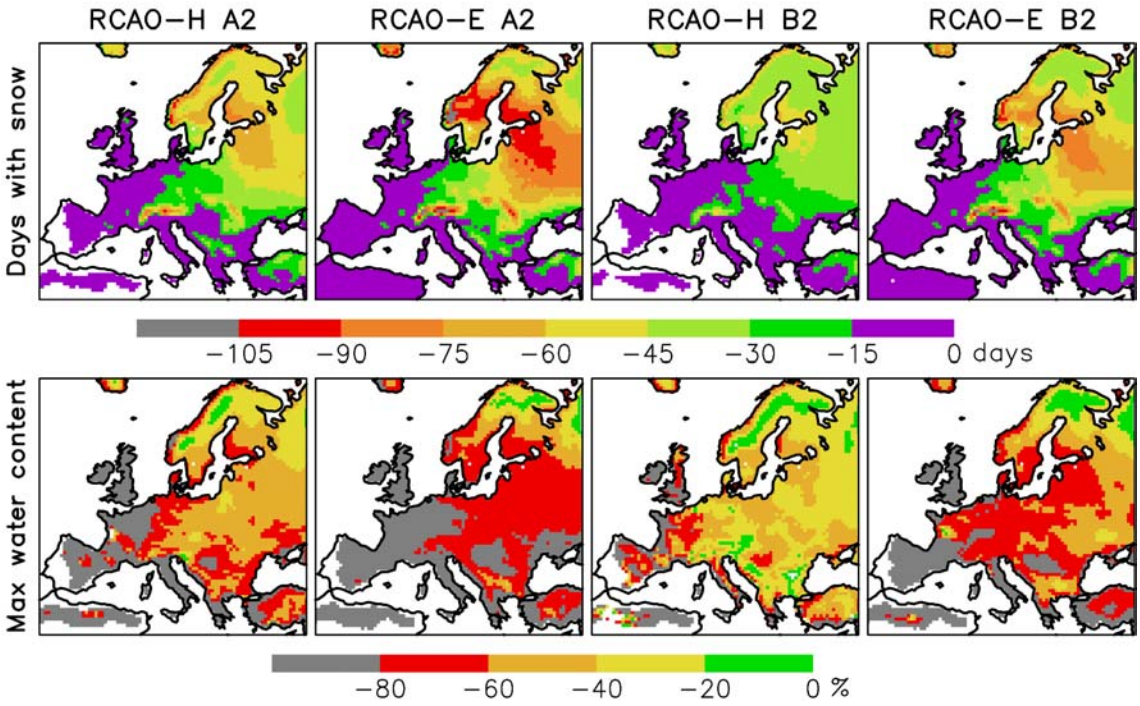

Figure 32. *Top: the change in the average duration of the snow season from the RCAO control runs to the A2 and B2 scenario runs (in days). Bottom: the change in the average annual maximum water content of the snow pack (in per cent of the control run mean).*

4.7 Other aspects of the surface hydrology

In this subsection we describe the changes in the three hydrological parameters whose control run behaviour was documented in Section 3.7: evaporation, runoff generation and soil moisture.

4.7.1 Evaporation

The simulated annual mean evaporation increases in northern Europe and most of central Europe in all four scenario runs (upper row of Fig. 33). The changes are largest in the A2 scenario runs, in which the annual increase in the Nordic area is about 20%. Even larger changes occur locally over the Scandinavian mountains. As illustrated in Fig. 33e-f for Sweden, evaporation increases in northern Europe in all seasons. However, the increase is in relative terms largest in winter and spring, especially in RCAO-E. This differs from the earlier RCA1 experiments in which evaporation decreased in winter (section 5.3). This difference is thought to be explained by the changes in the land surface scheme documented in Bringfelt et al. (2001), which act to reduce evaporation over snow-covered surfaces to more realistic levels. As there is more snow in the control than in the scenario runs, this tends to increase the scenario run minus control run differences in evaporation. In late summer, the simulated increases in Sweden mean evaporation are relatively small, probably because a decrease of soil moisture (Section 4.7.3) acts to suppress evaporation in the southern parts of the country.

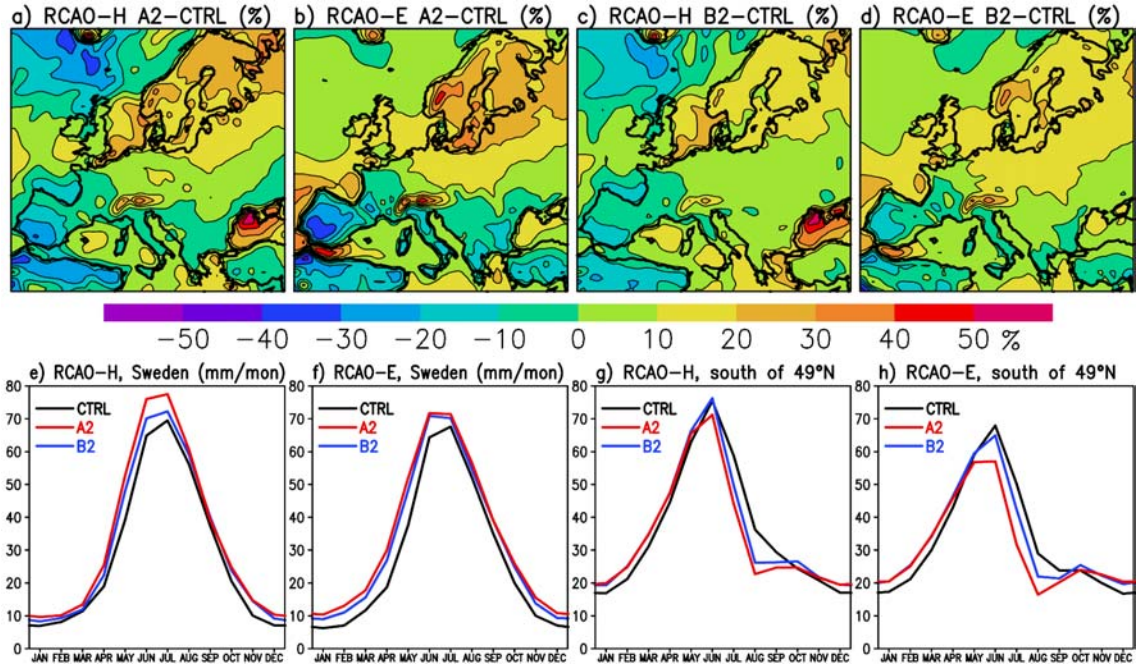

Figure 33. *Top: changes in the 30-year mean annual evaporation (per cent differences from the corresponding control run 30-year means) in the A2 and B2 scenario runs. Bottom: the average seasonal cycles of evaporation in Sweden and in the land area south of 49°N. The black, red and blue lines give the results for the control, A2 and B2 runs, respectively.*

In much of southern Europe, the simulated decreases in precipitation also lead to a decrease in annual evaporation. In all four scenario runs evaporation generally increases

in this area in winter and early spring, but decreases in summer and autumn (Fig. 33g-h) because of a marked decrease in soil moisture (Section 4.7.3). The decrease in evaporation leaves more radiation energy to drive the sensible heat flux, contributing in this way to the large increase in summer temperatures.

Over the northern North Atlantic, evaporation is reduced substantially in RCAO-H. In this experiment, wind speeds over the northern North Atlantic decrease (Section 4.5) and the increase in SSTs is small compared with the warming of the air that is advected from the surrounding continents. In RCAO-E, in which the average wind speeds increase and the increase in SSTs is larger, the changes in evaporation over the northern North Atlantic are small.

4.7.2 Runoff generation

The changes in the 30-year annual mean runoff generation (Fig. 34) are determined by the changes in precipitation and evaporation. In most of northern Europe, the annual runoff generation increases in all four scenario runs. In RCAO-E A2 and B2, in which the per cent increase in precipitation is larger than that in evaporation, the per cent increase in runoff generation exceeds the increase in precipitation. In RCAO-H, precipitation increases in absolute terms more but in relative terms less than evaporation. Consequently, runoff generation increases, but in per cent terms less than precipitation. Further south in central and southern Europe, and even in parts of southern Scandinavia, annual runoff generation decreases. An exception is southeastern Europe in RCAO-H B2, where, however, the control run runoff is low so that the large relative increase is relatively modest in absolute terms.

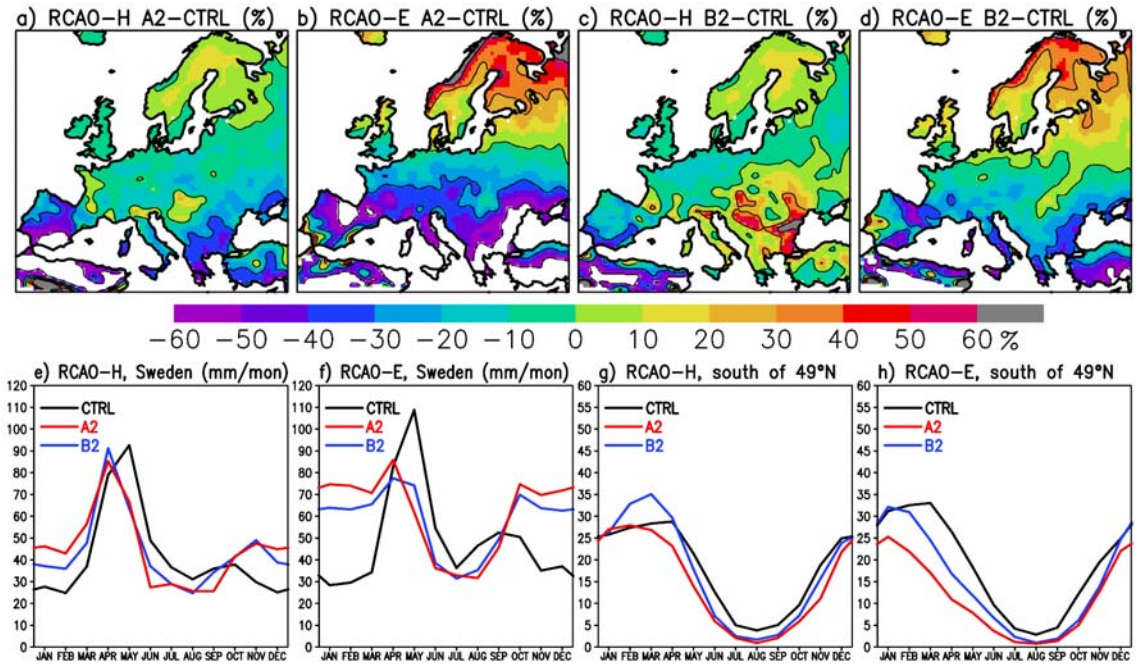

Figure 34. *Top: changes in the 30-year mean annual runoff generation (per cent differences from the corresponding control run 30-year means). Bottom: the average seasonal cycles of runoff generation in Sweden and in the land area south of 49°N. The black, red and blue lines give the results for the control, A2 and B2 runs, respectively.*

The seasonal cycle of runoff generation is affected by changes in snow conditions and soil moisture, as well as precipitation and evaporation (see the lower half of Fig. 34 for results for Sweden and for the land area south of 49°N). In Sweden, the earlier snowmelt gives an earlier spring peak in runoff generation in all four scenario runs. Increased precipitation and snowmelt during the late autumn and winter leads to a substantial increase in runoff generation in these seasons, most notably in the RCAO-E scenario runs. Conversely, the earlier snowmelt together with reduced summer precipitation and increased evaporation leads to a decrease in runoff generation in summer. In the area south of 49°N, the area mean runoff generation decreases almost throughout the year, at least excluding the midwinter and (in RCAO-H B2) early spring.

4.7.3 Soil moisture

On an annual mean basis, soil moisture decreases in most of Europe in all four scenario runs (upper row of Fig. 35), the main exception being northern Scandinavia and Russia in RCAO-E A2 and B2. The decrease is in absolute terms largest in central and southwestern Europe, and it is generally largest in the RCAO-E A2 simulation. Further south, the decrease in soil moisture is limited by the fact that the soil is very dry even in the control simulations.

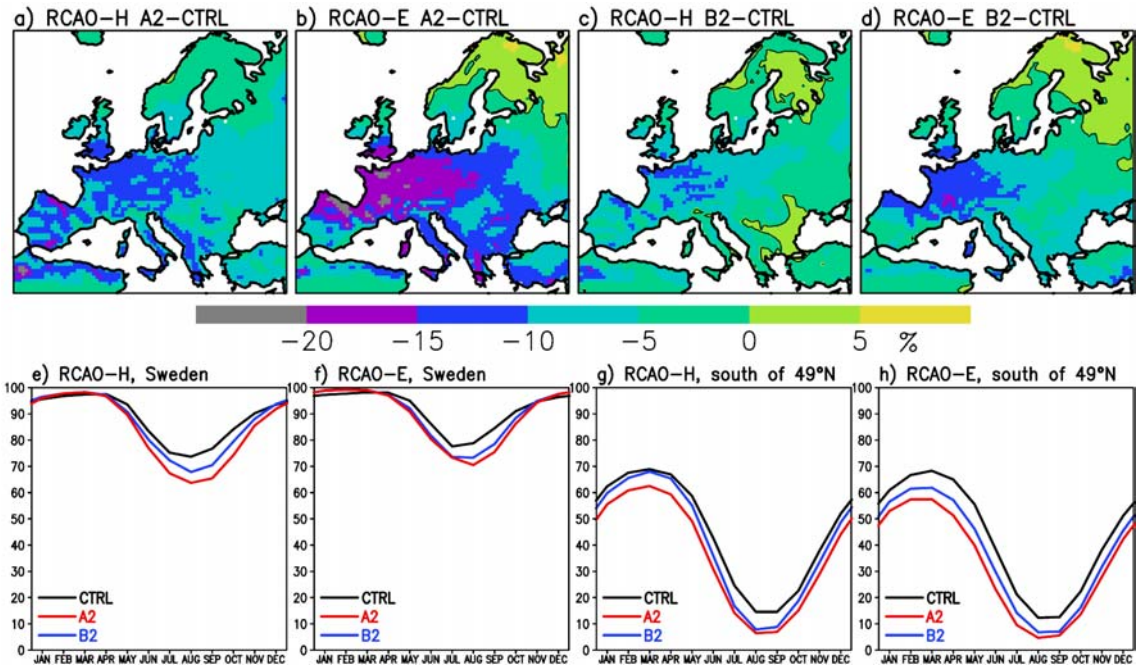

Figure 35. *Top: changes in the 30-year annual mean soil moisture (in per cent of a maximum of 242 mm). Bottom: the average seasonal cycles of soil moisture (per cent of 242 mm) in Sweden and in the land area south of 49°N. The black, red and blue lines give the results for the control, A2 and B2 runs, respectively.*

The average seasonal cycles of soil moisture in Sweden and the land area south of 49°N are shown in the lower part of Fig. 35. In Sweden, little change occurs in winter, when the soil is very wet in all the simulations. However, the seasonal decrease in soil moisture toward late summer is larger in the scenario runs than in the control runs, due to the earlier snowmelt, increased evaporation and reduced summer precipitation. South of 49°N, the area mean soil moisture is reduced throughout the year, but the most

remarkable feature is the extreme dryness of the soil in late summer. In RCA-E A2, the August mean for this large area is only 5% of the maximum.

4.8 Ice conditions

4.8.1 Lake ice

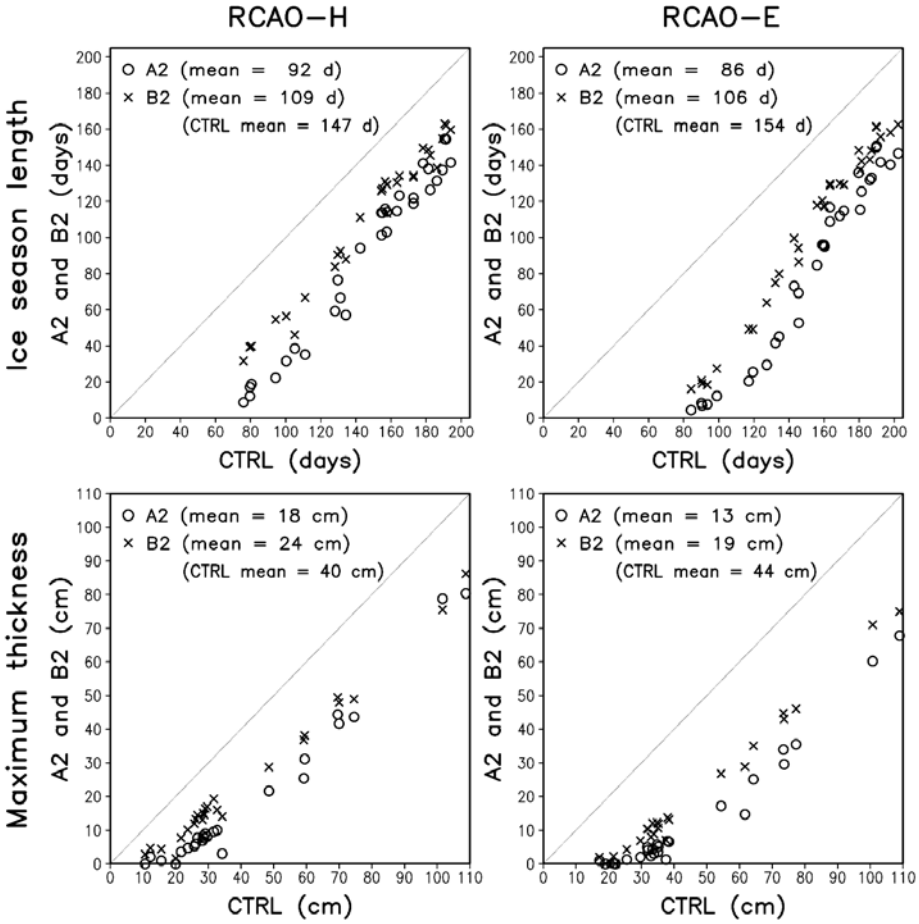

Figure 36. *Comparison of ice conditions in Swedish lakes in the control, A2 and B2 simulations, using the same sets of lakes as in Fig. 17. Top: scatter plots of the average duration of the ice season in 37 lakes in RCAO-H (left) and RCAO-E (right). The horizontal axis gives the ice season length in the control run and the vertical axis that in the A2 (open circles) and B2 (crosses) scenario runs. Bottom: the same for average yearly maximum ice thickness in 26 lakes.*

The changes in the simulated ice conditions in Swedish lakes are illustrated in Fig. 36 (see the figure caption for details). For the set of 37 lakes studied, the decrease in the average ice season length varies from 38 days in RCAO-H B2 to 68 days in RCAO-E A2. The decrease tends to be largest for the lakes in southern Sweden, where the winters are relatively mild even in the control simulations. In RCAO-E A2, in particular, many lakes in southern Sweden become virtually ice-free. Further north, where the control run winters are colder, the ice season length is reduced less even though the increase in winter temperatures is at least as large (Fig. 22). Similar conclusions apply to the changes in the average winter maximum ice thickness (lower part of Fig. 36). In many lakes in southern Sweden, no or only very thin ice develops in an average winter in RCAO-E A2, and this is the case to some extent even in the other simulations. Further

north ice thickness is also reduced substantially, but in the northernmost Sweden relatively thick lake ice still develops in all four scenario runs.

4.8.2 Baltic Sea ice cover

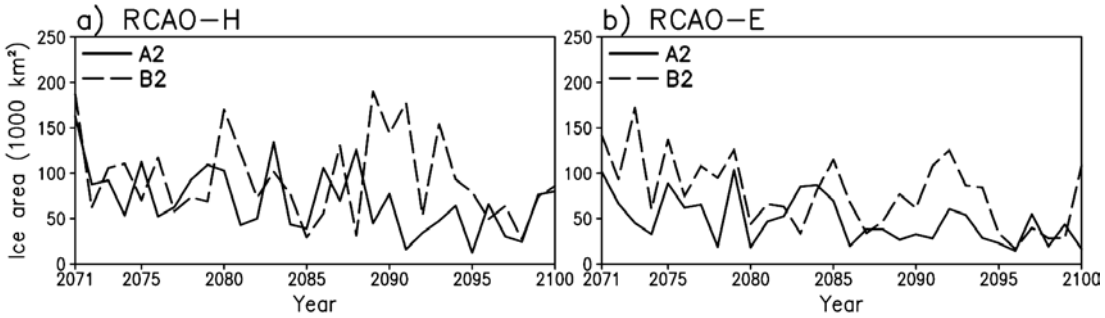

Figure 37. *Yearly maximum Baltic Sea ice area in the RCAO-H (solid) and RCAO-E (dashed) A2 and B2 scenario runs. Note that the scale differs from Fig.18.*

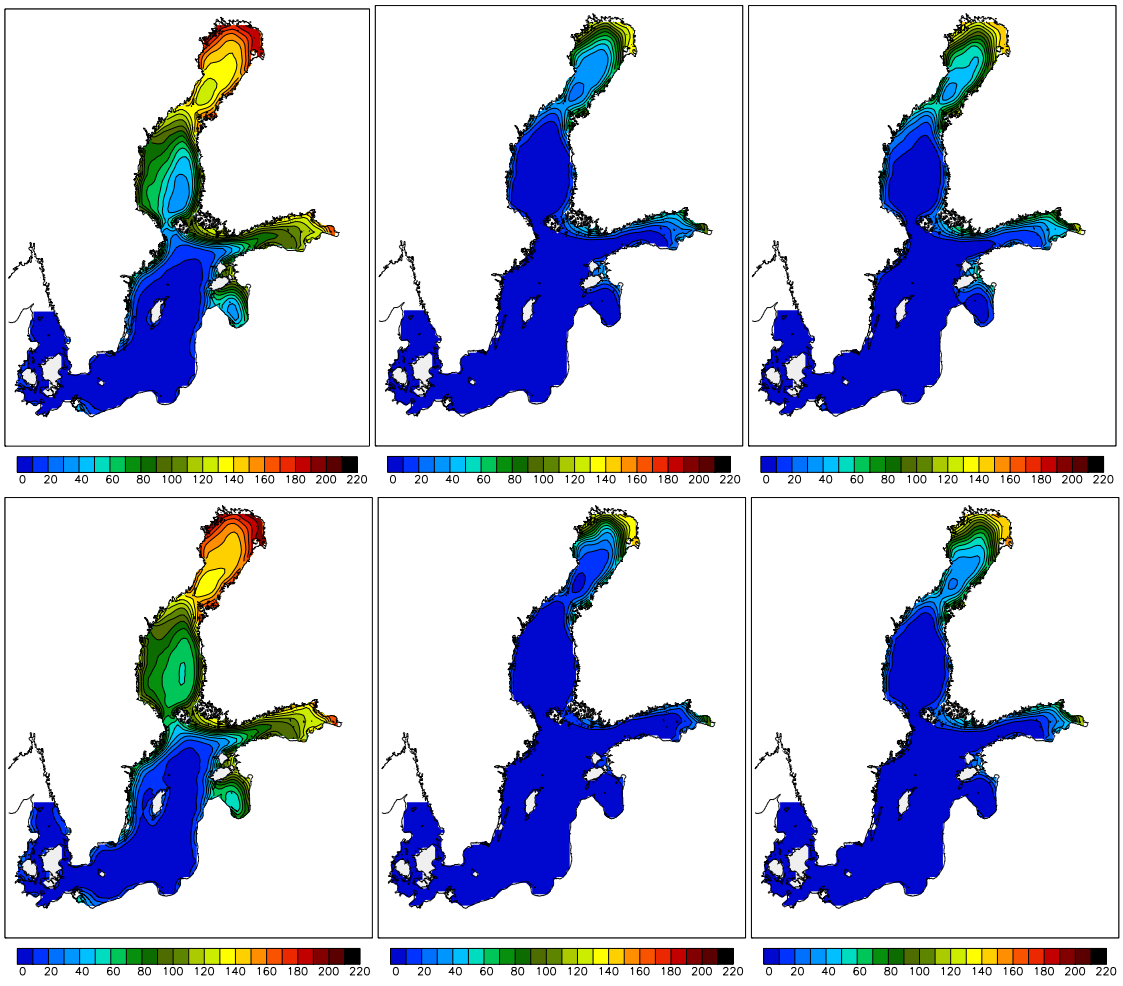

Figure 38. *Average annual number of days with ice cover in the Baltic Sea. Top left, middle and right: RCAO-H CTRL, A2 and B2. Bottom left, middle and right: RCAO-E CTRL, A2 and B2.*

The simulated warming also leads to a large decrease in the Baltic Sea ice extent (Figs. 37 and 38). Excluding the first winter which may still be affected by the initial spin-up,

the yearly maximum ice extent in RCAO-H A2 varies from 13×10^3 km^2 to 134×10^3 km^2 with a mean of 67×10^3 km^2, and that in RCAO-E A2 from 15×10^3 km^2 to 104×10^3 km^2 with a mean of 46×10^3 km. For RCAO-H B2 the range is from from 27×10^3 km^2 to 190×10^3 km^2 with a mean of 91×10^3 km^2, and for RCAO-E B2 from 17×10^3 km^2 to 172×10^3 km^2 with a mean of 76×10^3 km^2. In comparison with the control simulations (Section 3.8.2), the average maximum ice extent decreases by 54-80%, depending on the driving model and the forcing scenario. Some ice still forms in every winter, but even in the coldest winters in the B2 simulations the ice extent remains somewhat below the control run mean.

As shown by Fig. 38, the ice cover in the scenario runs is largely limited to the Gulf of Finland and the Bothnian Bay. In the northernmost Bothnian Bay, the average ice season length nevertheless exceeds four months in all four scenario runs.

5 Statistical analysis of simulated climate changes

This section is devoted to statistical tables characterising the simulated climate changes. In the first subsection (5.1), the statistical significance of the simulated changes and their magnitude relative to the simulated interal climate variability is addressed. In Section 5.2, the agreement between the HadAM3H- and ECHAM4-driven simulations is quantified and the contribution of internal variability to the differences between these simulations is estimated. Finally, because it is anticipated that these experiments will be used most actively within the Swedish climate change community, a table of Sweden area mean climate changes is given in Section 5.3. In this subsection some comparison is also made with the previous generation of Rossby Centre climate change simulations discussed by Räisänen et al. (2000a) and Räisänen and Joelsson (2001).

5.1 Simulated changes versus internal variability

Climate varies even under constant external conditions, both in the real world and in models. Any simulated climate change (computed as the difference between the climates in two different model runs) is therefore a combination of two parts: a reproducible signal associated with the external forcing, and noise associated with internal (i.e., unforced) variability. These two parts could be separated, in principle, by making a large ensemble of climate change simulations with the same external forcing but different initial conditions (in the case of regional climate change experiments, the initial conditions would need to be varied even in the driving global model). In that case, the ensemble mean climate change would approach the reproducible signal with increasing ensemble size. Without such ensembles, there is no exact way to separate between the signal and the noise. However, the magnitude of the simulated climate changes can still be compared with the magnitude of noise expected from statistical considerations.

A frequently used tool in this context is the *t* statistics, which is of the general form

$$t = \frac{\Delta X}{\sqrt{V(\Delta X)}} \tag{2}$$

Here, ΔX is the simulated change (e.g., 30-year annual or seasonal mean difference between two model runs) in variable X and $V(\Delta X)$ is the error variance of the simulated change. If the values of X in subsequent years are independent and the simulation is statistically stationary, then

$$V(\Delta X)_0 = \frac{1}{n}(V_{X,1} + V_{X,2}) \tag{3}$$

where $V_{x,1}$ and $V_{x,2}$ are the interannual ("n-1" definition) variances of X within the two model runs compared and n (here n = 30) is the number of years in each of them. However, (3) will underestimate $V(\Delta X)$ if the values of X in subsequent years are positively correlated, which is the case for at least some variables (sea surface temperature is the most obvious example). A first-order adjustment for this (Zwiers and von Storch 1995), which is adopted here, is to replace (3) with

$$V(\Delta X) = \frac{1+r_1}{1-r_1} V(\Delta X)_0 \tag{4}$$

where r_1 is the lag-1 autocorrelation estimated from the simulations (i.e., the correlation between the values of X in the years i and i+1). In practice, sampling variability makes it difficult to estimate r_1 precisely. To keep the estimate conservative (i.e., more likely too high than too low), r_1 is set to zero where the value derived directly from the data is negative. Another possible source of positive bias in our variance estimate is the fact that the 30-year simulations are not stationary due to the gradually increasing greenhouse gas forcing. However, this effect is expected to be small, with the possible exception of temperature for which the signal-to-noise ratio is highest and the issue of statistical significance is therefore less critical than for other variables.

For large enough samples, the t statistics is almost normally distributed, so that there is about a 5% probability to get $|t| > 2$ by pure chance. Table 6 lists the actual area fraction of changes with $|t| > 2$ for some variables. Results are given for both the A2 scenario run minus control run and the B2 scenario run minus control run climate changes, and for the difference between the A2 and B2 scenario runs. Finally, the two rightmost columns of the table address the question whether the climate changes in the B2 simulations differ significantly from what is expected from the changes in A2 and the evolution of the global mean temperature in the driving models. In this case, the null hypothesis is that the local RCAO-simulated climate changes should be linearly proportional to the change in the global mean temperature. Thus, we define the nonlinear part of the climate change in the B2 simulation as

$$\Delta X_{NL} = \Delta X_{B2-CTRL} - A\Delta X_{A2-CTRL} \tag{5}$$

where the scaling coefficient A is the ratio in global mean warming between the A2 and B2 scenarios in the driving model. We use for RCAO-H A = 0.72 (the global mean warming in HadAM3H from 1961-1990 to 2071-2100 is 2.3ºC in B2 and 3.2ºC in A2), and for RCAO-E A = 0.76 (in ECHAM4/OPYC3, the global warming is 2.6ºC in B2 and 3.4ºC in A2). For the error variance of ΔX_{NL}, simple algebra gives the estimate

$$V(\Delta X_{NL}) = \frac{1}{n}\frac{1+r_1}{1-r_1}(V_{X,B2} + A^2 V_{X,A2} + (1-A)^2 V_{X,CTRL}) \tag{6}$$

where the subindices A2, B2 and CTRL refer to the different 30-year simulations.

Table 6. *Fractional area of statistically significant (|t| > 2) climate changes in the RCAO experiments. Columns 3-4: changes from control to A2; columns 5-6: changes from control to B2; columns 7-8: differences between A2 and B2; columns 9-10: nonlinearity of the change between B2 and A2 (see text). RH = RCAO-H; RE = RCAO-E. T2 = mean 2 m temperature; Prec = mean precipitation; Wind = mean 10 m level wind speed; SLP = sea level pressure; Ntot = total cloudiness; T2max and T2min = average yearly 2 m temperature extremes; P24max = average yearly maximum one-day precipitation; Wmax = average yearly maximum 10 m wind speed. The results for SLP include the whole map domain used in this report, those for the other variables land grid boxes only. Cases with at least 50% of significant changes are shown in bold.*

		A2-CTRL		B2-CTRL		A2-B2		Nonlinearity	
Variable	Season	RH	RE	RH	RE	RH	RE	RH	RE
T2	DJF	**100**	**100**	**100**	**100**	**85**	**58**	34	41
	JJA	**100**	**100**	**100**	**100**	**98**	**92**	16	21
	Ann	**100**	**100**	**100**	**100**	**99**	**98**	0	1
Prec	DJF	**67**	**68**	**57**	**68**	22	10	9	7
	JJA	**60**	**65**	**52**	35	8	42	9	13
	Ann	38	**74**	25	**54**	17	43	10	21
Wind	DJF	14	**68**	6	**67**	22	9	19	4
	JJA	46	**50**	36	43	8	9	3	5
	Ann	13	**73**	9	**63**	4	15	5	2
SLP	DJF	33	**54**	26	**61**	6	26	9	22
	JJA	**75**	**71**	**64**	**67**	43	40	26	1
	Ann	26	**60**	31	**62**	0	22	13	0
Ntot	DJF	39	**51**	23	36	17	10	12	5
	JJA	**76**	**76**	**69**	**70**	23	35	14	8
	Ann	**83**	**86**	**61**	**76**	41	**60**	8	3
T2max	Ann	**100**	**100**	**89**	**100**	**70**	**73**	19	11
T2min	Ann	**99**	**100**	**97**	**100**	**55**	26	9	15
P24max	Ann	29	33	23	35	6	5	6	6
Wmax	Ann	7	**51**	9	32	7	8	8	5

The following general conclusions arise from Table 6.

- The A2 – control run climate changes are more frequently significant than the B2 – control run changes, whereas the differences between A2 and B2 are less frequently significant than either of A2 – control and B2 – control. The nonlinear part of the B2 – control run climate change [Eq. (5)] is in most cases significant in only a small part of the domain, in several cases in less than 5% of it, which is the fraction on the average expected to be obtained by pure chance. In the case of the DJF mean temperature, 34% of significantly nonlinear changes are found in RCAO-H and 41% in RCAO-E, but the two experiments disagree on the nature of the nonlinearity. In RCAO-H B2, the DJF mean warming in southern and central Europe is smaller than is expected from the B2 / A2 ratio in global temperature change, whereas the reverse is true for RCAO-E.

- The seasonal and annual A2 – control and B2 – control changes in mean surface air temperature are significant in the whole domain. Changes in precipitation are much less regularly significant than those in temperature, but as a whole more frequently significant than those in the mean wind speed, especially in RCAO-H in which the changes in wind speed are (excluding JJA) significant in only a small part of the domain. The changes in sea level pressure are also in most cases more significant in RCAO-E than in RCAO-H. The changes in total cloudiness are significant in quite a large part of the domain, especially in the summer and the annual mean when cloudiness decreases in most areas in these experiments.
- Although extremes are more strongly affected by internal variability than the mean climate, the changes in the average yearly temperature maximum and minimum are significant in almost the whole land area for both A2 – control and B2 – control. The local changes in the annual maximum one-day precipitation and (excluding RCAO-E A2 – control) maximum wind speed are significant in only a minority of the domain. However, the general increase in maximum precipitation seen in Fig. 29 is actually highly significant in an area mean sense, because the area means of maximum precipitation vary much less from year to year than individual grid box values (see Räisänen and Joelsson 2001).

The statistical significance of climate changes depends on the length of the averaging period, as well as the magnitude of the changes. With a long enough period, even very small changes would become statistically significant. To judge the practical significance of the changes, it is also useful to compare them directly with the simulated interannual variability. This is done in Fig. 39 for the change in annual precipitation in the RCAO-H A2 simulation. The left panel shows the t value of the change, the right the ratio between the change and the interannual standard deviation in the control run. A statistically significant increase ($t > 2$) occurs in northern Europe and a statistically significant decrease ($t < -2$) in the southern parts of the domain. However, even in most of those areas where the change is significant, the magnitude of the change is smaller than the interannual standard deviation, which indicates a good deal of overlap between the distributions in the control and the scenario run. As expected from Eqs. (2)-(4), the t value is generally almost four times the ratio between the mean and the standard deviation. In the absence of interannual autocorrelation (which tends to be very weak for precipitation) and if the magnitude of the variability would not change with changing climate, this factor would be $15^{1/2}$.

For Table 7, the analysis of Fig. 39b was repeated for a few other cases. Characteristic values of the change-to-standard-deviation ratio were computed by dividing the rms (root-mean-square) amplitude of the changes by the rms amplitude of the interannual standard deviation. For precipitation and wind speed, the changes of which have been expressed in this report in per cent units, both the change and the interannual standard deviation were normalized by the local control run mean before the calculation of the rms values. In the case of precipitation, however, very dry areas ($P_{ctrl} < 0.5$ mm day^{-1}) were excluded from this computation, because in such areas modest absolute changes sometimes translate to gigantic relative changes (this problem mainly occurs in the southern parts of the model domain in summer). Otherwise, the rms values were evaluated over all land grid boxes within the map domain used in this report.

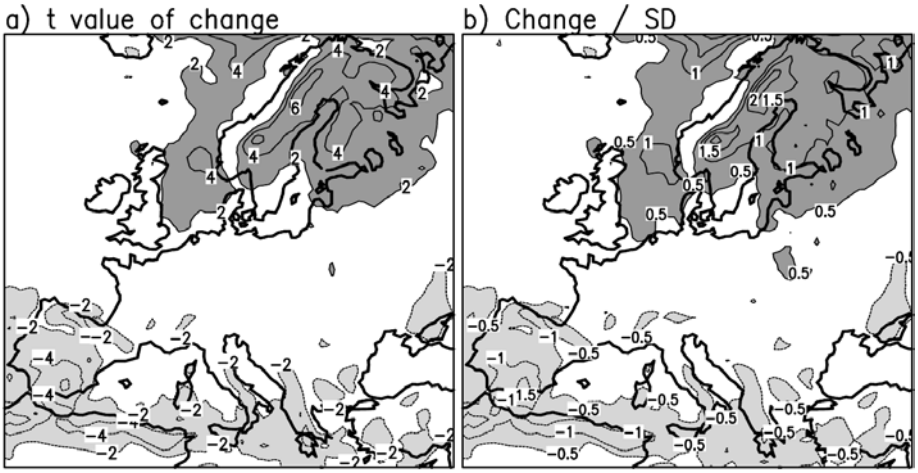

Figure 39. *Comparison of the annual precipitation change in RCAO-H A2 with the simulated variability. (a) the t value of the change (contour interval 2, zero contour omitted, values below -2 are shaded in light and values above 2 in dark). (b) the ratio between the change and the year-to-year standard deviation in the control run (contour interval 0.5, zero contour omitted, values below -0.5 are shaded in light and values above 0.5 in dark).*

Table 7. *Ratio between the root-mean-square amplitude of the simulated climate changes and the root-mean-square amplitude of the control run interannual standard deviation (see text). Results are given for the A2 – control run and B2 – control run climate changes in mean surface air temperature (T2), precipitation (Prec) and mean 10 m level wind speed (Wind). Values exceeding or equal to one are given in bold.*

		A2-CTRL		B2-CTRL	
Variable	Season	RH	RE	RH	RE
T2	DJF	**2.25**	**3.09**	**1.53**	**2.58**
	JJA	**4.16**	**5.41**	**2.92**	**3.72**
	Ann	**5.38**	**6.51**	**3.64**	**5.00**
Prec	DJF	0.70	**1.08**	0.48	0.92
	JJA	0.77	**1.02**	0.68	0.61
	Ann	0.58	**1.34**	0.39	0.97
Wind	DJF	0.44	**1.05**	0.33	0.84
	JJA	0.81	**1.12**	0.69	0.83
	Ann	0.54	**1.39**	0.40	**1.00**

The results in Table 7 demonstrate the large magnitude of the simulated temperature changes, even when compared directly with interannual variability. This is particularly the case with the summer and the annual mean temperatures, and of course more so for the A2 than the B2 scenario. In winter, the large interannual variability makes the change-to-standard deviation ratios somewhat lower. The changes in precipitation and mean wind speed are by this nondimensional measure several times smaller than those in temperature, in particular in the RCAO-H simulations. Thus, if a person familiar with

the current climate were transported with a time machine hundred years to the future, it would probably be the higher temperatures, rather than the changes in precipitation or windiness that would appear most different against his/her earlier experience.

5.2 Comparison between RCAO-H and RCAO-E

Although the maps in Section 4 give a general impression of what the HadAM3H- and ECHAM4-driven RCAO simulations agree and disagree on, it is worthwile to put the agreement in quantitative terms. Here, the similarity statistics of Räisänen et al. (2001) is used for that purpose. Denoting the climate changes in the HadAM3H- and ECHAM4-driven experiments with the same forcing scenario as ΔH and ΔE,

$$s = \frac{\overline{\Delta H \Delta E}}{\overline{[(\Delta H)^2 + (\Delta E)^2]/2}} \tag{7}$$

where the overline indicates averaging over a spatial domain (here, all land grid boxes excluding the boundary zones and the two outermost rows and columns of the ordinary model area). This statistics only attains its maximum value of 1 when $\Delta H = \Delta E$ in the whole area of comparison, whereas $s = -1$ indicates complete disagreement ($\Delta H = -\Delta E$ in the whole domain). $s = 0$ is what one would get on the average as a result of pure chance. In the special case that the area means of both ΔH and ΔE are zero and their variances are equal, s is identical to the standard spatial correlation. Its main advantage over spatial correlation is that it does not neglect the area mean change, which is in some cases a very important part of the whole (in particular for temperature changes).

The origin of the differences in climate change between RCAO-H and RCAO-E also needs to be addressed. There are two sources of difference: the different driving global models and the noise associated with internal variability (generated by both the global models and by RCAO). These two sources of difference are statistically additive in the sense that the expected value of the mean squared difference between RCAO-H and RCAO-E is the sum of global-model-related and noise-related squared differences (e.g., Räisänen et al. 2001). A suitable nondimensional measure estimating the relative importance of noise for the RCAO-H minus RCAO-E differences is

$$I = \frac{\overline{V(\Delta H) + V(\Delta E)}}{\overline{(\Delta H - \Delta E)^2}} \tag{8}$$

where V(ΔH) and V(ΔE) are the noise-related error variances estimated from (4). These variances need to be summed because the differences in climate change between RCAO-H and RCAO-E are affected by noise in both of these two experiments.

Results for mean 2 m temperature, precipitation and 10 m wind speed are given in Table 8. As expected, the RCAO-H and RCAO-E experiments agree best on temperature changes. Despite some pronounced regional differences, the overall agreement on precipitation changes may also be regarded as reasonable, although it is lower for the annual mean change than for the changes in winter and summer separately. The agreement on the changes in the mean wind speed is poor, most notably for the annual mean changes that are essentially orthogonal between RCAO-H and RCAO-E.

Table 8. *Similarity [Eq. (7)] of climate changes between RCAO-H and RCAO-E, and the per cent fraction of differences estimated to be explained by internal variability (in parentheses). Results are given for the A2 – control run and B2 – control run climate changes in mean surface air temperature (T2), precipitation (Prec) and mean 10 m level wind speed (Wind).*

Variable	Season	A2-CTRL	B2-CTRL
T2	DJF	0.95 (16%)	0.87 (10%)
	JJA	0.96 (11%)	0.96 (20%)
	Ann	0.96 (6%)	0.93 (6%)
Prec	DJF	0.76 (36%)	0.67 (40%)
	JJA	0.87 (48%)	0.75 (58%)
	Ann	0.67 (21%)	0.43 (29%)
Wind	DJF	0.38 (17%)	0.14 (21%)
	JJA	0.31 (13%)	0.31 (20%)
	Ann	0.04 (9%)	-0.08 (14%)

As indicated by the numbers given in parentheses in Table 8, only a minority of the differences in climate change between RCAO-H and RCAO-E can be explained by internal variability. In particular, this is the case for temperature and wind speed. In the case of precipitation change, internal variability plays a somewhat larger role, especially in summer when it appears to explain about a half of the differences between RCAO-H and RCAO-E. Thus, the differences between RCAO-H and RCAO-E in temperature change are larger than those in precipitation change in comparison with the internal variability, although the reverse is true when the differences are compared with the common features of change between the two experiments. Internal variability tends to explain a larger fraction of the differences between the changes obtained in the B2 than in the A2 simulations, simply because the absolute differences are larger for the A2 simulations.

5.3 Climate change in Sweden

A summary of the simulated climate changes in Sweden is given in Table 9, using area means over the whole country. Naturally, such area means often hide substantial local variations. In addition to the RCAO experiments, the table also includes results for the previous generation of the Rossby Centre climate change simulations, which were made with the RCA1 model at 44 km horizontal resolution (Räisänen et al. 2000; Räisänen and Joelsson 2001). Because of differences in forcing scenarios and periods (see Räisänen and Joelsson 2001), the RCA1 experiments are not directly comparable with RCAO. However, as measured by the global mean warming in the driving GCMs, the differences between the various experiments are not very large. The HadCM2 and ECHAM4/OPYC3 simulations used to drive the RCA1 simulations (abbreviated in Table 9 as RCA1-H and RCA1-E) both had a global mean warming of 2.6°C. The numbers for the HadAM3H A2 and B2 simulations used to drive RCAO are 3.2°C and 2.3°C, and those for ECHAM4/OPYC3 A2 and B2 3.4°C and 2.6°C. Thus, the RCAO A2 (B2) scenario simulations correspond to a slightly larger (similar or slightly smaller) global climate change than RCA1. Some comments related to the table follow below.

Table 9. *Changes in the Sweden area means of some parameters in the four RCAO climate change simulations and in the two 44 km resolution RCA1 experiments. Evap = evaporation; Runoff = runoff generation evaluated directly from RCAO or RCA1; NP1 = average yearly number of days with at least 1 mm of precipitation; other variables as in Table 6. Changes that are at the 95% level statistically significant are given in bold.*

Variable	Season	Unit	RH, A2	RE, A2	RH, B2	RE, B2	RCA1-H	RCA1-E
T2	DJF	ºC	**3.8**	**5.5**	**2.8**	**4.2**	**5.2**	**4.1**
	MAM		**3.6**	**4.8**	**2.5**	**3.7**	**3.6**	**3.0**
	JJA		**2.9**	**3.3**	**1.5**	**2.5**	**2.4**	**3.2**
	SON		**4.2**	**4.6**	**3.1**	**3.5**	**3.7**	**5.0**
	Ann		**3.6**	**4.5**	**2.5**	**3.5**	**3.7**	**3.8**
Prec	DJF	%	**32**	**49**	**19**	**37**	15	-3
	MAM		**23**	**36**	9	**24**	9	13
	JJA		-5	-6	-5	-5	**23**	0
	SON		7	**25**	**11**	**21**	**25**	**25**
	Ann		**12**	**23**	**8**	**17**	**18**	**8**
Wind	DJF	%	0.0	**13.0**	-0.1	**7.1**	**7.2**	2.1
	MAM		0.5	**12.7**	-2.5	**7.8**	1.7	4.3
	JJA		-1.8	-1.2	-0.7	-1.4	1.6	2.1
	SON		-3.1	**4.6**	1.6	**4.2**	6.3	**5.2**
	Ann		-1.0	**7.8**	-0.4	**4.7**	**4.3**	**3.4**
Ntot	DJF	%	**3.4**	-0.5	**1.7**	0.2	**-5.5**	**-5.0**
	MAM	of	-0.7	-1.3	0.2	-1.8	-2.9	**-4.3**
	JJA	sky	**-3.1**	**-2.0**	-0.3	-1.1	-0.2	-2.4
	SON		-1.5	-0.6	-1.1	-0.6	-2.5	-0.7
	Ann		-0.5	**-1.1**	0.2	-0.8	**-2.8**	**-3.1**
Evap	DJF	%	**36**	**68**	**21**	**44**	-18	-7
	MAM		**32**	**47**	**18**	**34**	-1	**12**
	JJA		**12**	**8**	**6**	**6**	**10**	**12**
	SON		**15**	**24**	**15**	**19**	**20**	**7**
	Ann		**18**	**23**	**11**	**17**	**6**	**10**
Runoff	DJF	%	**73**	**132**	**44**	**100**	**107**	24
	MAM		0	-3	-3	-4	1	-10
	JJA		**-30**	**-27**	**-22**	**-23**	-1	-17
	SON		11	**38**	**20**	**32**	**71**	**51**
	Ann		6	**22**	5	**17**	**29**	7
T2max	Ann	ºC	**3.6**	**3.7**	**1.2**	**2.4**	**2.0**	**3.6**
T2min	Ann	ºC	**10.5**	**12.4**	**8.2**	**9.3**	**10.2**	**6.9**
P24max	Ann	%	**13**	**14**	**7**	**11**	**18**	**18**
NP1	Ann	%	4	**11**	2	**8**	6	-2
Wmax	Ann	%	-2.8	**8.1**	-2.0	**6.3**	**5.0**	2.3

- **Mean surface air temperarature**. The largest annual mean warming among this set of simulations occurs in RCAO-E A2 and the smallest warming in RCAO-H B2. In the two RCAO-H simulations the Sweden mean warming is only about 10% larger than the global mean warming, whereas it is 30-50% larger in all the other simulations. There is no clear single explanation to this

result, although the slight decrease in the winter mean westerly flow (in contrast to an increase found in all other cases) most probably makes a contribution. The seasonal cycle of the warming has remained stable across the suite of the simulations, with all of them showing a maximum of warming in winter or autumn and a minimum in summer or (in RCA1-E) in spring.

- **Mean precipitation**. All six simulations indicate an increase in the Sweden annual mean precipitation, with the largest change again in RCAO-E A2. The seasonal cycle of the change is more variable. All four RCAO simulations indicate the largest increase in precipitation in winter and a slight decrease in summer (although with a north-south gradient across the country with a more pronounced decrease in the south and a slight increase in the north). This winter-summer contrast was absent in the RCA1 simulations, which both indicated a maximum of precipitation increase in the autumn. However, the short duration (10 years) of the RCA1 simulations suggests that the seasonal details of their results might have been affected substantially by the strong unforced variability of precipitation.
- **Mean wind speed**. The two RCAO-H simulations differ from the other four by showing a small (statistically insignificant) decrease in the Sweden annual mean wind speed. The changes in the summer mean wind speed are small in all six experiments, whereas there is a much larger inter-experiment variation in the other seasons. The largest increases occur in RCAO-E A2, especially in winter and in spring. As discussed above (Section 4.5), the changes in windiness and differences in them between different experiments appear to be primarily determined by changes in the large-scale atmospheric circulation.
- **Total cloudiness**. The four RCAO simulations show only small changes in the Sweden annual mean cloud cover, in contrast to the larger decreases obtained in the RCA1 simulations. A particularly large difference between the two generations of experiments occurs in winter. It seems likely that the changes in physical parameterisations from RCA1 to RCA2 explain at least a part of these differences. However, the issue has not yet been investigated in any detail.
- **Evaporation**. The increase in Sweden mean annual evaporation is larger in the RCAO (11-23%) than in the RCA1 simulations (6-10%). There is little difference between RCAO and RCA1 summer, but in winter and spring the RCAO simulations indicate a much larger increase than RCA1 (in which winter evaporation actually decreased). As discussed in Section 4.7.1, this difference likely reflects the smaller snow evaporation produced by the RCA2 land surface scheme.
- **Runoff generation**. All six simulations indicate an increase in the average annual runoff generation, the magnitude of which depends on the precipitation and evaporation changes. All the simulations also indicate increased winter and reduced summer runoff, but with large differences in the magnitude of the seasonal changes.
- **Average yearly temperature extremes**. The average highest yearly maximum temperatures increase in all six simulations approximately as much as the summer mean temperature, even though there is a suggestion in the RCAO-E results that the absolute extremes in southern Sweden might increase somewhat more (Table 3). The lowest winter minimum temperatures increase in all the simulations more than the winter mean temperature, and this difference has actually become larger in RCAO than in RCA1. Although the tendency of the

model to simulate excessively cold temperatures in some situations (Section 3.3.4) calls for some care in the interpretation of this result, we expect it to be at least qualitatively realistic.

- **Yearly maximum one-day precipitation.** The daily precipitation extremes increase in all the RCAO and RCA1 simulations, but not necessarily by a larger per cent amount than the mean annual precipitation. In both the two RCAO-E simulations, the mean precipitation increases markedly more than the extremes. This is explained by a large increase in the annual number of precipitation days (up to 11% or 19 more days per year with at least 1 mm of precipitation in RCAO-E A2) in these simulations. However, the change in the number of precipitation days varies a lot seasonally and between the different experiments, whereas an increase in extreme precipitation occurs in all four seasons and all six experiments (not shown).
- **Yearly extremes of wind speed** change approximately as much as the annual mean wind speed. Thus, there are large differences between the RCAO-H and RCAO-E results.

Many users of Rossby Centre climate simulation data may like to ask which of these different results they should rely on. The best answer may be that it is too early to disregard any of them. After all, all these simulations have been based on GCM results from just two global climate modelling centres, only one (although developing) regional model system, and a limited set of forcing scenarios. The actual uncertainty associated with future Swedish climate may therefore be larger than is indicated by the scatter of the numbers in Table 9. On the other hand, because the earlier RCA1 simulations were only 10 years long, some of their results (for example, regarding precipitation change and changes in extremes in general) may have been affected substantially by unforced climate variability. In this respect, the 30-year RCAO simulations provide a more stable basis for estimating long-term climate changes. In addition, it is likely that some of the differences between the RCAO and RCA1 results have resulted from improvements made to the regional model (e.g., the larger increase in evaporation in RCAO). This also suggests that somewhat more weight should be given to the RCAO than the RCA1 simulations.

6 Conclusions

This report provides the first documentation of a series of regional climate simulations made at the Rossby Centre, SMHI, during the year 2002. Six 30-year runs have been made with the regional atmosphere – Baltic Sea model RCAO, using boundary data from the two GCMs HadAM3H (experiment RCAO-H) and ECHAM4/OPYC3 (RCAO-E). Two of these runs represent the recent (1961-1990) climate and the remaining four the climate in the late 21st century (2071-2100) under two different assumptions of future atmospheric composition. Together with other regional climate simulations being conducted within the PRUDENCE project, these experiments are expected to be actively used in European climate change and climate impacts research in the next few years.

A series of six 30-year simulations provides a huge amount of data for exploration. Although this report has only scratched the surface, it is not practicable to present here a systematic summary of all the findings. Rather, a few main points are taken up below.

- **Control simulations**. Many aspects of the RCAO-simulated control run climate compare favourably with observations, even when the model is driven by boundary data from the two global models. Some problems are evident in the simulated cloudiness and precipitation, with generally too cloudy and wet conditions in northern Europe (although biases in precipitation measurements complicate the interpretation) and too clear and dry conditions in southern Europe. The average simulated diurnal temperature range is too small in northern Europe, at least in part because of excessive cloudiness, but in some rare winter situations temperature falls to questionably low levels. The extremes of daily precipitation and wind speed appear relatively modest, even though this may be partly because the model resolution (49 km) is too coarse to capture the truly local-scale extremes. There is a lot of similarity between the HadAM3H- and ECHAM4/OPYC3-driven control simulations, although the problems associated with the hydrological cycle and cloudiness are somewhat larger in the latter. However, it is important to remember that ECHAM4/OPYC3 as a coupled atmosphere-ocean general circulation model has a larger freedom to generate problems than the atmospheric model HadAM3H, the control run of which used observed sea surface conditions.
- **Changes in time mean climate**. The magnitude of the simulated changes depends on both the forcing scenario (the changes are generally larger for the A2 than the B2 scenario) and the driving global model (the largest changes tend to occur in RCAO-E). In all four scenario simulations, the warming in northern Europe is largest in winter or autumn. In central and southern Europe, the warming peaks in summer and reaches in the RCAO-E A2 simulation locally 10°C. This is associated with substantial decreases in precipitation, soil moisture and cloudiness. The four experiments agree on a general increase in precipitation in northern Europe especially in winter and on a general decrease in precipitation in southern and central Europe in summer, but the magnitude and the geographical patterns of the change differ a lot between RCAO-H and RCAO-E. This reflects very different changes in the atmospheric circulation during the winter half-year. The different changes in atmospheric circulation inherited from the driving global models also have a large impact on the simulated changes in windiness. As expected, the warming is accompanied by reduced snow and reduced ice in inland lakes and in the Baltic Sea.
- **Changes in extremes**. The change in the highest summer maximum temperatures follows broadly the change in average summer temperatures in northern Europe, but it generally exceeds the time mean warming further south where variability is enhanced by reduced soil moisture and cloudiness. A very large increase in the lowest minimum temperatures occurs in large parts of Europe, most probably due to reduced snow cover. Extreme daily precipitation increases even in most of those areas where the time mean precipitation decreases. Like the changes in the mean wind speed, the changes in wind extremes differ substantially between RCAO-H and RCAO-E.

These results highlight the need of further research at least in two important areas. First, as long as the response of the atmospheric circulation to anthropogenic forcing is in gross disagreement between different global models, many aspects of regional climate change will remain very uncertain. This uncertainty can only be reduced by painstaking improvement of global climate models. Second, the dramatic summertime warming and drying in central and southern Europe suggested by some of the simulations might have serious consequences. It is therefore important to address the sensitivity of this result to model formulation, including especially the description of land surface, cloud and precipitation processes. The suite of regional climate change simulations being conducted within the PRUDENCE project is hoped to give some information on this issue.

Acknowledgments

This work is part of the SWECLIM programme, mainly funded by MISTRA and SMHI, and of the European PRUDENCE project (project EVK2-CT2001-00132 in the EU 5th Framework program for Energy, environment and sustainable development).

Appendix. Modification of the RCAO-H monthly mean files to reduce the ice thickness problem

To minimise the impact of the ice thickness problem described in Section 2.5, the following procedure was applied to the RCAO-H monthly mean files.

1. All points that had had very thick ice (over 1.5 m) during the previous nine months were flagged. The nine-month period accounts for the time required by a 1.5 m ice layer to melt and the water temperature to forget the late ice melt.
2. For each grid box and each variable X, the 30-year mean seasonally varying difference between the local X and the mean of X in the surrounding eight points was calculated, using only unflagged values.
3. The flagged values were replaced using the means over the surrounding eight points and the differences calculated in 2.
4. Some bound checks were made to eliminate unphysical results, for example negative snow depths.

This procedure was applied to most surface variables, although the resulting changes were generally very small excluding surface air temperature and other more or less directly temperature-related variables. No adjustments were made to surface pressure, sea level pressure and pressure level variables, which were judged to be virtually unaffected by the problem. This correction procedure is local, that is, the effect of the anomalous ice conditions on neighbouring grid boxes is neglected. However, this effect is most probably a secondary one.

References

Blackmon M. L., 1976. A climatological spectral study of the 500 mb geopotential height of the Northern Hemsiphere. *Journal of the Atmospheric Sciences*, **33**, 1607-1623.

Bringfelt B., Räisänen J., Gollvik S., Lindström G., Graham L. P. and Ullerstig A., 2001. The land surface treatment for the Rossby Centre Regional Atmospheric Climate Model – version 2 (RCA2). SMHI Reports Meteorology and Climatology No. 98, SMHI, SE-60176 Norrköping, Sweden, 40 pp.

Cuxart J., Bougeault P. and Redelsperger J.-L., 2000. A turbulence scheme allowing for mesoscale and large eddy simulations. *Quarterly Journal of the Royal Meteorological Society*, **126**, 1-30.

Delworth T. L. and Manabe S., 1988. The influence of potential evaporation on the variabilities of simulated soil wetness and climate. *Journal of Climate*, **1**, 523-546.

Delworth T. L. and Manabe S., 1989. The influence of soil wetness on near-surface atmospheric variability. *Journal of Climate*, **2**, 1447-1462.

Eklund A., 1998. Istjocklek på sjöar – en statistisk bearbetning av SMHIs mätningar (Thickness of lake ice – a statistical analysis of measurements made by SMHI; in Swedish). SMHI Hydrologi No. 76, SMHI, SE-60176 Norrköping, Sweden, 19 + 9 pp.

Eklund A., 1999. Isläggning och islossning i svenska sjöar (Freezing and melting of ice in Swedish lakes; in Swedish). SMHI Hydrologi No. 81, SMHI, SE-60176 Norrköping, Sweden, 18 + 6 pp.

Fritsch M. and Chappell C. F., 1980. Local prediction of convectively driven mesoscale pressure systems. Part 1. Convective parameterisation. *Journal of the Atmospheric Sciences*, **37**, 1722-1733.

Gordon C., Cooper C., Senior C. A., Banks H., Gregory J. M., Johns T. C., Mitchell J. F. B. and Wood R. A., 2000. The simulation of SST, sea ice extents and ocean heat transports in a version of the Hadley Centre coupled model without flux adjustments. *Climate Dynamics*, **16**, 147-166.

Hahn C. J., Warren S. G. and London J., 1995. The effect of moonlight on observation of cloud cover at night, and application to cloud climatology. *Journal of Climate*, **8**, 1429-1446.

Houghton J. T., Ding Y., Griggs D. J., Noguer M., van der Linden P. J., Dai. X., Maskell K. and Johnson C. A. (Eds.), 2001. *Climate Change 2001: The Scientific Basis*. Cambridge University Press, 881 pp.

Huffman G. J. and Coauthors, 1997. The global precipitation climatology project (GPCP) combined precipitation dataset. *Bull. Amer. Meteor. Soc.*, **78**, 5-20.

Jones C., 2001. A brief description of RCA2 (Rossby Centre Atmosphere Model Version 2). *SWECLIM Newsletter*, **11**, 9-14.

Jones C. and Ullerstig A., 2002. The representation of precipitation in the RCA2 model (Rossby Centre Atmosphere Model Version 2). *SWECLIM Newsletter*, **12**, 27-39.

Kain J. and Fritsch M., 1990. A one dimensional entraining/detraining plume model and its application in convective parameterisation. *Journal of the Atmospheric Sciences*, **47**, 2784-2802.

Kalnay E. and Coauthors, 1996. The NCEP/NCAR 40-year Reanalysis Project. *Bull. Amer. Meteor. Soc*., **77**, 437-471.

Karlsson K.-G., 2001. A NOAA AVHRR cloud climatology over Scandinavia covering the period 1991-2000. SMHI Reports Meteorology and Climatology No. 98, SMHI, SE-60176 Norrköping, Sweden, 95 pp.

Kistler R. and Coauthors, 2001. The NCEP/NCAR 50-year reanalysis: Monthly means CD-ROM and documentation. *Bull. Amer. Meteor. Soc*., **82**, 247-268.

Latif M., Roeckner E., Mikolajewics U. and Voss R., 2000. Tropical stabilization of the thermohaline circulation in a greenhouse warming simulation. *Journal of Climate*, **13**, 1809-1813.

Ljungemyr P., Gustafsson N. and Omstedt A., 1996. Parameterization of lake thermodynamics in a high resolution weather forecasting model. *Tellus*, **48A**, 608–621.

McDonald A., 1994. Using 2nd, 4th and 6th order implicit horizontal diffusion to control noise in a 3D semi-Lagrangian, semi-implicit, limited area grid point model. Report from *HIRLAM3 Workshop on Numerical Integration Techniques*, 17-20. Available from SMHI, S-60176 Norrköping, Sweden.

McDonald A. and Haugen J. E., 1992. A two time level, three dimensional semi-Lagrangian, semi-implicit limited area grid point model of the primitive equations. *Monthly Weather Review*, **120**, 2603-2621.

McDonald A. and Haugen J. E., 1993. A two time level, three dimensional semi-Lagrangian, semi-implicit limited area grid point model of the primitive equations. Part II: extension to hybrid coordinates. *Monthly Weather Review*, **121**, 2077-2087.

Meier H. E. M., 2001. On the parameterization of mixing in 3D Baltic Sea models. *J. Geophys. Res.,* **106**, 30997-31016.

Meier H. E. M., Döscher R., Coward A. C., Nycander J. and Döös K., 1999. RCO – Rossby Centre regional Ocean climate model: model description (version 1.0) and first results from the hindcast period 1992/1993. SMHI Reports Oceanography No. 26, SMHI, S-60176 Norrköping, Sweden,102 pp.

Meier H. E. M., Döscher R. and Faxén T., 2002. A multiprocesssor coupled ice-ocean model for the Baltic Sea: application to salt inflow. *J. Geophys. Res*., submitted.

Nakićenović N. and Coauthors, 2000. Emission Scenarios. A Special Report of Working Group III of the Intergovernmental Panel on Climate Change. Cambridge University Press, 599 pp.

New M., Hulme M. and Jones P., 1999. Representing twentieth-century space-time climate variability. Part I: Development of a 1961-90 mean monthly terrestrial climatology. *Journal of Climate*, **12**, 829-856.

New M., Hulme M. and Jones P., 2000. Representing twentieth-century space-time climate variability. Part II: Development of 1901-96 monthly grids of terrestrial surface climate. *Journal of Climate*, **13**, 2217-2238.

Noguer M., Jones R. and Murphy J., 1998. Sources of systematic errors in the climatology of a regional climate model over Europe. *Climate Dynamics*, **14**, 691-712.

Raab B. and Vedin H. (Special Editors), 1995. Climate, Lakes and Rivers. National Atlas of Sweden, vol. 14. SNA Publishing, Box 45029 S-10430 Stockholm, Sweden, 176 pp.

Ramaswamy V. and Coauthors, 2001. Radiative forcing of Climate Change. In: *Climate Change 2001: The Scientific Basis* (ed: J. T. Houghton, Y. Ding, D. J.Griggs, M. Noguer, P. J. van der Linden, X. Dai, K. Maskell and C. A. Johnson). Cambridge University Press, 349-416.

Rasch P. J. and Kristjánsson J. E., 1998. A comparison of the CCM3 model climate using diagnosed and predicted condensate parameterizations. *J. Climate*, **11**, 1587-1614.

Roeckner E., Bengtsson L., Feichter J., Lelieveld J. and Rodhe H., 1999. Transient climate change simulations with a coupled atmosphere-ocean GCM including the tropospheric sulfur cycle. *J. Climate*, **12**, 3004–3032.

Rubel F. and Hantel M., 2001. BALTEX 1/6-degree daily precipitation climatology 1996-1998. *Meteorol. Atmos. Phys.*, **77**, 155-166.

Rummukainen M., Räisänen J., Ullerstig A., Bringfelt B., Hansson U., Graham P. and Willén U. 1998. RCA - Rossby Centre regional Atmospheric climate model: model description and results from the first multi-year simulation. SMHI Reports Meteorology and Climatology No. 83, SMHI, SE-60176 Norrköping, Sweden, 76 pp.

Rummukainen M., Räisänen J., Bringfelt B., Ullerstig A, Omstedt A., Willén U, Hansson U. and Jones C., 2001. A regional climate model for northern Europe: model description and results from the downscaling of two GCM control simulations. *Climate Dynamics*, **17**, 339-359.

Räisänen J., 2000. CO_2-induced climate change in northern Europe: comparison of 12 CMIP2 experiments. SMHI Reports Meteorology and Climatology No. 87, SMHI, SE-60176 Norrköping, Sweden, 59 pp.

Räisänen J., 2002. CO_2-induced changes in interannual temperature and precipitation variability in 19 CMIP2 experiments. *Journal of Climate*, **15**, 2395-2411.

Räisänen J. and Joelsson R., 2001. Changes in average and extreme precipitation in two regional climate model experiments. *Tellus*, **53A**, 547-566.

Räisänen J., Rummukainen M., Ullerstig A., Bringfelt B., Hansson U. and Willén U., 1999. The first Rossby Centre regional climate scenario – dynamical downscaling of CO_2-induced climate change in the HadCM2 GCM. SMHI Reports Meteorology and Climatology No. 85, SMHI, SE-60176 Norrköping, Sweden, 56 pp.

Räisänen J., Ullerstig A, Bringfelt B. and Räisänen P., 2000a. Two new RCA1 climate change experiments. *SWECLIM Newsletter*, **7+8**, 5-12.

Räisänen P., Rummukainen M. and Räisänen J., 2000b. Modification of the HIRLAM radiation scheme for use in the Rossby Centre regional atmospheric climate model. Report No. 49, Department of Meteorology, University of Helsinki, 71 pp.

Räisänen J., Rummukainen M. and Ullerstig A., 2001. Downscaling of greenhouse gas induced climate change in two GCMs with the Rossby Centre regional climate model for northern Europe. *Tellus*, **53A**, 168-191.

Räisänen J., Hansson U. and Ullerstig A., 2002. First GCM-driven RCAO runs of recent and future climate. *SWECLIM Newsletter*, **12**, 16-21.

Sass B. H., Rontu L. and Räisänen P., 1994. HIRLAM-2 radiation scheme: documentation and tests. HIRLAM Technical Report No. 16, SMHI, SE-60176 Norrköping, Sweden, 43 pp.

Savijärvi H., 1990. Fast radiation parameterization schemes for mesoscale and short-range forecast models. *Journal of Applied Meteorology*, **29**, 437-447.

Slingo J., 1987. The development and verification of a cloud prediction scheme for the ECMWF model. *Quarterly Journal of the Royal Meteorological Society*, **113**, 899-928.

Stocker T. F. and Coauthors, 2001. Physical Climate Processes and Feedbacks. In: *Climate Change 2001. The Scientific Basis*. J. T. Houghton et al., Eds., Cambridge University Press, 417-470.

Tett S. F. B., Johns T. C. and Mitchell J. F. B., 1997. Global and regional variability in a coupled AOGCM. *Climate Dyn*., **13**, 303-323.

Wetherald R. T. and Manabe S., 1995. The mechanisms of summer dryness induced by greenhouse warming. *Journal of Climate*, **8**, 3096-3108.

Zwiers F. W. and von Storch H., 1995. Taking serial correlation into account in tests of the mean. *Journal of Climate*, **8**, 336-351.

SMHI's publications

SMHI publishes six report series. Three of these, the R-series, are intended for international readers and are in most cases written in English. For the others the Swedish language is used.

Names of the Series	**Published since**
RMK (Report Meteorology and Climatology)	1974
RH (Report Hydrology)	1990
RO (Report Oceanography)	1986
METEOROLOGI	1985
HYDROLOGI	1985
OCEANOGRAFI	1985

Earlier issues published in serie RMK

1 Thompson, T., Udin, I., and Omstedt, A. (1974)
Sea surface temperatures in waters surrounding Sweden.

2 Bodin, S. (1974)
Development on an unsteady atmospheric boundary layer model.

3 Moen, L. (1975)
A multi-level quasi-geostrophic model for short range weather predictions.

4 Holmström, I. (1976)
Optimization of atmospheric models.

5 Collins, W.G. (1976)
A parameterization model for calculation of vertical fluxes of momentum due to terrain induced gravity waves.

6 Nyberg, A. (1976)
On transport of sulphur over the North Atlantic.

7 Lundqvist, J.-E., and Udin, I. (1977)
Ice accretion on ships with special emphasis on Baltic conditions.

8 Eriksson, B. (1977)
Den dagliga och årliga variationen av temperatur, fuktighet och vindhastighet vid några orter i Sverige.

9 Holmström, I., and Stokes, J. (1978)
Statistical forecasting of sea level changes in the Baltic.

10 Omstedt, A., and Sahlberg, J. (1978)
Some results from a joint Swedish-Finnish sea ice experiment, March, 1977.

11 Haag, T. (1978)
Byggnadsindustrins väderberoende, seminarieuppsats i företagsekonomi, B-nivå.

12 Eriksson, B. (1978)
Vegetationsperioden i Sverige beräknad från temperaturobservationer.

13 Bodin, S. (1979)
En numerisk prognosmodell för det atmosfäriska gränsskiktet, grundad på den turbulenta energiekvationen.

14 Eriksson, B. (1979)
Temperaturfluktuationer under senaste 100 åren.

15 Udin, I., och Mattisson, I. (1979)
Havsis- och snöinformation ur datorbearbetade satellitdata - en modellstudie.

16 Eriksson, B. (1979)
Statistisk analys av nederbördsdata. Del I. Arealnederbörd.

17 Eriksson, B. (1980)
Statistisk analys av nederbördsdata. Del II. Frekvensanalys av månadsnederbörd.

18 Eriksson, B. (1980)
Årsmedelvärden (1931-60) av nederbörd, avdunstning och avrinning.

19 Omstedt, A. (1980)
A sensitivity analysis of steady, free floating ice.

20 Persson, C., och Omstedt, G. (1980)
En modell för beräkning av luftföroreningars spridning och deposition på mesoskala.

21 Jansson, D. (1980)
Studier av temperaturinversioner och vertikal vindskjuvning vid Sundsvall-Härnösands flygplats.

22 Sahlberg, J., and Törnevik, H. (1980)
A study of large scale cooling in the Bay of Bothnia.

23 Ericson, K., and Hårsmar, P.-O. (1980)
Boundary layer measurements at Klock-rike. Oct. 1977.

24 Bringfelt, B. (1980)
A comparison of forest evapotranspiration determined by some independent methods.

25 Bodin, S., and Fredriksson, U. (1980)
Uncertainty in wind forecasting for wind power networks.

26 Eriksson, B. (1980)
Graddagsstatistik för Sverige.

27 Eriksson, B.(1981)
Statistisk analys av nederbördsdata. Del III. 200-åriga nederbördsserier.

28 Eriksson, B. (1981)
Den "potentiella" evapotranspirationen i Sverige.

29 Pershagen, H. (1981)
Maximisnödjup i Sverige (perioden 1905-70).

30 Lönnqvist, O. (1981)
Nederbördsstatistik med praktiska tillämpningar.
(Precipitation statistics with practical applications.)

31 Melgarejo, J.W. (1981)
Similarity theory and resistance laws for the atmospheric boundary layer.

32 Liljas, E. (1981)
Analys av moln och nederbörd genom automatisk klassning av AVHRR-data.

33 Ericson, K. (1982)
Atmospheric boundary layer field experiment in Sweden 1980, GOTEX II, part I.

34 Schoeffler, P. (1982)
Dissipation, dispersion and stability of numerical schemes for advection and diffusion.

35 Undén, P. (1982)
The Swedish Limited Area Model. Part A. Formulation.

36 Bringfelt, B. (1982)
A forest evapotranspiration model using synoptic data.

37 Omstedt, G. (1982)
Spridning av luftförorening från skorsten i konvektiva gränsskikt.

38 Törnevik, H. (1982)
An aerobiological model for operational forecasts of pollen concentration in the air.

39 Eriksson, B. (1982)
Data rörande Sveriges temperaturklimat.

40 Omstedt, G. (1984)
An operational air pollution model using routine meteorological data.

41 Persson, C., and Funkquist, L. (1984)
Local scale plume model for nitrogen oxides. Model description.

42 Gollvik, S. (1984)
Estimation of orographic precipitation by dynamical interpretation of synoptic model data.

43 Lönnqvist, O. (1984)
Congression - A fast regression technique with a great number of functions of all predictors.

44 Laurin, S. (1984)
Population exposure to SO and NO_x from different sources in Stockholm.

45 Svensson, J. (1985)
Remote sensing of atmospheric tempera-ture profiles by TIROS Operational Vertical Sounder.

46 Eriksson, B. (1986)
Nederbörds- och humiditetsklimat i Sverige under vegetationsperioden.

47 Taesler, R. (1986)
Köldperioden av olika längd och förekomst.

48 Wu Zengmao (1986)
Numerical study of lake-land breeze over Lake Vättern, Sweden.

49 Wu Zengmao (1986)
Numerical analysis of initialization procedure in a two-dimensional lake breeze model.

50 Persson, C. (1986)
Local scale plume model for nitrogen oxides. Verification.

51 Melgarejo, J.W. (1986)
An analytical model of the boundary layer above sloping terrain with an application to observations in Antarctica.

52 Bringfelt, B. (1986)
Test of a forest evapotranspiration model.

53 Josefsson, W. (1986)
Solar ultraviolet radiation in Sweden.

54 Dahlström, B. (1986)
Determination of areal precipitation for the Baltic Sea.

55 Persson, C. (SMHI), Rodhe, H. (MISU), De Geer, L.-E. (FOA) (1986)
The Chernobyl accident - A meteorological analysis of how radionucleides reached Sweden.

56 Persson, C., Robertson, L. (SMHI), Grennfelt, P., Kindbom, K., Lövblad, G., och Svanberg, P.-A. (IVL) (1987)
Luftföroreningsepisoden över södra Sverige 2 - 4 februari 1987.

57 Omstedt, G. (1988)
An operational air pollution model.

58 Alexandersson, H., Eriksson, B. (1989)
Climate fluctuations in Sweden 1860 - 1987.

59 Eriksson, B. (1989)
Snödjupsförhållanden i Sverige - Säsongerna 1950/51 - 1979/80.

60 Omstedt, G., Szegö, J. (1990)
Människors exponering för luftföroreningar.

61 Mueller, L., Robertson, L., Andersson, E., Gustafsson, N. (1990)
Meso-γ scale objective analysis of near surface temperature, humidity and wind, and its application in air pollution modelling.

62 Andersson, T., Mattisson, I. (1991)
A field test of thermometer screens.

63 Alexandersson, H., Gollvik, S., Meuller, L. (1991)
An energy balance model for prediction of surface temperatures.

64 Alexandersson, H., Dahlström, B. (1992)
Future climate in the Nordic region - survey and synthesis for the next century.

65 Persson, C., Langner, J., Robertson, L. (1994)
Regional spridningsmodell för Göteborgs och Bohus, Hallands och Älvsborgs län. (A mesoscale air pollution dispersion model for the Swedish west-coast region. In Swedish with captions also in English.)

66 Karlsson, K.-G. (1994)
Satellite-estimated cloudiness from NOAA AVHRR data in the Nordic area during 1993.

67 Karlsson, K-G. (1996)

Cloud classifications with the SCANDIA model.

68 Persson, C., Ullerstig, A. (1996)
Model calculations of dispersion of lindane over Europe. Pilot study with comparisons to measurements around the Baltic Sea and the Kattegat.

69 Langner, J., Persson, C., Robertson, L., and Ullerstig, A. (1996)
Air pollution Assessment Study Using the MATCH Modelling System. Application to sulfur and nitrogen compounds over Sweden 1994.

70 Robertson, L., Langner, J., Engardt, M. (1996)
MATCH - Meso-scale Atmosperic Transport and Chemistry modelling system.

71 Josefsson, W. (1996)
Five years of solar UV-radiation monitoring in Sweden.

72 Persson, C., Ullerstig, A., Robertson, L., Kindbom, K., Sjöberg, K. (1996)
The Swedish Precipitation Chemistry Network. Studies in network design using the MATCH modelling system and statistical methods.

73 Robertson, L. (1996)
Modelling of anthropogenic sulfur deposition to the African and South American continents.

74 Josefsson, W. (1996)
Solar UV-radiation monitoring 1996.

75 Häggmark, L., Ivarsson, K.-I. (SMHI), Olofsson, P.-O. (Militära vädertjänsten). (1997)
MESAN - Mesoskalig analys.

76 Bringfelt, B, Backström, H, Kindell, S, Omstedt, G, Persson, C, Ullerstig, A. (1997)
Calculations of PM-10 concentrations in Swedish cities- Modelling of inhalable particles

77 Gollvik, S. (1997)
The Teleflood project, estimation of precipitation over drainage basins.

78 Persson, C., Ullerstig, A. (1997)
Regional luftmiljöanalys för Västmanlands län baserad på MATCH modell-beräkningar och mätdata - Analys av 1994 års data

79 Josefsson, W., Karlsson, J.-E. (1997)
Measurements of total ozone 1994-1996.

80 Rummukainen, M. (1997)
Methods for statistical downscaling of GCM simulations.

81 Persson, T. (1997)
Solar irradiance modelling using satellite retrieved cloudiness - A pilot study.

82 Langner, J., Bergström, R. (SMHI) and Pleijel, K. (IVL) (1998)
European scale modelling of sulfur, oxidized nitrogen and photochemical oxidants. Model development and evaluation for the 1994 growing season.

83 Rummukainen, M., Räisänen, J., Ullerstig, A., Bringfelt, B., Hansson, U., Graham, P., Willén, U. (1998)
RCA - Rossby Centre regional Atmospheric climate model: model description and results from the first multi-year simulation.

84 Räisänen, J., Döscher, R. (1998)
Simulation of present-day climate in Northen Europé in the HadCM2 OAGCM.

85 Räisänen, J., Rummukainen, M., Ullerstig, A., Bringfelt, B., Ulf Hansson, U., Willén, U. (1999)
The First Rossby Centre Regional Climate Scenario - Dynamical Downscaling of CO_2-induced Climate Change in the HadCM2 GCM.

86 Rummukainen, Markku. (1999)
On the Climate Change debate.

87 Räisänen, Jouni (2000)
CO_2-induced climate change in northern Europé: comparison of 12 CMIP2 experiments.

88 Engardt, Magnuz (2000)
Sulphur simulations for East Asia using the MATCH model with meteorological data from ECMWF.

89 Persson, Thomas (2000)
Measurements of Solar Radiation in Sweden 1983-1998.

90 Daniel B. Michelson, Tage Andersson
Swedish Meteorological and Hydrological Institute (2000)
Jarmo Koistinen, Finnish Meteorological Institute
Christopher G. Collier, Telford Institute of Environmental Systems, University of Salford
Johann Riedl, German Weather Service
Jan Szturc, Instiute of Meteorology and Water Management
Uta Gjertsen, The Norwegian Meteorological Institute
Aage Nielsen, Danish Meteorological Institute
Søren Overgaard, Danish Meteorological Institute
BALTEX Radar Data Centre Products and their Methodologies.

91 Josefsson, Weine (2000)
Measurements of total ozone 1997 – 1999.

92 Andersson, Tage (2000)
Boundary clear air echos in southern Sweden.

93 Andersson, Tage (2000)
Using the Sun to check some weather radar parameters.

94 Rummukainen, M.,S. Bergström, E. Källén, L. Moen, J. Rodhe, M. Tjernström (2000)
SWECLIM – The First Three Years.

95 Meier, H. E Markus (2001)
The first Rossby Centre regional climate scenario for the Baltic Sea using a 3D coupled ice-ocean model.

96 Landelius, Tomas, Weine Josefsson, Thomas Persson (2001)
A system for modelling solar radiation parameters with mesoscale spatial resolution

97 Karlsson, Karl-Göran (2001)
A NOAA AVHRR cloud climatology over Scandinavia covering the period 1991-2000

98 Bringfelt, B., Räisänen, J., Gollvik, S., Lindström, G., Graham, P., Ullerstig, A., (2001)
The land surface treatment for the Rossby Centre Regional Atmospheric Climate Model - version 2 (RCA2).

99 Kauker, Frank, Alfred Wegener Institute for Polar and Marine Research, Germany and Meier, H.E. Markus, Swedish Meteorological and Hydrological Institute, Rossby Centre, Sweden (2002)
Reconstructing atmospheric surface data for the period 1902-1998 to force a coupled ocean-sea ice model of the Baltic Sea.

100 Klein, Thomas, Bergström, Robert, Persson, Christer (2002)
Parameterization of dry deposition in MATCH.

SMHI
Swedish Meteorological and Hydrological Institute
SE 601 76 Norrköping, Sweden.
Tel +46 11-495 80 00. Fax +46 11-495 80 01

ISSN 0347-2116